SPATIAL CHARACTERISTICS OF COOPERATIVE INTERACTIONS IN THE STRIATE CORTEX

By

Zhiyi Zhou

Dissertation

Submitted to the Faculty of the

Graduate School of Vanderbilt University

in partial fulfillment of the requirements

for the degree of

DOCTOR OF PHILOSOPHY

in

Biomedical Engineering

December, 2007

Nashville, Tennessee

Approved:

Professor A. B. Bonds, III

Professor Jon H. Kass

Professor Peter Konrad

Professor Joseph S. Lappin

Professor Richard G. Shiavi

ACKNOWLEDGMENTS

First, I would like to thank my wonderful research advisor, Dr. A. B. Bonds for his guidance and patience during my graduate school study. I am also indebted to the members of my committee: Drs. Jon Kaas, Peter Konrad, Richard Shiavi, and Joseph Lappin, for their time and assistance. Thanks also to the past and present members in our lab, Dr. Jason Samonds and Melanie Bernard, for their help in my research.

My deeply appreciation goes to my wife, Jingqi Wang, for her understanding and support throughout my graduate research at Vanderbilt University.

TABLE OF CONTENTS

LIST OF FIGURES

CHAPTER I

SPECIFIC AIMS

Traditionally, the visual system has been thought to encode visual scenes by changes in response rate of visual neurons, with the individual neurons acting as feature detector (Barlow, 1972). However, the dimensionality of visual scenes overwhelms even the large number of visual neurons, suggesting that independent firing rate modulation may not be the only coding mechanism employed by the visual system. With the aid of multi-channel recording, synchronized neural responses have been found at multiple stages in the visual pathway. The stimulus dependence of synchrony implies that neural cooperation may play an important role in visual perception (Eckhorn et al., 1988; Gray et al., 1989; Engel et al., 1991; Singer and Gray, 1995; Castelo-Branco et al., 2000). The goal of this work is to explore the fundamental sources of neural synchronization and the potential functional role of correlated neural responses in visual perception tasks such as contour integration and pattern recognition.

Aim #1

To determine the relationship between stimulus properties and receptive field features that encourages neural synchrony. Earlier work suggests that cortical neurons with similar orientation preferences and overlapped receptive fields are more likely to synchronize their activities (Eckhorn et al., 1988; Engel et al., 1991a; Gray et al., 1989; Kreiter & Singer, 1996; Kohn & Smith, 2005). However, using linear gratings or bars as

the major experimental stimulus cannot reflect the broad range of visual stimuli in the real world and this strategy potentially underestimates the functional role of neural synchrony in visual perception. The fact that neural synchrony is stimulus-driven implies that spatial or temporal features in the visual stimuli may be more important than intrinsic receptive field characteristics in the development of neural synchrony. The influence of receptive field features in the development of synchrony remains unresolved. We have analyzed neural responses, including average response rate and neural synchrony, to the stimulation of collinear (regular drifting sinusoid gratings) and cocircular contours (drifting sinusoid concentric rings). The goal of this study is to test whether non-collinear stimuli can induce synchronized activity between cells, and whether this activity is emergent, i.e., provides a more sensitive discrimination between collinear and non-collinear stimuli than does firing rate.

Aim #2

To study the relationship between the time domain and frequency domain estimates of neural synchronization and to clarify the importance of fine temporal structures in maintaining neural correlation. Correlation between neural responses normally expresses as synchronization of spike timing and/or coherence of specific frequency components (oscillation). Cross-correlation (Perkel et al., 1967; Aertsen et al., 1989) and coherence (Mitra and Pesaran, 1999; Jarvis and Mitra, 2001) analysis are the primary methods for analyzing the timing and frequency association between neurons, but few studies have been conducted to address the direct relationship between these two approaches. In this aim, we analyzed the synchronized neural activities in cat primary

visual cortex with both cross-correlation and coherence analysis and conducted regression analysis to study the correlation between the results from these two methods. We also perturbed the fine temporal structures in the original spike trains by randomly jittering spikes in different time ranges to observe how correlation is disrupted by systematically destroying the fine temporal structure in the response.

Aim #3

To clarify the contribution of spatial integrity to the generation of neural synchrony. Coherent spatial and temporal structures within visual space lead to the perception of discrete visual features as a whole (Koffka, 1935). Neural assemblies, defined by correlated firing, can be constructed among cells with similar tuning properties once those cells are coactivated by stimuli with appropriate spatial characteristics such as drifting gratings with preferred orientation and direction of motion (Eckhorn et al., 1988; Engel et al., 1991a; Gray et al., 1989; Kreiter & Singer, 1996; Samonds et al., 2004). Gray et al. (1989) showed that neural synchrony is sensitive to contour integrity. These findings suggest that synchronized neural responses not only depend on common temporal coherence but are also sensitive to spatial integrity. What remains unknown is the specific degree to which synchrony depends on spatial coherence of the visual stimulus. In the third aim, we used drifting sinwave gratings with fixed temporal features but systematically deconstructed contour integrity to determine the dependence of neural synchronization on spatial coherence. We also examined how neural synchronization in the time and frequency domains developed to explore the relationship between spike timing synchronization and associated frequency component oscillation.

REFERENCES

Aertsen AM, Gerstein GL, Habib MK, Palm G (1989) Dynamics of neuronal firing correlation: modulation of "effective connectivity". J Neurophysiol 61:900-917.

Barlow HB (1972) Single units and sensation: a neuron doctrine for perceptual psychology? Perception 1:371-394.

Castelo-Branco M, Goebel R, Neuenschwander S, Singer W (2000) Neural synchrony correlates with surface segregation rules. Nature 405:685-689.

Eckhorn R, Bauer R, Jordan W, Brosch M, Kruse W, Munk M, Reitboeck HJ (1988) Coherent oscillations: A mechanism of feature linking in the visual cortex? Biological Cybernetics V60:121-130.

Engel AK, Kreiter AK, Konig P, Singer W (1991) Synchronization of oscillatory neuronal responses between striate and extrastriate visual cortical areas of the cat. Proc Natl Acad Sci USA 88:6048-6052.

Gray CM, Konig P, Engel AK, Singer W (1989) Oscillatory responses in cat visual cortex exhibit inter-columnar synchronization which reflects global stimulus properties. Nature 338:334-337.

Jarvis MR, Mitra PP (2001) Sampling properties of the spectrum and coherency of sequences of action potentials. Neural Comput 13:717-749.

Mitra PP, Pesaran B (1999) Analysis of Dynamic Brain Imaging Data. Biophys J 76:691-708.

Perkel DH, Gerstein GL, Moore GP (1967) Neuronal spike trains and stochastic point processes. II. Simultaneous spike trains. Biophys J 7:419–440.

Singer W, Gray CM (1995) Visual feature integration and the temporal correlation hypothesis. Annu Rev Neurosci 18:555-586.

CHAPTER II

INTRODUCTION

Visual coding hypothesis

The dimensionality of a complex visual scene, involving different objects with specific spatial and temporal features, such as colors, brightness, shapes and motion, is enormous. This raises the challenging question of how the visual system is capable of segregating and identifying specific objects within the huge amount of information it receives every moment. The Gestalt principle, which embraces a series of rules such as common fate, closure, familiarity, and proximity etc. (Figure 2-1), defines the basic framework about how our brain combines discrete elements to create a "whole" object (Koffka, 1935). However, the biological mechanisms within the visual pathway that support the representation and integration of those individually incomplete features are still under debate. Different coding schemas have been proposed to address the solution. Based on the response properties of individual neurons, a classic model called the “Cardinal cell” theory (Barlow, 1972) proposed that each visual neuron serves as a feature detector and each cell will display an elevated firing rate once an appropriate feature is presented in a specific location in the visual field. Visual information then converges onto neurons in the next cortical level in the visual pathway, where the structure of effective stimulus features is further developed. "Cardinal" cells located on the top of the mental hierarchy would have the ability to represent features that have the highest complexity, which also implies the highest degree of selectivity. The "Cardinal

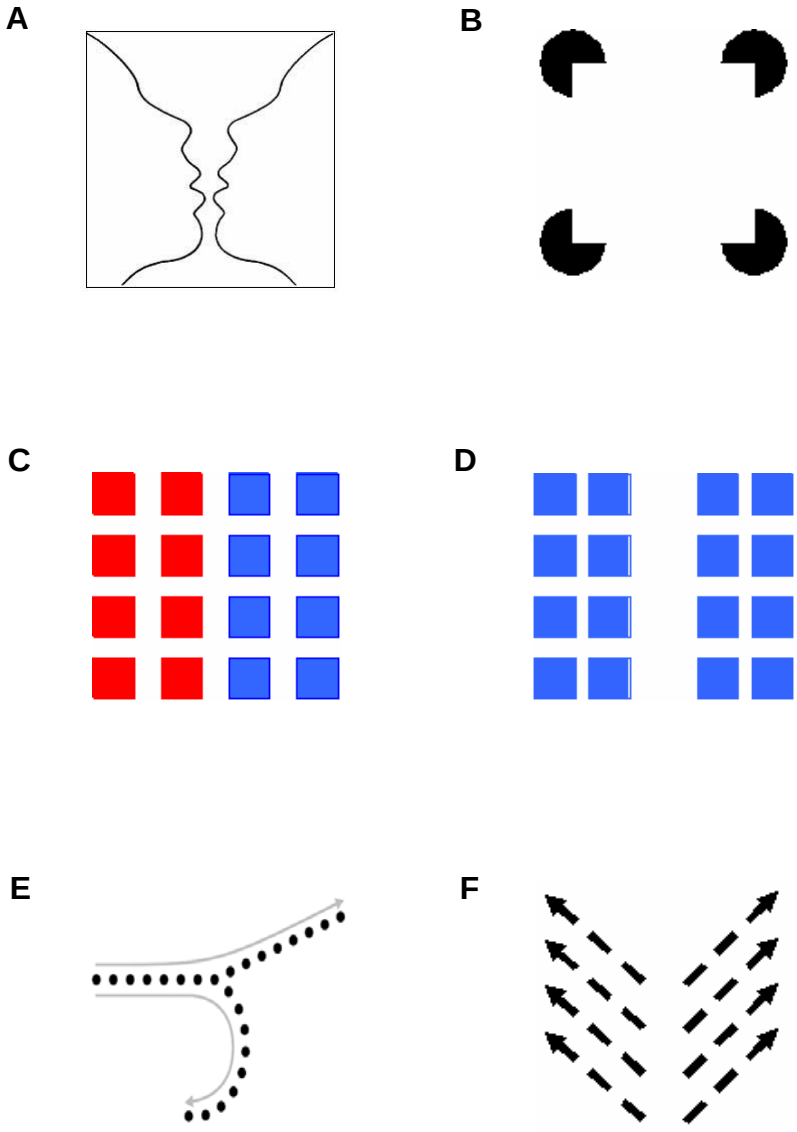

Figure 2-1: Perception rules of Gestalt psychology (A) Figure-ground segregation (B) Closure (C) Similarity (D) Proximity (E) Continuity (F) Common fate.

cell" theory describing perception through integrated firing rate has received support from extensive experimental studies. In the primary visual cortex, neurons are generally dependent on the simplest features of the visual input including location, orientation and spatial and temporal frequencies (Hubel and Wiesel, 1962; Albrecht et al., 1980; De Valois et al., 1982; Webster and De Valois, 1985; Bonds, 1989). Cells in higher cortical areas are selective to more complicated features. For example, some cells in area V4 of macaque monkey will show an elevated response rate only if concentric rings or radial gratings are presented in their receptive fields (Gallant et al., 1996). A small group of cells located in the inferior temporal (IT) cortex in macaque monkeys are reported to respond selectively to faces (Desimone et al., 1984). If the internal features of the face such as eyes or snout are removed or scrambled, the response is greatly reduced, which suggests that a particular configuration of the internal features is essential to drive those cells. Furthermore, other stimuli such as a picture of a hand or sine-wave gratings elicit almost no response in these face-selective IT neurons.

However, the coding mechanism described by this classic model has been criticized for its inefficiency and ambiguity. The “cardinal cell” theory requires cells at the highest levels of the visual cortex to have the ability to detect a specific object or complicated feature, but the finite number of total available neurons in the central nervous system seems inadequate to support the apparently unlimited perceptual ability of the brain. On the other hand, neurons may respond to stimuli consisting of different feature parameters with the same response magnitude. For example, the response rate of cells in area 17 may not change if a cell is stimulated by a moving grating with less optimal orientation but high contrast or a grating with more optimal orientation but low

contrast. The information provided to cells in the extra-striate cortical areas will thus be ambiguous if response rate modulation is the only coding methodology in the visual system. The theory of perception through the independent firing rate of distributed feature-triggered cells thus cannot account for the entire capability of the visual system to represent information.

The concept of population coding was proposed early in the last century. Sherrington (1941) presented a reflex model defining cooperation between different groups of neurons, in which a "center" received converging input from afferent nerve fibers and the output pulses were transmitted over a compound efferent nerve tract. The sum of the central excitatory and central inhibitory states decided the activity of the pool. A “neural assembly” theory proposed by Hebb (1949) considers that connections and interactions between neurons are more functionally significant than the specific properties of individual neurons. Hebb suggested that a group of neurons that tend to fire together under specific stimulation forms a “cell assembly” in which numbers of cells act simultaneously as an entity to represent and deliver certain information. The efficacy of connection among neurons increases in proportion to the degree of correlation between pre- and post- synaptic activities (Hebb, 1949). Guided by Hebb’s “cell assembly” theory, brain researchers and vision scientists further explored the theoretical and experimental evidence supporting the notion that neural correlation may play an important role in brain function. Milner (1974) elaborated on the drawback of the "feature detector" theory in shape perception and explained in detail how synchronized cell assemblies might improve the deficiency and ambiguity of the feature detector model. Von der Malsburg (1981) presented a theory in which the term "correlation" was defined as the

measurement of similarity between the time of occurrence of neural signals expressed on a fine temporal scale. Correlation between neural signals could then modulate the synaptic strength or refine the synaptic plasticity that von der Malsburg proposed as the biological basis for short-term and long-term memory respectively.

Neural synchronization and temporal correlation

After the late 1970's, when practical multi-channel recording became available, vision researchers began to seek experimental support for theories involving correlated neural responses and have found that neural synchrony may play an important role in visual perception. Numerous studies have shown that synchronized neural activity exists throughout the entire visual pathway and that it is stimulus-dependent, implying that it carries useful information. Meister et al (1995) studied correlated signaling in ganglion cells of the salamander retina. They found that cell pairs that have more closely spaced receptive fields have higher correlation in their activity. The plot of a synchronous receptive field of a cell pair derived from reverse correlation with a pseudorandom flickering checkerboard was generally smaller than the sum of the receptive fields of both neurons and was located in the overlapping portion of the receptive fields, which implied that these two cells were not firing independently. With multiunit recordings from cat retina and lateral geniculate nucleus (LGN), Neuenschwander & Singer (1996) found oscillatory synchronization between cells with non-overlapping receptive fields, with synchronized responses occurring over distances greater than 20^{o}. Synchronization has also been described between cells located in the same or different levels of the visual

cortex or even between cells in different hemispheres (Gray et al., 1989; Gray and Singer, 1989; Engel et al., 1991a; Engel et al., 1991b).

A number of studies provide evidence suggesting that neural synchronization may act as a versatile coding mechanism in the perceptual binding of features detected by individual cells. Synchronized neural responses in multi-unit activity (MUA) of cat area 17 are dependent on global features such as spatial continuity. When stimulating with a long moving light bar, strong oscillatory behavior with zero phase lock was found between two recording sites with separate receptive fields if these two sites were co-activated by the same stimulus. If the same two recording sites were separately stimulated with two short light bars moving in the same or different directions, synchronization was considerably reduced (Gray et al., 1989). Similarly, in MT area of awake behaving monkey, the strength of synchrony was higher when two cells were stimulated with a single bar moving in a direction midway between the preferred directions than when the two cells were stimulated independently with two bars moving in the preferred directions of the individual cells. Castelo-Branco et al. (2000) tested neurons in cat area 18 and PMLS with a plaid stimulus created by superimposing two gratings with different moving directions. By manipulating the luminance of the grating intersections, the plaid stimulus is perceived as either two surfaces, in which two gratings are moving independently, or as a single pattern, in which two gratings are moving coherently. Neurons responding to one of the two grating components would synchronize with neurons responding to the other component when the components were perceived to move coherently or desynchronize when the components were perceived to move independently. Response rate modulation, however, failed to differentiate the above two patterns. Gamma band oscillation may also

act as a brain mechanism for scene segmentation. Gail et al. (2000) used a grating pattern in which a rectangular area with (figure-ground condition) or without (continuous condition) spatial phase shift was defined as an object. Analysis of V1 MUA and local field potential (LFP) responses from the recording sites corresponding to the figure and background areas showed that gamma coherence was dramatically reduced when the stimulus condition changed from figure-ground condition to the continuous condition.

Based on the above research findings, Singer and his colleagues extended earlier correlation theories and developed the "temporal correlation" hypothesis (Singer and Gray, 1995; Gray, 1999; Singer, 1999). Oscillatory synchronization between feature selective cells in the visual cortex is suggested as being sensitive to the global features of visual stimuli, such as continuity, orientation similarity and motion coherency and provides a binding mechanism to establish relations between features in different parts of the visual fields. Perceptual grouping and segmentation could be mediated by the formation of cell assemblies. Because of the precise (<10 msec) timing of synchrony, multiple cell assemblies could be formed simultaneously, and each assembly represents one set of grouped features. Cell assemblies are dynamic entities; the structure of an assembly would be determined not only by the anatomical organization of the cortical networks, but would also be constrained by the Gestalt properties of the stimulus features in the visual scene. Cell assemblies are formed based on the synchronization of neuronal firing among neural populations distributed within and across different levels of the cortical hierarchy. Different assemblies are distinguished from one another by the independence of their firing patterns. Since these neural ensembles are dynamic, different stimuli will create different coherent groupings. With such mechanisms, in primary visual

cortex even entirely novel stimuli can be represented by the coherent activity of a particular neural ensemble.

The role of neural synchrony in visual perception

The hypothesis of binding through neural synchrony has been challenged by some negative findings reported by other research groups. These inconsistent results should however be carefully interpreted before rejecting neural synchrony as a potential binding mechanism. The plaid experimental protocol (see Castelo-Branco et al., 2000) was reexamined by Thiele and Stoner (2003) in area MT of awake, behaving monkeys. Synchrony was not significantly higher in plaids perceived as coherent as opposed to those perceived as non-coherent. On the other hand, coherent plaids elicited a significantly greater response rate than non-coherent plaids. This result would appear to contradict any linkage between synchrony and image binding. However, neural synchrony may play different roles in different cortical areas. In the early stages of the visual pathway, such as the primary visual cortex, neurons are mainly responsible for processing the fundamental properties of the visual stimuli. If objects are bound via synchrony at lower levels due to coherent temporal or spatial characteristics of visual stimuli, there is no necessity for higher-order neurons to further synchronize their responses. The higher response rate for recognizing coherent plaids than for non-coherent plaids found in MT neurons in fact suggests that rate modulation of higher-order neurons might be induced by synchronized inputs from lower-order neurons (Singer, 1999; Castelo-Branco et al., 2000; Thiele and Stoner, 2003). Lamme and Spekreijse (1998) reported that neuron pairs in Area 17 of awake behaving monkeys, in which both

members respond to the figure in a visual stimulus, did not show significantly higher synchrony than neuron pairs with one responding to figure and the other to ground, which seems to conflict with the positive finding in Gail et al. (2000). However, synchrony can be exquisitely sensitive to the match between the form of the stimulus and the tuning of the receptive fields (Samonds et al., 2003; Kohn and Smith, 2005) and Lamme and Spekreijse (1998) did not provide information on the relationship between the orientation preference of recorded units and the orientation of the stimuli. Thus, averaging data across cell pairs with different receptive field configurations may mask the truly valuable information (Singer, 1999). Palanca and DeAngeles (2005) examined MUA and LFP synchrony in MT of awake monkey. Images were created that were identical within the recorded receptive fields, but either joined or independent outside those regions. In general there was little synchrony difference between the two conditions, suggesting that synchrony was not a primary means for signaling the integrity of global structures. However, these results do not necessarily reject the temporal correlation hypothesis. LFP gamma band synchrony was slightly but consistently higher for integral (vs. independent) stimuli, which agrees that gamma band activity is on the whole more sensitive to image structure. While this was not seen in MUA, unit activity is generally less effective for coherency analysis and a larger data set may have improved the results. We would also suggest that binding of image segments by synchrony may be less obvious at higher cortical levels because cells are already expressing more complex abstractions.

Though the evidence of synchrony as an active binding mechanism is not consistent in extracortical visual areas, research results have suggested that synchrony in the early stages of visual pathway can provide pre-processing of visual information for

higher-order correlations. Each ganglion cell in the area centralis of a cat receives convergent inputs from fewer than 10 closely distributed photoreceptors (Kolb, 1979). The subsequent divergent and convergent transmission from ganglion cells to LGN causes the firing of nearby neurons in LGN to represent local coherent spatial and temporal structures embedded in the visual stimulus. Coherence information encoded in the form of synchrony is propagated to striate and extrastriate cortex (Engel et al., 1991a; Engel et al., 1991b; Castelo-Branco et al., 2000). The spatial and temporal integrity in the stimulus yields similar response latencies that appear to be more important in generating neural synchrony than oscillation (Samonds and Bonds, 2005). Because of high convergence, cortical neurons may not be able to recognize the rich temporal information contained in the spike trains of retinal ganglion cells. If the individual rates can be translated into distributed, synchronized neural ensembles, the information could be more easily parsed by cortical neurons (Usrey and Reid, 1999). In the visual pathway from retina to LGN to visual cortex, when neurons receive two input spikes with a narrow interspike interval (ISI), i.e., less than 30 milliseconds, the second spike is much more likely to evoke spikes in the postsynaptic neurons. This paired-spike enhancement also increases the number of synchronous events in the target area (Alonso et al., 1996; Usrey et al., 1998). Therefore, synchrony should to be considered as a "reliable signal transmission mechanism that extracts higher-order visual relationships as a Gestalt rather than active structural binding mechanism that represents a secondary code within a system of simple feature extraction" (Samonds and Bonds, 2005). Synchronized neural firing induced by the coherent spatial and/or temporal structures in visual stimuli emphasizes the salience of the correlated signals, which can be recognized by a common

target neuron in the higher level of the visual pathway. Thus novel or unanticipated structures can by represented flexibly, allowing for an unlimited perceptual range of the visual system.

One conceptual framework that we consider consistent with the synchronous activity in V1 is association field theory. In a psychophysical study of the Gestalt law of "good continuation", Field et al. (1993) found that the observers' performance in detecting a curved contour defined by a group of Gabor patches was improved if these Gabor patches were closer to each other. Field et al. also found that even though the orientation difference between two adjacent patches can affect the detectability of the contour, the orientation variance of each patch relative to the overall contour is more important in determining whether those patches are perceived as being linked together. After alternating the polarity of some Gabor patches, the contour was still detectable with only a minor decrement in observer performance. These findings imply that the perception of the contour is not the output of a single linear filter with an elongated receptive field, but rather that this linking result is due to the joint contribution from a network, which more likely consists of complex cells (Field et al., 1993; Hess et al., 2003). Association field theory predicts linking between orientation-tuned cells that is dependent on their joint relative orientation and spatial position. In natural images, contours are predominantly linear with a decreasing probability of greater curvature (Geisler et al., 2001; Sigman et al., 2001; Elder and Goldberg, 2002). The probability for linking is strongest between elements with smaller orientation difference and closer separations. What is more important is the relative variance, the extent to which receptive fields are aligned along the notional contour (Field et al., 1993). Therefore, greater

separation can support greater angular differences because the relative variance to the contour linking the two elements is smaller with larger spatial separation. We conjecture that synchrony in the early stages of visual processing, i.e. primary visual cortex, can extend integration over broad regions and overcome the ambiguity of firing rate to identify salient contours, which then have the potential to be integrated at subsequent locations in the higher level cortical areas, e.g. V4. In Chapter 4, we examined the potential role of neural synchrony in cat areas 17 and 18 in contour integration. We tested cell response with both traditional drifting sinusoid gratings and more complex drifting sinusoid concentric rings. We found that the strength of synchrony between cells in the primary visual cortex is not only affected by the receptive field properties, such as orientation and location, but also determined by the effectiveness of visual stimulus in driving cells. What is more interesting in our results is that synchrony was found to be more reliable for detecting cocircular contours than independent firing rate, suggesting that contour integration could start as early as in the lowest level of visual cortex through synchronization between neural responses.

Time and frequency domain analysis

Spike timing synchronization is often accompanied by coherent frequency oscillation, especially in the gamma band (35 – 70 Hz). Coherent oscillation is said to occur when two neurons oscillate at the same frequency with a small phase difference, which can result in a central peak in their cross-correlogram (Usrey and Reid, 1999). From studies of oscillation patterns of single and multiple spikes as well as local field potentials recorded from the primary visual cortex, Eckhorn et al. (1988) proposed that

stimulus-evoked oscillation may serve to define global aspects of a visual scene by binding a group of neurons that have specific receptive field features into coherent ensembles. The membership in these coherent ensembles is dynamically defined such that the same neuron can join different groups depending on the stimulus configuration and its receptive field attributes.

Neural synchronization is normally assessed in the time and frequency domains by cross-correlation and coherence analysis respectively. In Chapter 5, we examined the synchronized neural response in cat areas 17 and 18 with JPSTH and multi-taper coherence analysis (Percival and Walden, 1993; Jarvis and Mitra, 2001) to explore the correlation between the time and frequency domain estimates. Linear regression analysis on the synchrony and coherence results obtained with JPSTH and multi-taper methods shows that cross-correlation analysis and coherence analysis are internally related, though these two methods study neural connectivity from different perspectives.

Fine temporal structure and neural correlation

Several studies have suggested that information beyond that provided by the firing rate could be added by fine temporal structure within the neural response. In very early work, Hubel (1959) observed the irregularity of single-unit discharges in cat visual cortex and described burst activity, which later is defined as a group of multiple spikes from a single neuron with an interspike interval (ISI) of $< 4 – 8$ msec preceded by at least 100 msec of silence (Lu et al., 1992; Debusk et al., 1997; Reinagel et al., 1999; Lesica and Stanley, 2004). In complex cells, neural responses to stimuli presented at or near the optimal orientation tend to have a higher percentage of spikes in bursts than responses to

stimuli at nonoptimal orientations. Spikes in the burst ("clustered spikes") and outside the burst ("isolated spikes") have detection sensitivities to different attributes of the stimulus (Cattaneo et al., 1981). Only the clustered spikes are tuned for orientation and spatial frequency while both the isolated and clustered spikes are sensitive to contrast change. At a given firing rate, the optimal orientation can induce bursts with greater length than nonoptimal orientations (Debusk et al., 1997). Bursts from a presynaptic cell are almost 100% more effective than isolated spikes in eliciting a time-related response in the driven cell, and longer bursts are more effective than shorter bursts (Snider et al., 1998). Studies of response patterns from neural populations also indicate that emergent information that is not found in independent neural responses can be provided by the fine temporal structure embedded in neural firing. With cost-based metrics analysis, Samonds and Bonds (2004) reported that, while information for discriminating large orientation differences (i.e. $> 10^{o}$) is contained mainly in the firing rate, spike timing and intervals provide information suitable for fine discrimination of orientation (i.e. $< 10^{o}$). Study of the correlated activity of cells in the lateral geniculate nucleus (LGN) of cats showed that a significant amount of information can be extracted if temporal correlation between cells is considered (Dan et al., 1998). However, the role of fine temporal structure in coding visual information is still under debate. For example, Shadlen and Newsome (1998) have argued that the fine temporal structures contained in neural spike trains may merely reflect the noise transmitted through the visual pathway and deliver little meaningful information.

To explore the importance of spike timing accuracy and fine temporal structure in maintaining neural correlation, we perturbed the spike timing in the original neural

response by randomly jittering the spikes over different time ranges. The result described in Chapter 5 shows that synchrony and coherence both systematically dropped with the increase of the jittering range. Functional dependency analysis discovered that information loss is introduced after the fine temporal structures in the spike trains are deconstructed by the jittering procedure.

Spatial integrity and neural synchronization

The principle of continuity in Gestalt psychology states that the visual system tends to group continuous figures as a whole (Koffka, 1935). To support the notion that synchrony provides a substrate for pre-processing simple features in order to develop more complex structures, it is necessary to understand how synchrony depends on the integrity of the input structures. Although psychophysical experiments have studied the interaction of temporal and spatial cues in perceptual grouping and demonstrated that binding and segmentation may be accomplished by exploiting both spatial or temporal cues either alone or in combination (Leonards et al., 1996), more neurophysiological studies on the cellular level are needed to quantify the contribution and interactions of temporal and spatial features in visual segmentation and perceptual grouping.

Our laboratory has shown earlier that synchrony is dependent on the similarity of latency in the responses of a cell pair. The strength of synchrony is strongly correlated with the inverse log of both the difference in response latency and the standard deviation of the latency difference (Samonds and Bonds, 2005). Fries et al. (2001) reported that with similar orientation preferences and overlapping receptive fields, the spontaneous response of cells in cat primary visual cortex tends to exhibit correlated fluctuations in

response latency and that this correlation only occurred when local field potentials (LFPs) oscillated in the gamma frequency range. This suggests that during visual perception coherent spontaneous excitability fluctuation in certain cells, which may originate from either anatomical connections or short-term synaptic plasticity in the pre-stimulus stage, could result in faster binding after stimulus onset. These observations lead to the speculation that synchrony is likely to arise from common fate, but cortical circuitry contributes to sustaining it (Samonds and Bonds, 2005). On the other hand, synchrony is clearly related to spatial structure since it is more dependent on orientation than is firing rate (Samonds et al., 2004). Gray et al. (1989) reported that a long light bar would evoke stronger synchrony in two collinearly aligned cells than that induced by using two short bars to drive the same two cells, suggesting synchrony is sensitive to spatial disorganization or discontinuity in stimuli. What remains unknown is the specific degree to which neural synchronization depends on spatial integrity, temporal integrity, or both. In Chapter 6, we explored the answer to this question by studying cells' response to stimuli with and without coherent spatial structure. By adding 10 – 55% spatial noise into regular sinewave gratings, the spatial integrity of the stimulus was systematically deconstructed while the temporal integrity of stimulus was maintained constant. We found that temporal integrity, and not spatial integrity, generates synchrony; spatial integrity however is critical in triggering subsequent gamma band synchronization.

Future research

So far, research regarding the role of population coding has mainly focused on analyzing the correlation between pairs of neurons. Although pairwise correlations imply

strongly correlated network states in the overall neural population (Schneidman et al., 2006), studies extending to larger neural assemblies beyond cell pairs are necessary to fully understand the role of neural correlation in brain processing and visual perception.

The paucity of reports on interactions among larger neural populations is partially due to the unavailability of valid computational tools to quantify correlation within groups of neurons larger than two, although current techniques of multi-channel recording have conquered the limitation of collecting simultaneous activities from multiple cells. Therefore, we have developed a novel method to quantify multi-cell synchrony in a neural assembly that contains more than two members. The implementation of this method will be briefly discussed in Chapter 7.

Since the late 1950s, vision research has emphasized study of responses to spectrally or spatially pure artificial images, such as lines, gratings or simple geometric figures, based on the understanding that interpretation of results would be easier and less prone to artifact. This has contributed greatly to our understanding of basic neural properties of the visual system (Hubel, 1959; Hubel and Wiesel, 1962, 1968; De Valois et al., 1979; De Valois et al., 1982; Ts'o et al., 1986; Bonds, 1989; Gallant et al., 1996) and has provided an essential foundation for future work. However, interactions such as receptive field reorganization due to stimulation of the “non-classical” periphery (Pettet and Gilbert, 1992) suggest that current models based on simple stimuli may not accurately predict cell behaviors in the context of complex images such as natural scenes. The importance of natural image stimulation in future research will be briefly discussed in Chapter 7.

REFERENCES

Albrecht DG, De Valois RL, Thorell LG (1980) Visual cortical neurons: are bars or gratings the optimal stimuli? Science 207:88-90.

Alonso J-M, Usrey WM, Reid RC (1996) Precisely correlated firing in cells of the lateral geniculate nucleus. Nature 383:815-819.

Barlow HB (1972) Single units and sensation: a neuron doctrine for perceptual psychology? Perception 1:371-394.

Bonds AB (1989) Role of inhibition in the specification of orientation selectivity of cells in the cat striate cortex. Vis Neurosci 2:41-55.

Castelo-Branco M, Goebel R, Neuenschwander S, Singer W (2000) Neural synchrony correlates with surface segregation rules. Nature 405:685-689.

Cattaneo A, Maffei L, Morrone C (1981) Two firing patterns in the discharge of complex cells encoding different attributes of the visual stimulus. Exp Brain Res V43:115-118.

Dan Y, Alonso J-M, Usrey WM, Reid RC (1998) Coding of visual information by precisely correlated spikes in the lateral geniculate nucleus. Nat Neurosci 1:501-507.

De Valois KK, De Valois RL, Yund EW (1979) Responses of striate cortex cells to grating and checkerboard patterns. J Physiol 291:483-505.

De Valois RL, Albrecht DG, Thorell LG (1982) Spatial frequency selectivity of cells in macaque visual cortex. Vision Res 22:545-559.

Debusk BC, Debruyn EJ, Snider RK, Kabara JF, Bonds AB (1997) Stimulus-dependent modulation of spike burst length in cat striate cortical cells. J Neurophysiol 78:199-213.

Desimone R, Albright TD, Gross CG, Bruce C (1984) Stimulus-selective properties of inferior temporal neurons in the macaque. J Neurophysiol 4:2051-2062.

Eckhorn R, Bauer R, Jordan W, Brosch M, Kruse W, Munk M, Reitboeck HJ (1988) Coherent oscillations: a mechanism of feature linking in the visual cortex? Biological Cybernetics V60:121-130.

Elder JH, Goldberg RM (2002) Ecological statistics of Gestalt laws for the perceptual organization of contours. J Vis 2:324-353.

Engel AK, Konig P, Kreiter AK, Singer W (1991a) Interhemispheric synchronization of oscillatory neuronal responses in cat visual cortex. Science 252:1177-1179.

Engel AK, Kreiter AK, Konig P, Singer W (1991b) Synchronization of oscillatory neuronal responses between striate and extrastriate visual cortical areas of the cat. Proc Natl Acad Sci USA 88:6048-6052.

Field DJ, Hayes A, Hess RF (1993) Contour integration by the human visual system: Evidence for a local "association field". Vision Research 33:173-193.

Fries P, Neuenschwander S, Engel AK, Goebel R, Singer W (2001) Rapid feature selective neuronal synchronization through correlated latency shifting. Nat Neurosci 4:194-200.

Gail A, Brinksmeyer HJ, Eckhorn R (2000) Contour decouples gamma activity across texture representation in monkey striate cortex. Cereb Cortex 10:840-850.

Gallant JL, Connor CE, Rakshit S, Lewis JW, Van Essen DC (1996) Neural responses to polar, hyperbolic, and Cartesian gratings in area V4 of the macaque monkey. J Neurophysiol 76:2718-2739.

Geisler WS, Perry JS, Super BJ, Gallogly DP (2001) Edge co-occurrence in natural images predicts contour grouping performance. Vision Research 41:711-724.

Gray CM (1999) The temporal correlation hypothesis of visual feature integration: still alive and well. Neuron 24:31-47.

Gray CM, Singer W (1989) Stimulus-specific neuronal oscillations in orientation columns of cat visual cortex. Proc Natl Acad Sci USA 86:1698-1702.

Gray CM, Konig P, Engel AK, Singer W (1989) Oscillatory responses in cat visual cortex exhibit inter-columnar synchronization which reflects global stimulus properties. Nature 338:334-337.

Hebb DO (1949) The organization of behavior: A neuropsychological theory. New York John Wiley and Sons, Inc.

Hubel DH (1959) Single unit activity in striate cortex of unrestrained cats. J Physiol 147:226-238.

Hubel DH, Wiesel TN (1962) Receptive fields, binocular interaction and functional architecture in the cat's visual cortex. J Physiol 160:106-154.

Hubel DH, Wiesel TN (1968) Receptive fields and functional architecture of monkey striate cortex. J Physiol 195:215-243.

Jarvis MR, Mitra PP (2001) Sampling properties of the spectrum and coherency of sequences of action potentials. Neural Comput 13:717-749.

Koffka K (1935) Principles of Gestalt psychology. New York: Harcourt

Kohn A, Smith MA (2005) Stimulus dependence of neuronal correlation in primary visual cortex of the macaque. J Neurosci 25:3661-3673.

Kolb H (1979) The inner plexiform layer in the retina of the cat: electron microscopic observations. J Neurocytol 8.

Lamme VAF, Spekreijse H (1998) Neuronal synchrony does not represent texture segregation. Nature 396:362-366.

Leonards U, Singer W, Fahle M (1996) The influence of temporal phase differences on texture segmentation. Vision Research 36:2689-2697.

Lesica NA, Stanley GB (2004) Encoding of natural scene movies by tonic and burst spikes in the lateral geniculate nucleus. J Neurosci 24:10731-10740.

Lu SM, Guido W, Sherman SM (1992) Effects of membrane voltage on receptive field properties of lateral geniculate neurons in the cat: contributions of the low-threshold Ca2+ conductance. J Neurophysiol 68:2185-2198.

Meister M, Lagnado L, Baylor DA (1995) Concerted signaling by retinal ganglion cells. Science 270:1207-1210.

Milner PM (1974) A model for visual shape recognition. Psychol Rev 81:521-535.

Neuenschwander S, Singer W (1996) Long-range synchronization of oscillatory light responses in the cat retina and lateral geniculate nucleus. Nature 379:728-733.

Palanca BJA, DeAngelis GC (2005) Does neuronal synchrony underlie visual feature grouping? Neuron 46:333-346.

Percival DB, Walden AT (1993) Spectral analysis for physical applications, multitaper and conventional univariate techniques: Cambridge University Press.

Pettet MW, Gilbert CD (1992) Dynamic changes in receptive-field size in cat primary visual cortex. Proc Natl Acad Sci USA 89:8366-8370.

Reinagel P, Godwin D, Sherman SM, Koch C (1999) Encoding of visual information by LGN bursts. J Neurophysiol 81:2558-2569.

Samonds JM, Bonds AB (2004) From another angle: differences in cortical coding between fine and coarse discrimination of orientation. J Neurophysiol 91:1193-1202.

Samonds JM, Bonds AB (2005) Gamma oscillation maintains stimulus structure-dependent synchronization in cat visual cortex. J Neurophysiol 93:223-236.

Samonds JM, Allison JD, Brown HA, Bonds AB (2003) Cooperation between area 17 neuron pairs enhances fine discrimination of orientation. J Neurosci 23:2416-2425.

Samonds JM, Allison JD, Brown HA, Bonds AB (2004) Cooperative synchronized assemblies enhance orientation discrimination. Proc Natl Acad Sci USA 101:6722-6727.

Schneidman E, Berry MJ, Segev R, Bialek W (2006) Weak pairwise correlations imply strongly correlated network states in a neural population. Nature 440:1007-1012.

Shadlen MN, Newsome WT (1998) The variable discharge of cortical neurons: implications for connectivity, computation, and information coding. J Neurosci 18:3870-3896.

Sherrington CS (1941) Men of His Nature. London: Cambridge University Press.

Sigman M, Cecchi GA, Gilbert CD, Magnasco MO (2001) On a common circle: Natural scenes and Gestalt rules. Proc Natl Acad Sci USA 98:1935-1940.

Singer W (1999) Neuronal synchrony: a versatile code for the definition of relations? Neuron 24:49-65.

Singer W, Gray CM (1995) Visual feature integration and the temporal correlation hypothesis. Annu Rev Neurosci 18:555-586.

Snider RK, Kabara JF, Roig BR, Bonds AB (1998) Burst firing and modulation of functional connectivity in cat striate cortex. J Neurophysiol 80:730-744.

Thiele A, Stoner G (2003) Neuronal synchrony does not correlate with motion coherence in cortical area MT. Nature 421:366-370.

Ts'o DY, Gilbert CD, Wiesel TN (1986) Relationships between horizontal interactions and functional architecture in cat striate cortex as revealed by cross-correlation analysis. J Neurosci 6:1160-1170.

Usrey WM, Reid RC (1999) Synchronous activity in the visual system. Annu Rev Physiol 61:435-456.

Usrey WM, Reppas JB, Reid RC (1998) Paired-spike interactions and synaptic efficacy of retinal inputs to the thalamus. Nature 395:384-387.

von der Malsburg C (1981) The correlation theory of brain function. In. Goettingen, Germany: Max-Planck-Institute for Biophysical Chemistry.

Webster MA, De Valois RL (1985) Relationship between spatial-frequency and orientation tuning of striate-cortex cells. J Opt Soc Am A 2:1124-1132.

CHAPTER III

EXPERIMENTAL METHODS

Data collection

Experimental data in support of the included projects were collected from areas 17 and 18 of seven adult cats (2.0 – 4.0kg). Cats were prepared for electrophysiological recording in accordance with the guidelines by the American Physiology Society and Vanderbilt University's Animal care and Use Committee. Neural signals were recorded with the Utah 10×10 microelectrode array (Figure 3-1, Cyberkinetics Neurotechnology Systems, Inc.). Before recording, the electrode array was inserted into primary visual cortex to a fixed depth of 0.6 mm with the aid of pneumatically-actuated impulse array inserter. The impedance of the electrodes ranges from 50 to 300 kΩ. The Cyberkinetics microelectrode array can provide reliable recordings with quality comparable to that from single-electrode recordings (Kelly et al., 2007). The neural signal amplifier amplifies the signals from each electrode (×5000) and reduces the noise with high-pass and low-pass filters with corner frequencies of 250 Hz and 7.5 kHz. After the amplified and filtered signals were collected by the neural signal processor, signals were further digitized at 30,000 samples/sec/electrode. Real-time neural responses were monitored with neural signal acquisition system user an interface program and activity map viewer program (Figure 3-2).

A

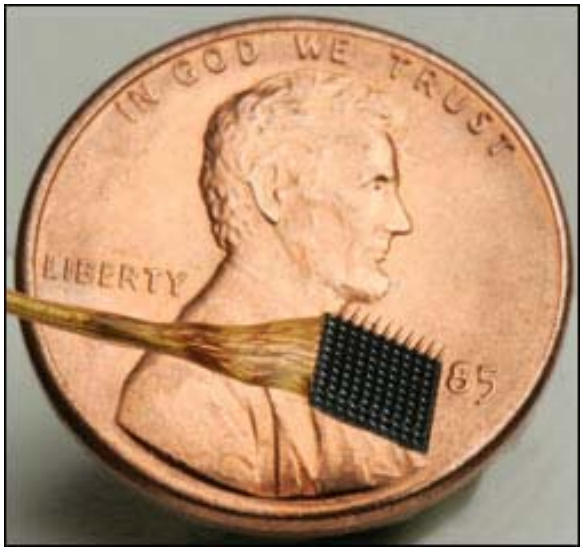

B

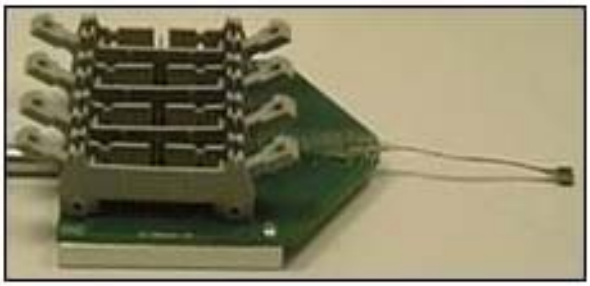

Figure 3-1: Microelectrode array (A) Cyberkinetics array consists of a 4 mm by 4 mm base that contains100 silicon spikes that are 1.0 mm long (B) Acute microelectrode array assembly with IDC connectors.

A

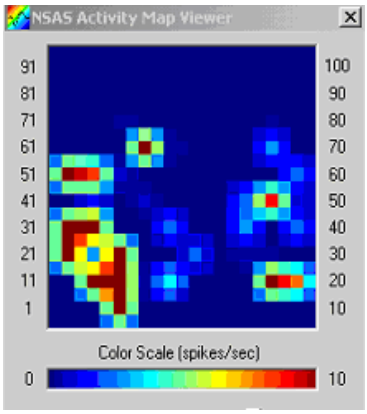

B

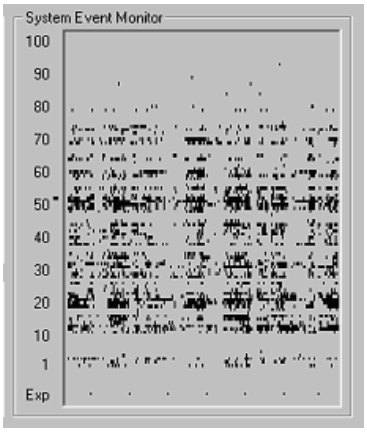

C

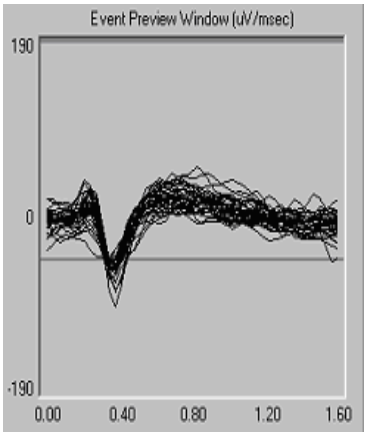

Figure 3-2: Example of recorded neural activity (A) Real-time neural activity viewer. (B) Raster plot of neural signals from 100 electrodes. (C) Neural spikes from one electrode.

Visual stimulation

Two stimulators were used in our projects. The first projected spots or bars of light onto a large tangent screen, and was used for rapid manual characterization of receptive field location and tuning properties. The second was a gamma-corrected SONY 21" graphics display driven either by a Cambridge Research Systems VSG2/3F controller board or a generic video controller using WinVis software package (Neurometrics Institute, CA). Images from monitor were projected into the cat's eyes through a mirror placed in front of animal at a 45^{o} angle, and the distance between image and cat's eyes was set at 57 cm so that 1 cm on the image subtended 1˚ of visual angle. Displays were refreshed at 120 Hz, which avoids entrainment artifact (Wollman and Palmer, 1995) that could be critically disruptive in our measurements. All stimulation loci were referenced to the area centralis, specified by projection of retinal landmarks onto the tangent screen with a reversible ophthalmoscope, and all stimulation was referenced to quantitative maps of receptive field loci. The size and location of the stimulation were chosen to cover the aggregated receptive fields from maximum number of cells that displayed robust tuning responses with stimulation by regular sinusoid gratings presented in a circular aperture (diameter = 18 degrees).

Time domain analysis

We quantify synchrony using the Cross-Correlation Histogram (CCH) derived from the Joint Post-Stimulus Time Histogram (JPSTH), which represents the joint occurrences of spikes from two neural spike trains at all possible time delays (Aertsen et al., 1989; Sillito et al., 1994; Snider et al., 1998; Samonds et al., 2004). The cross-

product of the post-stimulus time histograms (PSTHs) (expected correlation) is subtracted from the raw JPSTH (observed correlation, $\langle x(t_1)y(t_2)\rangle$) (Figure 3-3 A, Equation 3-1) and then normalized by the standard deviation of the PSTH predictor under the null hypothesis that two neurons are firing independently (Figure 3-3 B, Equations 3-2 to 3-4).

$$D_{x,y}(t_1,t_2) = \langle x(t_1)y(t_2)\rangle - \langle x(t_1)\rangle\langle y(t_2)\rangle \tag{3-1}$$

$$C_{x,y}(t_1,t_2) = \frac{D_{x,y}(t_1,t_2)}{\tilde{S}_{x,y}(t_1,t_2)} \tag{3-2}$$

$$\tilde{S}_{x,y}(t_1,t_2) = S_x(t_1)S_y(t_2) = \sqrt{D_{x,x}(t_1,t_1)D_{y,y}(t_2,t_2)} \tag{3-3}$$

$$S_x(t_1) = \sqrt{\frac{1}{K}\sum_{k=1}^{K}\left[x^k(t_1,t_1) - \langle x(t_1,t_1)\rangle\right]^2} = D_{x,x}(t_1,t_1) \tag{3-4}$$

In the above equations, *x* and *y* represents the neurons, *t* represents time bin, and *k* represents the stimulus trial index. The CCH is created by integrating along the principal diagonal of the normalized JPSTH matrix. Aertsen et al. (1989) refer to this CCH as the *normalized cross-correlogram* or *effective connectivity* (Figure 3-3 C). We quantify what we will refer to throughout the thesis as *synchrony* by measuring the 1-ms peak at or near zero in the normalized CCH. We consider synchrony significant when the peak is at least two times the random fluctuations or noise in the CCH (generally 0.1-0.3%).

Like conventional cross-correlation, the JPSTH contains a contribution from stimulus-related modulation of single-neuron firing rates (Perkel et al., 1967; Aertsen et al., 1989). Aerten et al. (1989) used the "residual" result after the cross-product of the PSTHs was subtracted from the "raw" JPSTH to represent the intrinsic neuronal dependencies. Although the cross-product of the PSTHs is conceptually the same as the shift predictor, the methods are distinct from each other and the cross-product provides a

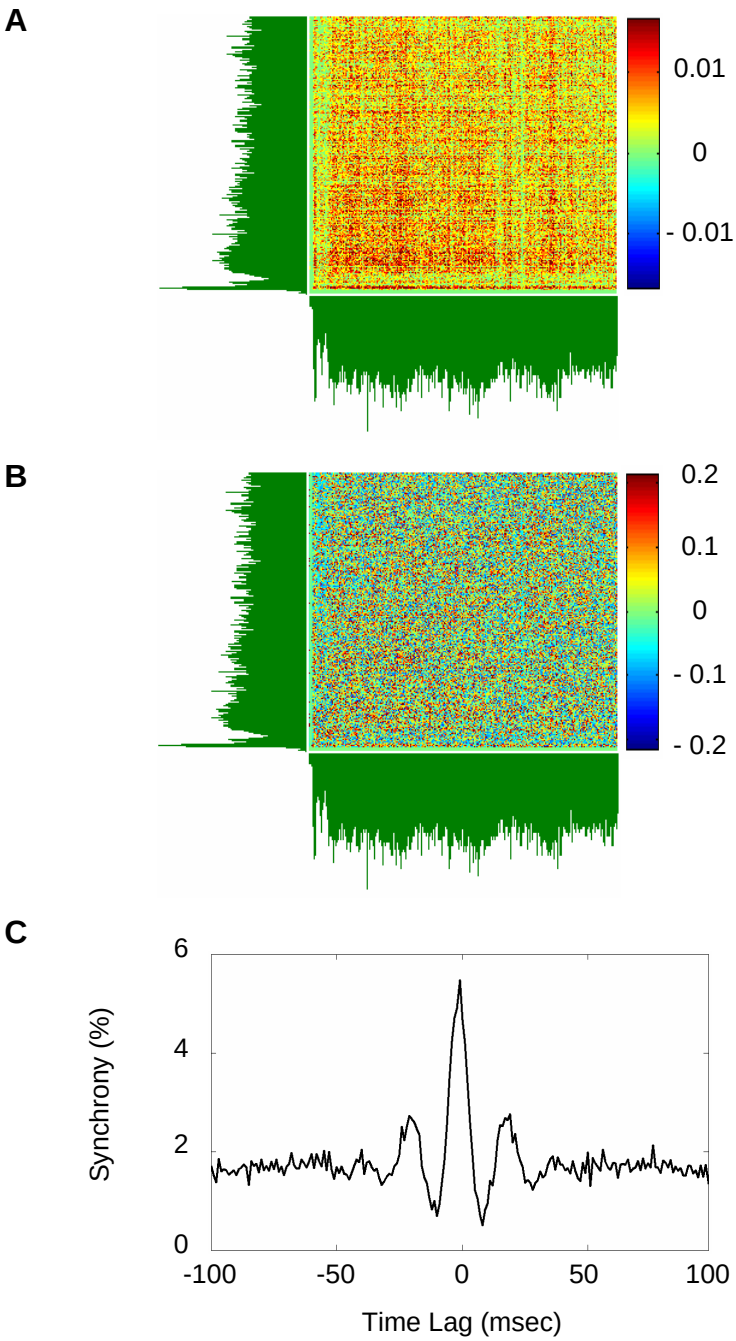

Figure 3-3: Example of JPSTH analysis (A) Raw JPSTH matrix. (B) Normalized JPSTH matrix. (C) Normalized cross-correlation histogram.

much smoother predictor function (Aertsen et al., 1989) since the PSTHs are the results averaged over many trials.

Frequency domain analysis

Besides analyzing correlation between neural spike trains in the time domain with the CCH, coherence analysis offers an alternative means to measure the coherent frequency association between neural signals. Compared with CCH analysis in the time domain, coherence analysis is much less susceptible to nonstationarity in neural responses, which provides an intrinsic normalized estimate. Coherency is calculated by deriving the power spectra ($S_{11}(f)$ and $S_{22}(f)$) and cross spectrum ($S_{12}(f)$) of cell responses with the Fourier transform of spike trains (Equation 3-5) and coherence is defined as the magnitude of coherency (Equation 3-6) since coherency is a complex value (Percival and Walden, 1993; Mitra and Pesaran, 1999; Jarvis and Mitra, 2001).

$$\gamma(f) = \frac{S_{12}(f)}{\sqrt{S_{11}(f)S_{22}(f)}} \tag{3-5}$$

$$C(f) = |\gamma(f)| \tag{3-6}$$

Indices 1 and 2 in Equation 3-5 indicate the two different simultaneously recorded neural spike trains. Spike trains were sampled at a rate of 250 or 500 Hz. To reduce bias of the spectrum estimate, we applied 5 orthogonal Slepian tapers during the windowing procedure of Fourier transform, which is also called multi-taper coherence analysis. We also utilized the jackknife resampling approach to calculate the 95% confidence intervals of the coherence result.

REFERENCES

Aertsen AM, Gerstein GL, Habib MK, Palm G (1989) Dynamics of neuronal firing correlation: modulation of "effective connectivity". J Neurophysiol 61:900-917.

Jarvis MR, Mitra PP (2001) Sampling properties of the spectrum and coherency of sequences of action potentials. Neural Comput 13:717-749.

Kelly RC, Smith MA, Samonds JM, Kohn A, Bonds AB, Movshon JA, Sing Lee T (2007) Comparison of recordings from microelectrode arrays and single electrodes in the visual cortex. J Neurosci 27:261-264.

Mitra PP, Pesaran B (1999) Analysis of dynamic brain imaging data. Biophys J 76:691-708.

Percival DB, Walden AT (1993) Spectral analysis for physical applications, multitaper and conventional univariate techniques: Cambridge University Press.

Perkel DH, Gerstein GL, Moore GP (1967) Neuronal spike trains and stochastic point processes. II. Simultaneous spike trains. Biophys J 7:419–440.

Samonds JM, Allison JD, Brown HA, Bonds AB (2004) Cooperative synchronized assemblies enhance orientation discrimination. Proc Natl Acad Sci USA 101:6722-6727.

Sillito AM, Jones HE, Gerstein GL, West DC (1994) Feature-linked synchronization of thalamic relay cell firing induced by feedback from the visual cortex. Nature 369:479-482.

Snider RK, Kabara JF, Roig BR, Bonds AB (1998) Burst firing and modulation of functional connectivity in cat striate cortex. J Neurophysiol 80:730-744.

Wollman DE, Palmer LA (1995) Phase locking of neuronal responses to the vertical refresh of computer display monitors in cat lateral geniculate nucleus and striate cortex. J Neurosci Methods 60:107-113.

CHAPTER IV

SYNCHRONOUS ACTIVITY IN CAT VISUAL CORTEX ENCODES COLLINEAR AND COCIRCULAR CONTOURS

Jason M. Samonds[*], Zhiyi Zhou[*], Melanie R. Bernard, A. B. Bonds

[*]*These authors contributed equally to this work*

Abstract

We explored how contour information in primary visual cortex might be embedded in the simultaneous activity of multiple cells recorded with a 100-electrode array. Synchronous activity in cat visual cortex was more selective and predictable in discriminating between drifting grating and concentric ring stimuli than changes in firing rate. Synchrony was found even between cells with wholly different orientation preferences when their receptive fields were circularly aligned, and membership in synchronous groups was orientation- and curvature-dependent. The existence of synchrony between cocircular cells reinforces its role as a general mechanism for contour integration and shape detection, as predicted by association field concepts. Our data suggest that cortical synchrony results from common and synchronous input from ealier visual areas and that it could serve to shape extrastriate response selectivity.

Introduction

The primary visual cortex has traditionally been viewed as a network of filters or feature detectors, each sampling localized regions of the visual field (Hubel and Weisel 1962). There remains considerable debate on how features are integrated for object recognition and segmentation. This question becomes especially critical when considering that the firing rate of each cell varies across multiple features (e.g., orientation, spatial frequency, temporal frequency, contrast, context) resulting in ambiguity. One proposed solution is that feature detectors are integrated through synchronous activity (Singer and Gray 1995). Synchronous integration is an intriguing solution because it could also provide an elegant resolution to the binding problem (von der Malsburg 1999; but see also Shadlen and Movshon 1999).

The first experimental evidence for the involvement of synchronous activity in feature integration used coherent collinear stimulation such as drifting light bars (Ts'o et al. 1986; Eckhorn et al. 1988; Gray et al. 1989). The observed synchrony required that pairs of cells had similar orientation preferences and collinear receptive fields (RFs). Collinearity is actually just one special case of the more general property of cocircularity (Parent and Zucker 1989). Cocircular RFs are defined as having orientation preferences with the same angle, but opposite sign, with respect to a line connecting the center of the two RFs—i.e., tangent to the same circle (Parent and Zucker 1989) (Figure 4-1). Cocircularity is a ubiquitous structure in natural scenes (Geisler et al. 2001; Sigman et al. 2001; Elder and Goldberg 2002; see also Chow et al. 2002) and has been proposed as the foundation of contour integration (Field et al. 1993). The framework is known as the *association field,* where the chances of contour segments being part of one continuous

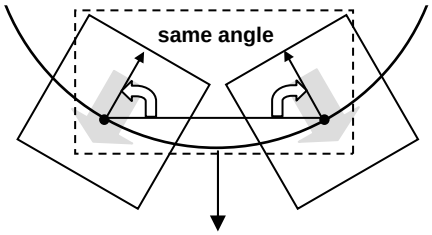

Figure 4-1: Mathematical Definition of Cocircularity: A line passing through the centre of each RF at the preferred orientation must be tangent to the same circle.

contour increase with proximity and similarity in their orientation. Each segment of an integrated contour falls on the same circle as another segment. The idea is that in nature, contours are predominantly linear with a decreasing probability of greater curvature (aligning on progressively smaller circles).

The goal of our current study was to see if synchronous activity predictably exists for cell pairs that differed in orientation preference, but whose receptive fields still followed cocircularity and association field rules. Extending the collinear synchrony results to cocircular RFs in general is necessary if synchrony is to be considered to play some role in integrating complex contours and shapes. We recorded from large groups of cells simultaneously in areas 17 and 18 of anesthetized cats and found that particular subgroups of cells dynamically synchronize depending on the incoming visual information (based on cocircularity). Synchronous activity matched the association field rules and stimulus curvature much more reliably than the average firing rate because synchrony depended primarily on local contour information and was not prone to response ambiguities outside of the local RFs. We conjecture that the integration of global contour information begins with synchronous activity within cell groups in early visual areas such as V1. Extrastriate cortex could then respond to complex shapes and curvature by detecting this synchronous activity.

Materials and Methods

Physiological Preparation and Recording

Experimental procedures were performed under the guidelines of the American Physiological Society and Vanderbilt University's Animal Care and Use Committee and

are described in detail elsewhere (Samonds et al. 2003, 2004; Samonds and Bonds 2005). Two cats were anesthetized with propofol and N_2O and paralyzed with pancuronium bromide. A Bionics (now Cyberkinetics) 10 x 10 multi-electrode array (400-μm spacing) was pneumatically inserted to a fixed depth of 0.6 mm (Figure 4-2). Seventy and 98 channels recorded single-unit or multi-unit activity for each cat, respectively. However, we could not isolate spiking activity with thresholding for all channels due to low signal-to-noise.

Details about the reliability of single-unit recordings with this array and spike sorting procedures can be found in Samonds and Bonds (2005). Here we did not include multiple units that were recorded and resolved from a single channel (i.e., all single units reported in this article are from different electrodes). Spike sorting was used to isolate the most robust single-unit (e.g., see Figure 4-2 B, *right*) and remove noise and artifact on each channel (Shoham et al. 2003). We isolated 28 and 23 single-units that had stable orientation-selective activity driven by drifting sinusoid gratings (Figure 4-2 A and B, respectively). The response to the preferred orientation had to be at least two times that from the worst orientation (orientation tuning was typically robust and narrow). The 51 cells provided 631 pairs of cells, for cross-correlation analysis.

Due to tissue damage caused by removing the array, we were unable to perform histological analysis on the recording sites following recording. However, based on the relationship between electrode positions and Horsley-Clark coordinates and response characteristics, we believe that >92% (47/51 cells) of our sample was in area 17 while the remaining 8% (4 cells) was in area 18 (see Figure 4-2). Based on our estimation, the area 18 cells contributed 9 pairs (<5%) to our sample of synchronous pairs (N = 188 pairs)

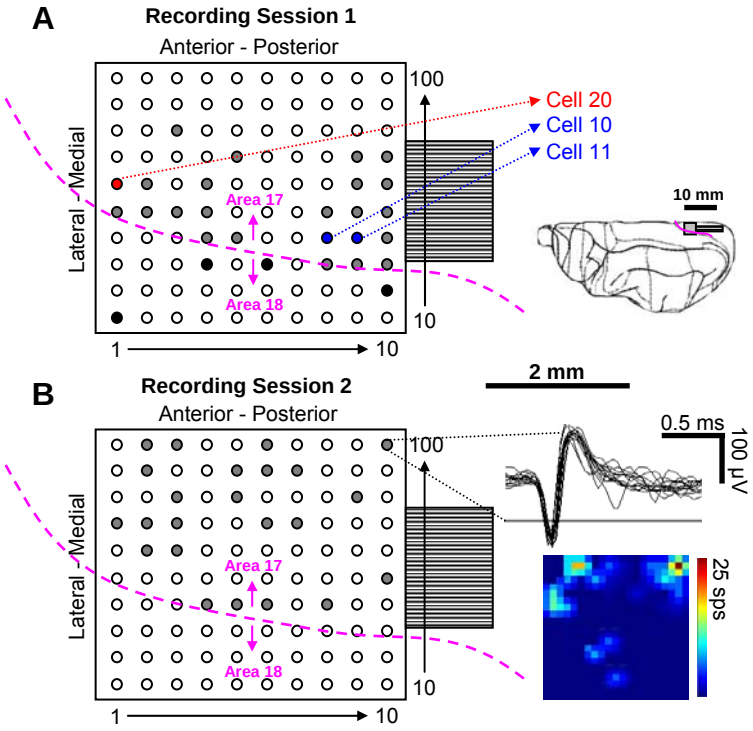

Figure 4-2: Positioning of microelectrode array (A) Layout of microelectrode array with respect to Horsley-Clark coordinates. Magenta line represents estimated border between areas 17 and 18 (see left hemisphere view on the right). Gray dots represent electrodes with reliable single-unit responses (Recording Session 1). Red and blue dots correspond to cells used as representative examples in Figures 8 and 11. (B) Same as (A) for Recording Session 2. Images on the right show examples of spiking activity—waveform (horizontal line: threshold) and instantaneous firing rates.

with all pairs comprised of one area 17 and one area 18 cell. The fixed insertion depth virtually ensures recordings were in superficial layers. The curvature of the brain leads to some variation of electrode depth with a maximum depth of 0.6 mm. This depth combined with the possibility of recording activity a few hundred microns below the electrode leaves only a very small probability of our sample including layer 4 cells. Forty-nine out of the 51 cells were complex (Hubel and Weisel 1962; Skottun et al. 1991) with a mean $F1/F0 = 0.34 \pm 0.03$ ($N = 51$ cells).

Quantifying Synchrony

We quantified synchrony using the "effective connectivity" Cross-Correlation Histogram (CCH) derived from the Joint Post-Stimulus Time Histogram (JPSTH) (Aertsen et al. 1989; see also Sillito et al. 1994; Snider et al. 1998; Samonds et al. 2003; Samonds and Bonds 2005). The cross-product of the post-stimulus time histograms (PSTH) (expected correlation) is subtracted from the JPSTH (observed correlation) and then normalized by the standard deviation of the PSTH predictor (*normalized JPSTH*: equation 9 in Aertsen et al. 1989). We then create a CCH by integrating along the principal diagonal of this two-dimensional matrix (Aertsen et al. 1989). Aertsen et al. (1989) refer to this CCH as the *normalized cross-correlogram* or *effective connectivity*. We represent the magnitude as the percentage of the maximum possible effective connectivity (all spikes correlated; correlation coefficient ranging from -100% to 100%). We quantify what we will refer to throughout the article as *synchrony* by measuring the 1-ms peak at or near zero in the CCH. We considered synchrony significant when the peak was at least two times the random fluctuations or noise in the CCH (0.1-0.3%).

Although the cross-product of the PSTHs is conceptually the same as the shift predictor, the methods are distinct from each other and the cross-product provides a much smoother predictor function (Aertsen et al. 1989). The normalization strategy of the JPSTH was also chosen to contribute as little noise as possible to the cross-correlation estimate (Aertsen et al. 1989). Based on models with known correlation strengths and temporal profiles, Aertsen et al. (1989) found the standard deviation of the PSTH-based predictor (described above) as the best choice for true normalization (due to its relatively small dynamic range; see also Palm et al. 1988; Ito and Tsuji 2000). In addition, the standard deviation of the predictor is equal to the square root of the product (geometric mean) of the auto-covariation histograms and the resulting normalized value is equivalent to Pearson's correlation. We find that with this normalization procedure, there is only a weak relationship between synchrony and firing rate ($r^2 = 0.13$ for sum of rates and $r^2 = 0.16$ for product of rates; see also Fig. 13 in Samonds and Bonds, 2005).

The second concern with any cross-correlation method is that fast correlations (10's of ms) may not necessarily represent true connectivity-based (anatomic) correlation. Brody (1998, 1999a,b) has shown that long-term (10's of seconds) or trial-by-trial covariation of firing rates, covariation of response latency, and covariation of excitability can produce what might be easily interpreted as correlated activity resulting from anatomical connections (short-term correlations) (however see also Kirkland et al. 2000). We explicitly chose the relatively vague and benign term *synchrony* for this very reason. Correlation and connectivity both implicitly suggest knowledge of the underlying causes for the observed firing rate statistics. What is not debatable is that the Aertsen et al. (1989) measurement describes the deviation of the activity from independence (Brody

1998, 1999a,b; Ito and Tsuji 2000). Although deciphering the origins of this deviation is important, we are at present primarily interested in describing the stimulus-dependence and dynamic behavior of the synchrony. For more recent progress on these topics, see Gerstein and Kirkland (2001) and Kass et al. (2005). We see very little covariation or correlation among the trial-by-trial firing rates ($r^2 << 0.1$ and always $<< 0.3$) and there are not clear relationships between PSTHs and CCHs. There is some weak broad correlation (beyond ±100 ms) observed that is likely caused by common inhibitory input (Moore et al. 1970; Ts'o et al. 1986).

Visual Stimulation

We tested responses to coherent cocircular stimulation using drifting sinusoidal concentric rings (Figure 4-3 A). The rings drifted outwards and were presented within a 16º circular aperture on a mean luminance background. The center locations were strategically chosen based on RF loci of the population to test conditions that would bias predicted synchrony between cells with clear orientation preference differences (>30º) (see Figure 4-3 C and D). However, each experiment included hundreds of pairs of cells, most requiring a unique ring origin, so 9-16 locations were chosen to test as many pairs as possible in an individual experiment. Our approach was highly probabilistic. Even though there were large numbers of cell pairs, it was not axiomatic that every cell pair would demonstrate constructive interactions, so stimuli had to be optimized for the population to maximize our yield of data that could be analyzed in detail. Pair-by-pair testing for 631 pairs of cells is not possible with our preparation in just two recording sessions. We chose concentric rings because this stimulus is very efficient since it

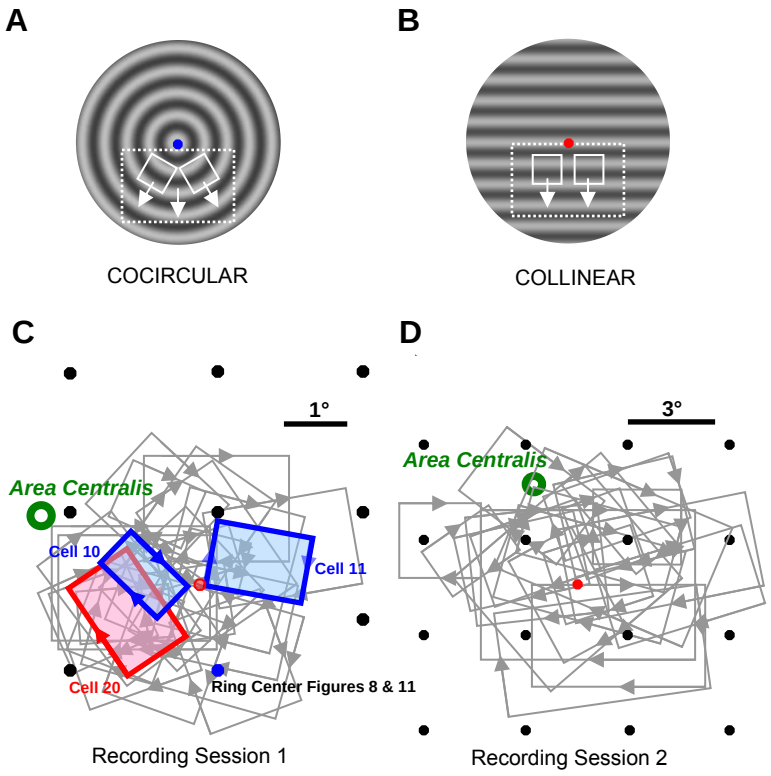

Figure 4-3: Visual stimuli and aggregated receptive fields (A) Drifting concentric rings were used for optimal stimulation of pairs with differing orientation preferences and co-circular RFs. (B) Drifting gratings were used for optimal collinear stimulation. (C) RF plots for Recording Session 1. Black dots represent centre locations of rings stimuli (blue dot for examples in Figures 4-8 and 4-11). Red dot is the center location of the gratings stimuli. Highlighted RFs correspond to examples in Figures 4-8 and 4-11. (D) Same as (C) for Recording Session 2.

minimizes trials by testing for varying curvature and cocircular relationships at multiple locations simultaneously. This strategy allowed us to synchronize 51 pairs of cells with differences in orientation preference ranging from 10-80º during the two experiments with rings stimulation

We used drifting sinusoidal gratings to test responses to coherent collinear stimulation (Figure 4-3 B). The orientation and direction were varied in 10º increments over all possible orientations and directions, while all other grating parameters were fixed (spatial frequency = 0.5 c/deg, temporal frequency = 2.0 Hz, contrast = 50%). All properties except orientation were the same for cocircular and collinear stimulation.

Linear and circular gratings on a mean luminance background provided the strongest responses, enhancing reliable estimation of response properties. Based on psychophysical considerations, we predicted that the rings and gratings offered the greatest chance of revealing the underlying mechanisms of contour integration because their contours are parallel (Polat and Norcia 1998; Polat and Tyler 1999; Geisler et al. 2001; Alais and Lorenceau 2002; however see Solomon and Morgan 2000), circular (Field et al. 1993; Pizlo et al. 1997; Pettet et al. 1998; Pettet 1999; Geisler et al. 2001; Alais and Lorenceau 2002), and are enclosed (Kovács and Julesz 1993; Pettet et al. 1998). We were interested in clearly revealing the dynamics of response properties from collinear to curvilinear stimulation. We did not explore segmented contours or contours embedded within noisy elements because we wanted to maximize our chances of contour integration among a variety of cells. We believe it is important to extend our results to some of the psychophysics tests such as segmented contours, but because the segmented contours are still detected and grouped together, they do not really provide a definitive

test for contour integration (the psychophysics results suggest the response properties or synchrony would simply deteriorate: Pizlo et al. 1997; Alais and Lorenceau 2002; Beaudot and Mullen 2003; see also corresponding neurophysiologic data: Gray et al. 1989; Kapadia et al. 1995).

Selection Criteria

A total of 127 out of a possible 631 pairs of cells were chosen for cocircularity analysis based on responsiveness and the spatial relationship between the RFs and the stimulus (Figure 4-4). In addition to requiring that each cell had orientation tuning (described above), we required that the pair of cells responded with a total average firing rate of at least 5 sps for either gratings or rings *and* had significant synchrony (see above) for one of the two stimulus conditions. Our detailed analysis (Figures 4-8, 4-9, 4-12) on only a limited portion of our entire dataset was important to ensure that we made direct comparisons between the two stimulus conditions and direct reliable comparisons between the two measured response properties. At least with respect to firing rates, this smaller sample was not significantly different from the entire sample ($p > 0.38$).

We used bars of light rear-projected onto a large tangent screen to estimate RF sizes (mean = 3.9 ± 0.2°) and locations (Figure 4-3 C and D). Receptive fields of cells in a pair had to have minimal overlap so that stimulus-response predictions were unambiguous. The mean RF overlap for each cell for pairs of cells with unambiguous RF relationships was 35.0 ± 1.8%. Firing rate and synchrony measurements were made for the rings and gratings that provided the best match with the preferred orientation of *both* cells. In order to make predictions about which stimulus would lead to a greater

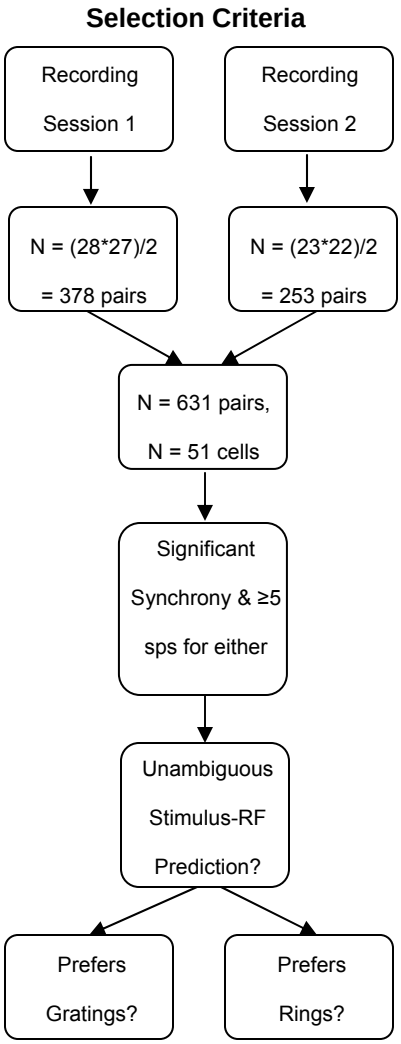

Figure 4-4: Flow diagram of the selection procedure for various stages of analysis.

response, it had to be clear whether the segment of the rings or the gratings passing through the two respective RFs was closer to the preferred orientation for *both* cells. Therefore, the quantitative criterion for the classes was that the corresponding rings or gratings contour had to match the RF orientations better than the complementary stimulus by ≥10º (because we used 10º increments). For example, rings would drive a pair of cells with a >40º difference in orientation preference better than gratings only if the ring segments are within ±20º of the preferred orientation for both cells. This criterion for both cells is impossible with larger amounts of receptive overlap—hence the ambiguity. Additionally, pairs of cells that were not aligned with the rings (because a limited number of locations were tested) were also not included because we could not make a direct comparison with the gratings condition.

Cocircularity Analysis

For each pair of cells, we calculated the ratio (*RPI, Rings Preference Index*) for both the total average firing rate and synchrony for rings (*R*) versus gratings (*G*) (the optimal rings and gratings):

$$RPI = \frac{R - G}{R + G} \qquad (4\text{-}1)$$

We specify this ratio as RPI_f when it is calculated on the basis of firing rate and RPI_s when it is calculated on the basis of synchrony. We used a standard sigmoid model fit for *RPI* versus the orientation preference difference between the cell pair (which we term *cocircularity*) *x* to see how well the synchrony or total average firing rate varied with cocircularity on a pair-by-pair basis:

$$RPI(x) = \frac{A}{1 + e^{B(x_0 - x)}} \quad (4\text{-}2)$$

We used a standard Gaussian model fit for our synchrony and firing rate measurements for grating stimulation, where *x* is cocircularity and *f(x)* is the total average firing rate or synchrony:

$$f(x) = Ae^{-B(x-x_0)^2} \quad (4\text{-}3)$$

The Gaussian fit was chosen because the total average firing rate and synchrony should decline with collinear gratings with increasing or decreasing cocircularity (i.e., both are absolute increases in the orientation preference difference). We used the sigmoid fit (equation 4-2) for synchrony and firing rate measurements for rings stimulation because the total average firing rate and synchrony should decline only for decreasing cocircularity. The models were otherwise arbitrarily chosen simply to show how much the variance of the total average firing rate and synchrony was related to stimulus-RF relationships (i.e., cocircularity) with regression analysis. The difference between R^2 measurements for total average firing rate and synchrony are more important than the absolute R^2 values, which are likely to be degraded by both response properties being dependent on additional spatiotemporal stimulus properties beyond contour/orientation information (e.g., spatial frequency, temporal frequency), which were not optimized for each pair of cells. Confidence intervals were calculated by bootstrapping pairs (Efron and Tibshirani 1993).

Results

In order to provide an adequate sample of cells with a variety of cocircular RF relationships, we recorded simultaneously, with 100-electrode arrays, from 28 and 23

cells in striate cortex of two cats, providing a total of 51 cells and 631 pairs of cells (see Figure 4-2). We tested responses to coherent cocircular stimulation using drifting sinusoid concentric rings (Figure 4-3 A) and tested responses to coherent collinear stimulation using drifting sinusoid gratings (Figure 4-3 B). Nine to sixteen locations in the visual field were strategically chosen for the ring centers in order to match the ring contours to the preferred orientations of pairs of cells with obvious differences in preferred orientation (see Figure 4-3 C and D). For gratings, orientations were varied in 10º increments over a range of 360°. All other stimulus properties were the same for both rings and gratings. Our stimulation paradigm produces data with a distribution that tends to be bimodal rather than continuous with respect to stimulus feature space. This allows us to show significant differences among the distributions. We chose this strategy because the physiological data would not be reliable enough to make significant parametric comparisons to psychophysical (access to all cells) and natural scene (very large databases) statistical distributions with respect to association field concepts.

Synchrony was quantified as the peak height of the rate-normalized cross-correlogram (Aertsen et al. 1989), with the quantity expressed as the percentage of the maximum possible synchrony (i.e., percent correlation; ranging from -100 to 100%). Peak widths were consistent (~10 ms width) so area under the peak provides qualitatively similar results. All of our pairs were recorded in the same layer (600 μm, putatively II-III) and thus would have some chance of integration at the next stage of visual processing. An evaluation of the utility of synchrony in propagating information requires that it be compared against some other mechanism. Here we compare it against the firing rate, which is the usual metric for neural signaling. There are however two different

ways of quantifying the firing rate of cell pairs, depending on the time constants of the recipient cell layer. If the time constant is reasonably long, then the firing rate is simply integrated without regard to temporal structure, and its effectiveness can be modelled by adding the average firing rate of the two cells. If the time constant is short, then only coincident spikes are effective. The probability of coincident spikes is simply equal to the product of the probabilities of each cell firing within the time constant interval, so the receiving layer acts as an effective multiplier of firing rates. Both mechanisms may be represented at different times, in that time constants are dynamic and dependent on the activity of the cell (e.g., Azouz and Gray 2003). In this paper we chose to analyze firing rate on the basis of the sum, because it provides a test of the relative effectiveness of two different processing strategies. We have also performed similar analyses using the product metric and found that the results remain qualitatively unchanged with regard to the relationships between contour information and firing rates. Our synchrony measurements are only weakly related to both the sum and product of the firing rates (see *Materials and Methods*) and provide an additional critical dimension to encode visual information.

We first examine our data with a broad perspective to see how firing rate and synchrony match the predictions made by the association field theory. We then take a closer look at the data by characterizing the RF properties. We use these properties to make predictions on how pairs of cells will respond to gratings and rings stimulation (i.e., varying degrees of curvature). We then test these predictions first very generally based on population statistics and rings and gratings stimuli. Next we systematically test these predictions on a pair-by-pair basis with respect to the degree of curvature. Finally, we

examine cross-correlation properties to gain insight into the possible underlying mechanisms of synchronous integration of contour information.

Visual Cortical Pairs and Association Field Predictions

Collinear contours exceed cocircular contours in natural scenes (Geisler et al. 2001; Sigman et al. 2001) and collinear contours are more easily detected psychophysically than curvilinear contours (Field et al. 1993; Polat and Sagi 1994; Pizlo et al. 1997; Pettet et al. 1998; Pettet 1999; Geisler et al. 2001; Beaudot and Mullen 2001). This is consistent with one of the primary rules of the association field theory—segments are less likely to be part of the same contour with greater differences in their orientations (i.e., greater curvature) (Field et al. 1993; Polat and Sagi 1994; Geisler et al. 2001; Sigman et al. 2001; Elder and Goldberg 2002). A second rule is that segments are less likely to be integrated with increasing distance between them. Cortical organization should reflect these principles in two ways: (1) Orientation tuned cells are connected when their RFs have cocircular alignment and (2) The number of connections decreases with increasing RF distance and increasing difference in orientation preference. Anatomical evidence tends to support these concepts (Malach et al. 1993; Bosking et al. 1997; Lund et al. 2003). Overall we would therefore predict enhanced activity (firing rate and/or synchrony) for drifting sinusoid gratings versus drifting concentric sinusoid rings.

Analysis of the firing rate suggests that there is not a clear preference for linear contours versus curved contours within our sample. The greatest average firing rate for each cell was chosen across 36 orientations (10° increments) for gratings and 16 center locations for rings. For $N = 51$ single cells and 631 pairs, the average firing rate is nearly

the same for gratings and rings—13.7 ± 1.9 sps versus 16.2 ± 2.0 sps (*t*-test; $p>0.18$) for the two stimuli, respectively. We would expect to underestimate the activity from rings because we tested a relatively limited number of ring locations and were therefore unable to match the preferred orientations and directions for the entire population. We were however able to match the preferred orientation and direction for all 51 cells with gratings. Therefore, overall the firing rate alone is inconsistent with the psychophysical data and discourages the notion of an association field organization in primary visual cortex.

Synchrony conversely does appear to show an overall preference for gratings over rings as the behavioral tests suggest. When we include all pairs of cells ($N = 47$ cells and 188 pairs) that showed significant synchrony (a central peak that was at least two times the random fluctuation in the CCH), the preference for gratings is substantial: gratings (collinear) = 0.90 ± 0.06% versus rings (curvilinear) = 0.36 ± 0.04% (*t*-test; $p<1.3\times10^{-12}$). If we examine only pairs of cells with RFs aligned with the rings contour orientation and direction ($N = 47$ cells and 127 pairs), the average synchrony for gratings (0.66 ± 0.04%) is still significantly (*t*-test; $p<5.0\times10^{-6}$) greater than that found for rings (0.40 ± 0.04%). For the same 47 cells, there is still no significant difference in the average firing rate between gratings and rings—14.5 ± 2.0 sps vs. 17.0 ± 2.1 sps (*t*-test; $p>0.19$).

The probability of observing synchrony for a given pair of cells also matches the orientation rule of the association field theory (Figure 4-5, *left*). If the pair of cells has orientation preferences within 30º (N = 185 pairs), the probability of measuring significant synchrony is 80.0% (see also Ts'o et al. 1986; Gray et al. 1989; Samonds et al. 2004). If the pair of cells has orientation preference differences greater than 30º, their

RFs are cocircular (e.g., Figure 4-1), and the pair was tested with an appropriately aligned ring stimulus (N = 76 pairs), the probability is reduced to 50.0%. Our data are insufficient to explore systematically the relationship between probability of synchrony and orientation preference difference, but clearly the trend matches the prediction. Overall, the change in strength in synchrony and the probability of observing synchrony appear to depend strongly on the relationship of orientation preference between pairs of cells in visual cortex that is consistent with the predictions of the association field model.

Our synchrony data do not at first glance appear to support the proximity rule of association field theory. Across all synchronous pairs (N = 188) the greatest synchrony found for gratings or rings did not covary with respect to average RF overlap or maximum RF overlap (e.g., 100% when the RF of one cell is completely within the RF of the other cell): $r^2 = 0.01$ for both measurements.

However, this might be attributed to including only pairs of cells with significant synchrony. Pairs of cells without significant synchrony would essentially have synchrony measurements of zero or near zero. If these pairs tend to have greater distance between their RFs, then the trend with respect to proximity would be stronger. Therefore, the proximity rule might be more apparent by measuring the probability of observing synchrony based on RF overlap. Figure 4-5 (*right*) illustrates the probability of observing synchrony for three subpopulations of pairs based on average RF overlap (<25%, 25-50%, >50%). For pairs of cells with orientation preferences within 30º (collinear), we do not find any difference among the three groups (all are ~80%). For cocircular pairs (with orientation preferences >30º), the probability of observing

synchrony increases with increasing proximity (29.2% to 55.6% to 64.0%) matching the association field prediction.

For any given orientation preference difference, the association field model predicts decreasing probability of integration with respect to distance between segments. The results above show this to be true for the probability of synchrony only for cells with >30º differences in preferred orientation. In order to see if there still might be some support for the proximity rule for orientation preference differences ≤30º, we measured the strength of synchrony with respect to average and maximum RF overlap for the orientation preference difference with both the strongest and most reliable synchrony measurements. Pairs of cells with orientation preferences within ±10° of each other (N = 64 pairs) should have significant synchrony across the entire spectrum of proximity. Even for these pairs, however, the relationship between the strength of synchrony and greater RF proximity (defined as average and maximum RF overlap) is still rather weak (r^2 = 0.13 and 0.14; Figure 4-6 A and B, respectively).

Although we did not find a clear general relationship between synchrony and proximity for probability of observation or magnitude, the trends we did observe were in the right direction. This weak proximity relationship and the progression to larger RFs from striate to extrastriate cortex might suggest that contour integration needs to extend beyond V1.

Classification Based on RF Organization

In the next three sections, we take a closer look at RF relationships and their connection to stimulus contour to characterize how these interactions shape firing rate and

synchrony. Based on the relationship between the RF locations and orientation preferences for each cell pair, we classified pairs *a priori* either as *Prefers Rings (PR)* or *Prefers Gratings (PG)*. PR pairs of cells had cocircular RFs (Figure 4-1) so they were predicted to have greater activity for drifting concentric rings versus drifting collinear gratings (Figure 4-7 A). Concentric rings, if properly centered, can present the preferred orientations for both cells simultaneously. Gratings would present intermediate non-optimal orientations for one or both cells.

We predicted that gratings would drive PG pairs of cells better than rings because they either had collinear RFs (Figure 4-7 B) or cocircular RFs with curvature opposite to that (Figure 4-7 C) of the rings stimulus. Collinear pairs are both driven by the same (preferred) orientation with the grating. While the example pair shown in Figure 4-7 C is driven by non-optimal grating orientations; with rings of the opposite curvature, orientations are yet more non-optimal (e.g., orthogonal).

Many cell pairs were unsuitable for this analysis. When RFs have excessive overlap, PG/PR classification is ambiguous (Figure 4-7 D). Additionally, the most appropriate center location for the rings could not be chosen for each of the 631 pairs—nearly all require a unique location. Because recording time was limited, we chose a limited number of ring centers (see Figure 4-3 C and D) selected to maximize our yield of data with an adequate number of samples (100-200 stimulus repetitions). A large portion (81%) of the 631 pairs of cells recorded with the 100-electrode arrays were disqualified for at least one of these two reasons, and these pairs were not subjected to further analysis (see selection criteria details in *Materials and Methods*).

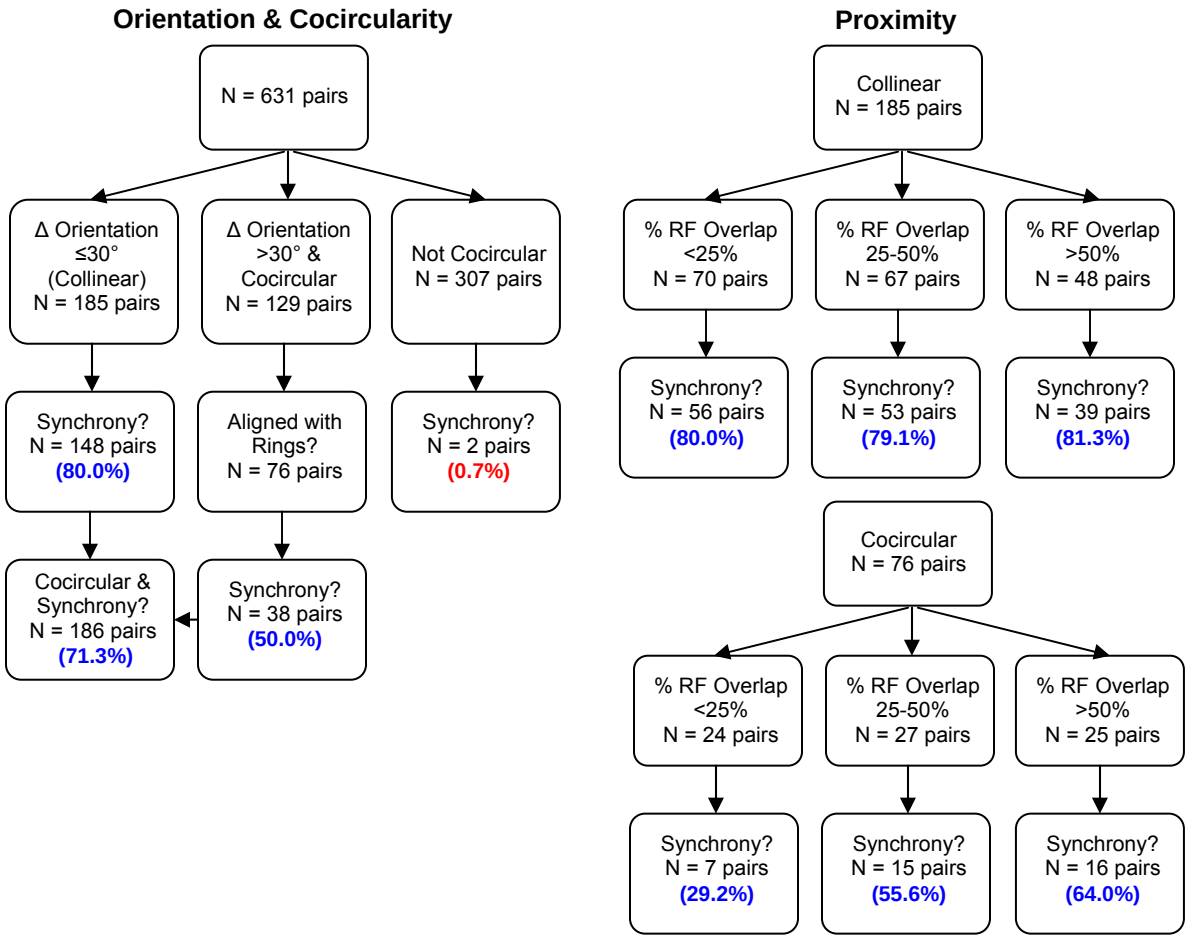

Figure 4-5: *Left*: Probability calculations of observing synchrony based on the orientation preference of cells. *Right*: Probability calculations of observing synchrony based on the RF overlap of cells (proximity).

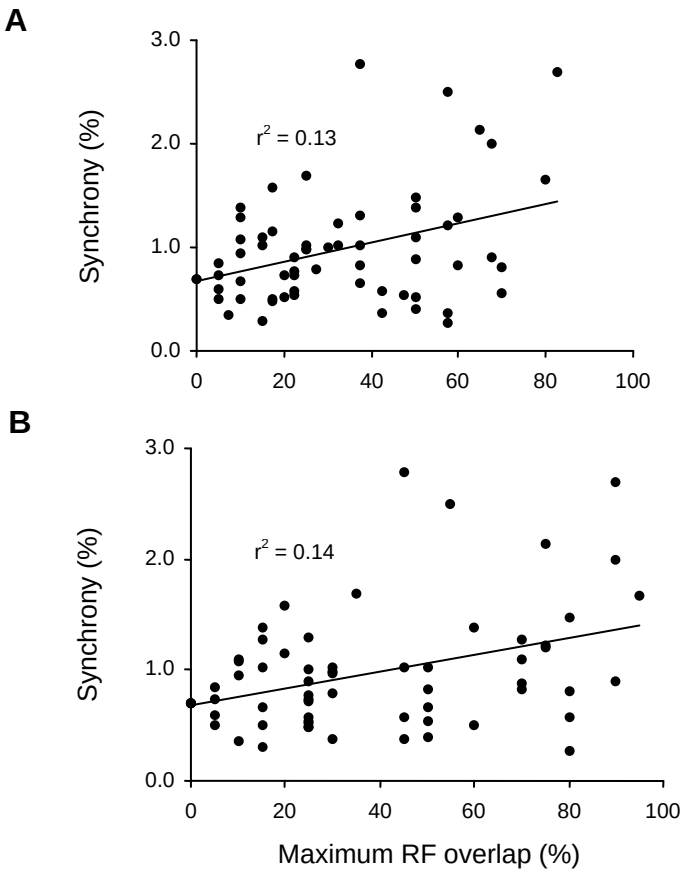

Figure 4-6: Relationship between Synchrony and Proximity (A) Scatter plot of synchrony versus average RF overlap for pairs of cells with orientation preferences with ±10° of each other (N = 64 pairs). (B) Same as (A) using the maximum RF overlap of one cell with respect to the other in each pair.

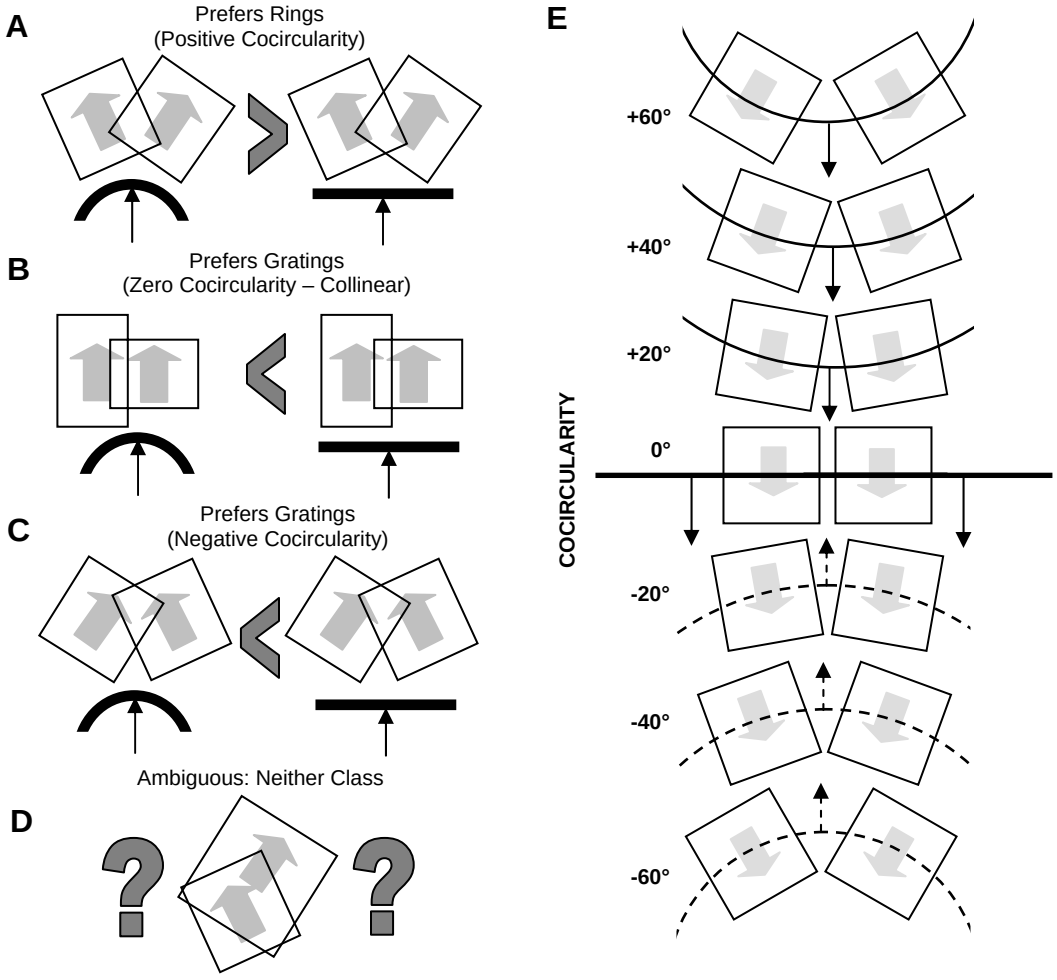

Figure 4-7: Stimulus-RF Classification (A) Prefers Rings (PR): The activity should be greater for a curve versus a line passing through both RFs. (B) Prefers Gratings (PG), Collinear: The activity should be greater for a line versus a curve passing through both RFs. (C) PG, Negative Cocircularity: Again, the activity should be greater for a line versus a curve because the RFs are oriented for the opposite curvature. (D) Ambiguous: Determining whether a line or curve passing through the RFs will cause greater activation is not possible. (E) Cocircularity Coordinate System: Pairs of cocircular and collinear RFs are assigned a cocircularity value, which is the difference in preferred orientation for the two cells. The RFs progressively prefer the curves of the concentric rings versus the lines of the gratings as you move up the coordinate system. The lower portion of the coordinate system is assigned negative cocircularity because the RFs prefer the opposite curvature of the rings stimulus (dashed curve) or an inward direction of motion.

The remaining sample that we analyze in detail seems representative of our entire population. First, this sample includes 47 of the 51 total cells and the overall firing rates of the two samples are not significantly different (*t*-test; $p>0.38$ and $p>0.39$ for gratings and rings, respectively). Second, the fact that we limit our analysis to pairs with significant synchrony does not lead to a small unique sample of cells. If this were true, we might deceptively imply a more dramatic role for synchrony in contour integration merely because we were seeking out synchronous pairs. In fact, choosing synchrony as a selection criterion is nearly the same as explicitly choosing cocircular RF relationships. As shown above (see Figure 4-5), 71.3% of cocircular (which includes collinear) pairs (N = 186 of 261 pairs) have significant synchrony in one of the two stimulus conditions when appropriately matched with the stimulus (<30% of the sample produces false negatives). We measured significant synchrony in 0.7% of the pairs (N = 2 of 307 pairs) that did not have any clear cocircular RF relationships (<1% of the sample produces false positives).

Each pair of cells that was classified as either PR or PG was assigned a *cocircularity* value (measured in degrees) calculated as the *difference between the cells' orientation preferences*. Cocircularity should not be confused with the definition *cocircular* described in Figure 4-1. All 127 pairs in this population are implicitly cocircular because they are aligned with the rings or gratings stimulus. Cocircularity simply characterizes the degree of curvature for each cocircular pair. Cocircularity was negative for the curvatures opposite those of the stimulus. Greater cocircularity for a cell pair predicts a better match between their RF properties and the rings stimulus (as

opposed to the grating stimulus), provided the location of the rings center was appropriate (Figure 4-7 E). Dashed lines represent the opposite curvature of the rings stimulation.

Do the Response Properties for PR and PG Pairs Match Our Predictions?

We measured the response of cell pairs to rings and to gratings with an orientation that best matched the preferred orientations of the two cells. We would predict (Figure 4-7) that the response for PR pairs should be maximized with rings and the response for PG pairs should be maximized with gratings. Figure 4-8 A-C shows the synchrony and firing rate statistics for PR pairs of cells. For this group, the rings nearly doubled the synchrony found with gratings (Figure 4-8 A). As expected, the total average firing rate for this group is also greater for rings versus gratings (Figure 4-8 C).

Figure 4-8 B shows two cells with an 80º difference in preferred orientation that synchronize for rings and do not synchronize for gratings. In this case, the absence of synchrony for gratings is unsurprising because with a linear grating at the orientation midway between the cells' preferences, the cells are barely being driven (total average firing rate 4.9 sps). However, synchrony between two cells with discrete RFs and a difference in orientation preference of 80º is surprising. Synchrony has traditionally been viewed as strictly orientation dependent (Ts'o et al. 1986; Eckhorn et al. 1988; Gray et al. 1989). Counterexamples are sparse, with only Das and Gilbert (1999) measuring predictable significant synchrony between cells with differing orientation preferences and discrete RFs for T-junction and corner configurations. Castelo-Branco et al. (2000) also found synchrony among cells with differing orientation preferences in areas 18 and PMLS when stimulated by plaid patterns.

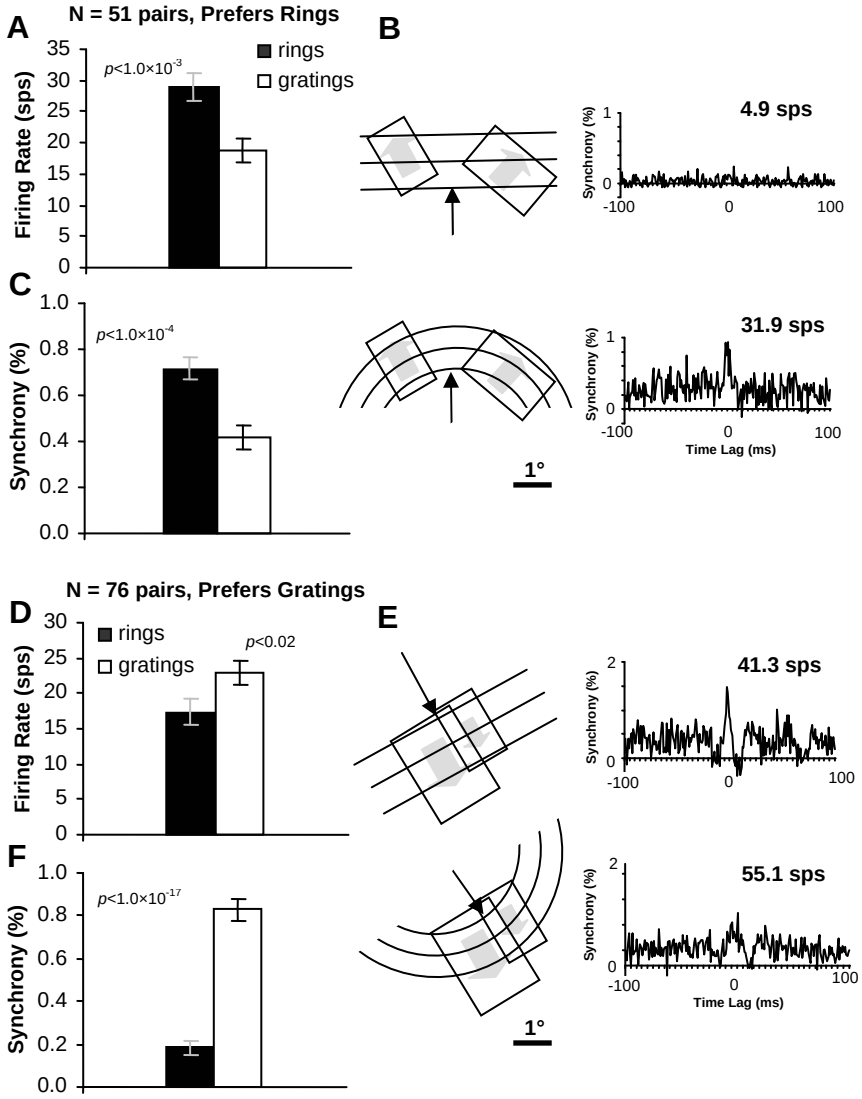

Figure 4-8: Activity of PR Pairs vs. PG Pairs (A-C) PR pairs of cells. (A) Average synchrony for 51 PR pairs for rings and gratings stimuli (standard error bars). (B) Cross-correlation histograms for a cocircular pair of cells driven by gratings (*above*) and rings (*below*). (C) Average total firing rate for same data described in (A). (D-F) PG pairs of cells. (D) Average synchrony for 76 PG pairs for rings and gratings stimuli. (E) Cross-correlation histograms for a collinear pair of cells driven by gratings (*above*) and rings (*below*). (F) Average total firing rate for same data described in (D).

The synchrony and firing rate statistics for pairs of cells classified as PG (Figure 4-8 D-F) show a pattern complementary to that found with PR pairs. Drifting concentric rings are less effective than drifting gratings at synchronizing these pairs (as predicted). Overall, for PG pairs of cells, synchrony from rings was about a quarter that found with gratings (Figure 4-8 D). The total average firing rate also decreased for rings versus gratings (Figure 4-8 F), but considerably less than the change in synchrony (Figure 4-8 D). Figure 4-8 E shows two cells with the same preferred orientation that generate more synchronization for gratings than for rings. This occurred despite a decrease in the total average firing rate of these two cells from 55.1 sps for rings to 41.3 sps for gratings (contradicting the prediction based on RF organization and orientation preferences).

Classification Based on Responses

Figure 4-8 suggests that synchrony and firing rate provide essentially the same contour information, but that synchrony does so more robustly (Figure 4-8 A vs. C and Figure 4-8 D vs F). That alone is not very surprising and it is consistent with past results showing that the spatial acuity (orientation tuning) of synchrony is narrower than that of firing rate (Snider et al. 1998; Frien et al. 2000; Samonds et al. 2003, 2004). The averaged results also suggest that local orientation filtering extends to multiple cells in a straightforward manner.

However, the response difference between rings and gratings contradicting the prediction based on RFs demonstrated in Figure 4-8 E was not an isolated case, which we will demonstrate in this section. Even though the average statistics across the population of cell pairs imply that synchrony and firing rate provide essentially the same

information, on a pair-by-pair basis the total average firing rate failed much more often than synchrony in tests of PR and PG predictions. The firing rates of the two cells did not predictably reflect the relationship between the orientations displayed in their RFs and their orientation preferences. Responses to rings were generally higher than responses to gratings despite the latter having a much better match with the orientation tuning of both cells.

In order to assess the reliability of a given coding scheme, we reclassified each pair of cells as either PR or PG on the basis of either synchrony or total average firing rate (as opposed to RF structure) and compared the results to our original classification described in Figure 4-7. For example, if grating stimulation yielded greater synchrony than ring stimulation, we classified pairs as PG, and vice versa. The classification errors can then be used to calculate transmitted information (Victor and Purpura 1996). With this simple strategy, synchrony provided 0.40 bits of information while the total average firing rate provided only 0.13 bits of information (the most information possible is one bit). Confidence intervals and bias for the information measurements were estimated with the bootstrap method (Efron and Tibshirani 1993) and the difference between synchrony and firing rate information was significant (α<0.005).

Figure 4-9 shows pair-by-pair results for the response-based (Figure 4-9 A, synchrony; Figure 4-9 B, firing rate) classification described above. The data for each pair of cells is plotted as the *rings preference index RPI* (see *Materials and Methods* for details), which ranges from -1 to 1 and represents the difference in synchrony (for RPI_s, Figure 4-9 A) or firing rate (for RPI_f, Figure 4-9 B) for rings versus gratings divided by the sum of the synchrony or firing rate, respectively (equation 4-1). RPI should vary

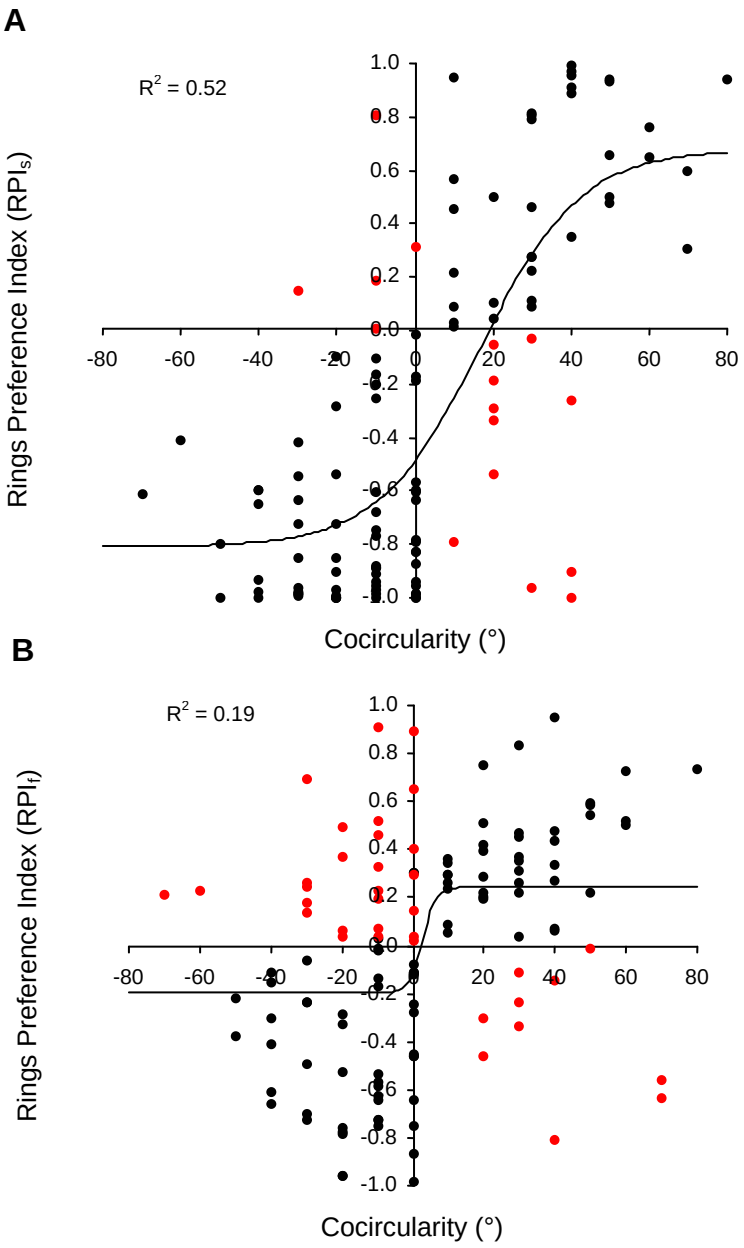

Figure 4-9: Rings Preference Index (RPI) vs. Cocircularity (A) The gain in synchrony (RPI_s, equation 2) for rings stimulation with respect to gratings stimulation (red points contradict the prediction based on RF organization). (B) The gain in the total average firing rate (RPI_f, equation 2) for rings stimulation with respect to gratings stimulation.

from -1 to 1 with respect to cocircularity (which represents the preference for rings stimulation based on RF relationships). There should also be a slight positive bias for RPI with respect to cocircularity (rightward shift) because zero cocircularity has a preference for gratings stimulation. Red data points in Figure 4-9 represent classification errors—i.e., when the response behavior did not match the prediction based on the RF properties. The total average firing rate clearly resulted in more classification errors (more red data points) than the synchrony as illustrated above with the information measurements.

Figure 4-9 also shows whether RPI varied systematically with cocircularity. One would predict a direct dependence between the two quantities, since both quantities are related to the degree of stimulus curvature. The data points should cluster in the lower-left and upper-right quadrants, approaching -1 and 1 in the two quadrants with decreasing and increasing cocircularity, respectively. Again, by comparing Figure 4-9 A with Figure 4-9 B, the synchrony clearly outperforms the total average firing rate on a pair-by-pair basis. The data points cluster in the appropriate quadrants in Figure 4-9 A while the data points appear to be equally scattered around the origin in Figure 4-9 B. Regression analysis of a sigmoid fit confirms that the synchrony varies systematically with the cocircularity more reliably than the total average firing rate ($R^2 = 0.52$ versus $R^2 = 0.19$; $\alpha<0.001$). The best-fit sigmoid for synchrony also matches the expected RP-cocircularity relationship (described above) much better than the fit for the total average firing rate. However, both functions at least show the slight positive bias with respect to cocircularity.

Converging and Diverging Inputs?

Even though there was only a slight dependence on RF overlap, we wanted to take a closer look at common input as a possible source of our synchrony. The average receptive field overlap for the entire population with significant synchrony (N = 188) was 41.5 ± 1.6%, which was expected since the majority of the significant synchrony that we measured was between electrodes that are within the range of overlapping RFs for area 17 in cats (5 mm^2; Albus 1975; see Figure 4-10).

In addition, the lag times of our cross-correlograms support common input as the probable source of synchrony. A large percentage (43%) of the synchrony peaks we measured were at 0 ms and the average center of the synchrony peaks was displaced only 1.4 ± 0.2 ms. Again, this is predicted by the anatomy since electrode pairs yielding synchrony fell within the extent of the most distant projections measured from layer 4 to layers 2/3 in cats (5 mm; Martin and Whitteridge 1984). We see a clear drop-off in synchronous pairs that lay outside of this region but still within the array dimensions (Figure 4-10).

However, within this region where common input is expected we do not see a clear systematic relationship with electrode distance and the strength of synchrony (N = 188 pairs) (r^2 = 0.01; Figure 4-10). Our data only weakly suggests that the strength of synchrony decreases with increasing distance between electrodes (Das and Gilbert, 1999). However, we were unable to investigate pairs closer than 400 μm (electrode spacing on the array), which were examined by Das and Gilbert (1999). Figures 4-6 A and B also show that within the 5 mm window there is not a strong systematic relationship between the RF overlap and the strength of synchrony. These two points,

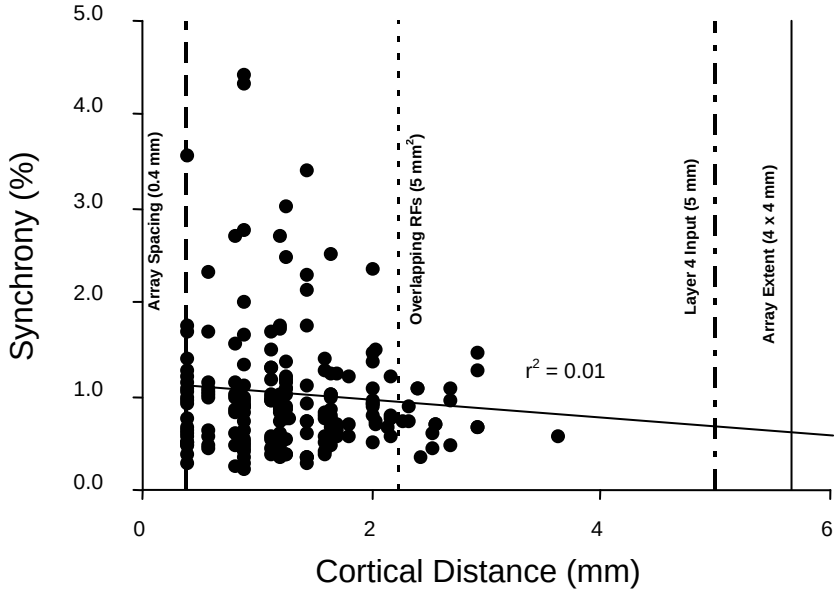

Figure 4-10: Relationship between Synchrony and Electrode Distance. Scatter plot of synchrony versus the distance between electrodes for each recorded pair. Vertical lines represent Bionics array dimensions and cat area 17 dimensions of regions of RF overlap (Albus, 1975) and maximum distance of Layer 4 projections to Layers 2/3 (Martin and Whitteridge, 1984).

together with the observation that 5% of our pairs had wholly separate RFs and over 12% of our pairs had less than 10% overlap, suggest that the synchrony we observe does not simply reflect common inputs. Nonetheless, both the lag times and the physical extent of the interactions suggest that synchrony arises from the bottom-up converging and diverging inputs from earlier levels of the visual system. One explanation for the lack of any clear systematic relationship with anatomy is that the synchrony is dynamic, which we will describe in the following section. Due to the overlap of these converging and diverging inputs, the synchrony cannot be resolved exclusively with a connectionist description of the cortical network.

Stimulus-Dependent Dynamic Synchrony

We also examined how synchrony within cell groups larger than pairs depended on the form of stimulation. One theory for cortical representation of information is that cells change their membership within a particular subpopulation (defined by synchrony) as stimuli vary (von der Malsburg 1981). Figure 4-11 (*left*) shows the RFs of three cells simultaneously recorded. When a drifting grating is presented, the two upper cells (*red*), which are essentially collinear, synchronize while the lower cell does not synchronize with either of the upper two (Figure 4-11 A, *middle*). When drifting concentric rings are presented, the lower two cells (*blue*), which are nearly orthogonal but positioned to prefer this ring stimulus, synchronize while the upper cell does not synchronize with either of the lower two cells (Figure 4-11 B, *middle*).

The firing rate tuning of the cells (Figure 4-11 A and B, *right*) roughly predicts the groupings for changing stimulation. However, the synchrony is much more precise,

acting like a logical AND gate that only allows the stimulus to synchronize the cells at the intersection of the tuning. For collinear contours, the strongest synchrony occurs for the orientation between the two cells' preferred orientations (Figure 4-11 A; *right, red arrow*) and weakens with changes in either direction (*green curve* is synchrony measurements). We see this behavior consistently across our entire sample, which matches several previous reports (see quantitative description in Ghose et al. 1994; Samonds et al. 2003, 2004; Samonds and Bonds 2005; Kohn and Smith 2005). For curved contours, the rings need to be precisely aligned with both RFs to allow cells with nonoverlapping orientation tuning to synchronize (*blue arrows* are direction of the ring with respect to each cell's RF). We again see the synchrony weaken or disappear with changes in the ring center location. However, the number of ring centers that we used was too sparse to characterize systematically the dependency of synchrony with respect to alignment for curved contours.

Figure 4-12 shows how the example of dynamic grouping in Figure 4-11 extends to our entire population of pairs. A scatter plot of all synchrony measurements (Figure 4-12 A) shows that the strongest synchrony for gratings occurs for cell pairs with zero cocircularity (i.e., strictly collinear), which matches previous reports (Ts'o et al. 1986; Gray et al. 1989; Samonds et al. 2004). The synchrony is both more reliable and more selective than the firing rate at predicting whether a stimulus is collinear (Figure 4-12 A vs. 4-12 B; $\alpha<0.005$). If synchrony is a general mechanism for contour integration, it must also play a role in detecting cocircular contours. Figure 4-12 C illustrates that ring stimuli tend to shift the strongest synchronization from collinear pairs to pairs with higher cocircularity, synchronizing pairs with differing orientations (note that overall the

Figure 4-11: Example of dynamic binding (A) Cross-correlation histogram (CCH) between cell 10 and cell 20 (collinear RF relationship) for gratings (red CCH) and for rings (lower black CCH). The firing rate tuning is shown to the right (red arrow is the orientation of the grating). The green points and curve are synchrony measurements. (B) Cell 10 synchronizes with cell 11 (cocircular RF relationship) for rings (blue CCH), but not for gratings (upper black CCH). The firing rate tuning is shown to the right (blue arrows are the orientation of the rings with respect to cell 10's and cell 11's RFs).

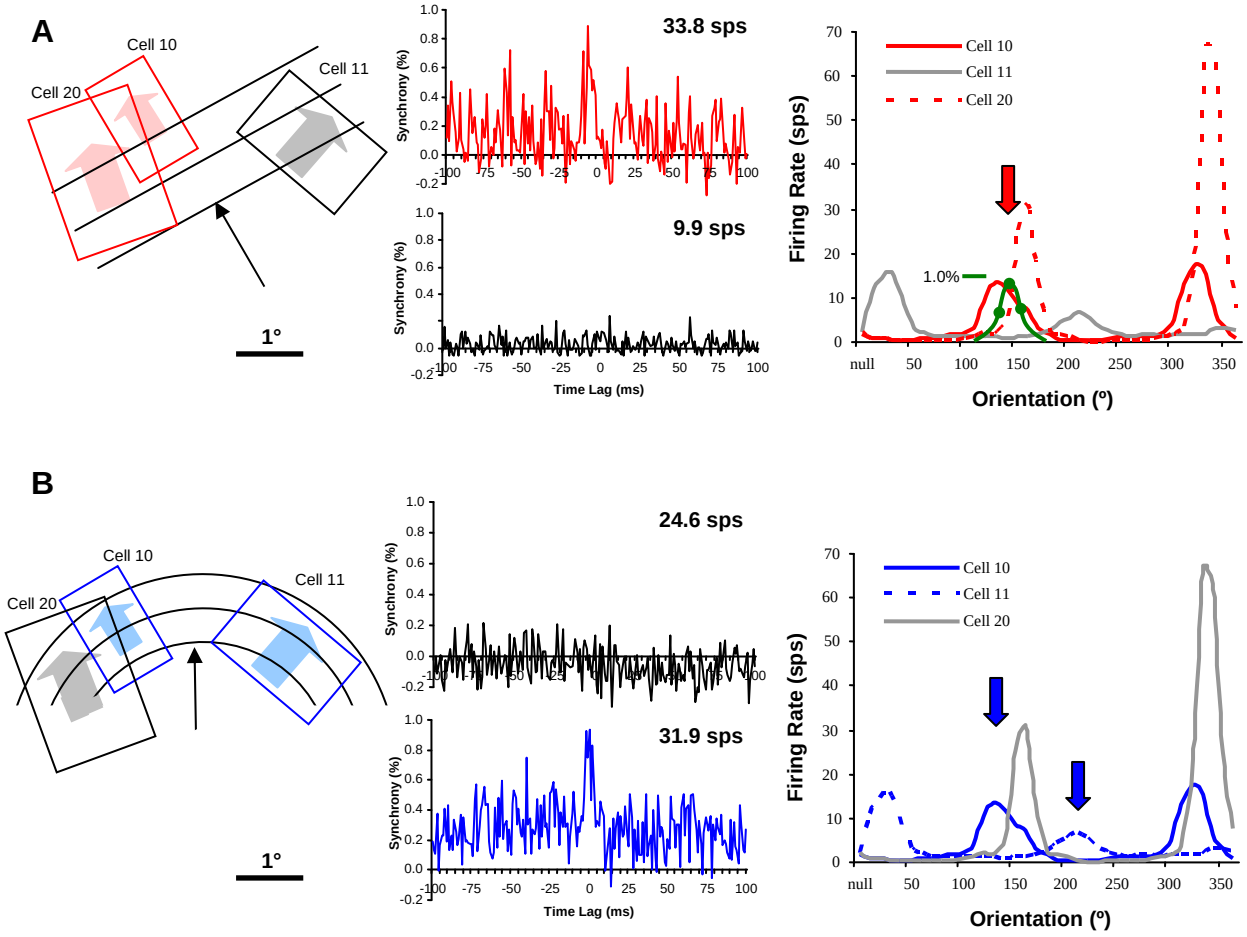
A
Cell 10
Cell 11
Cell 20
1°
33.8 sps
9.9 sps
Synchrony (%)
Time Lag (ms)
Cell 10
Cell 11
Cell 20
1.0%
Firing Rate (sps)
Orientation (º)
B
Cell 10
Cell 11
Cell 20
1°
24.6 sps
31.9 sps
Synchrony (%)
Time Lag (ms)
Cell 10
Cell 11
Cell 20
Firing Rate (sps)
Orientation (º)

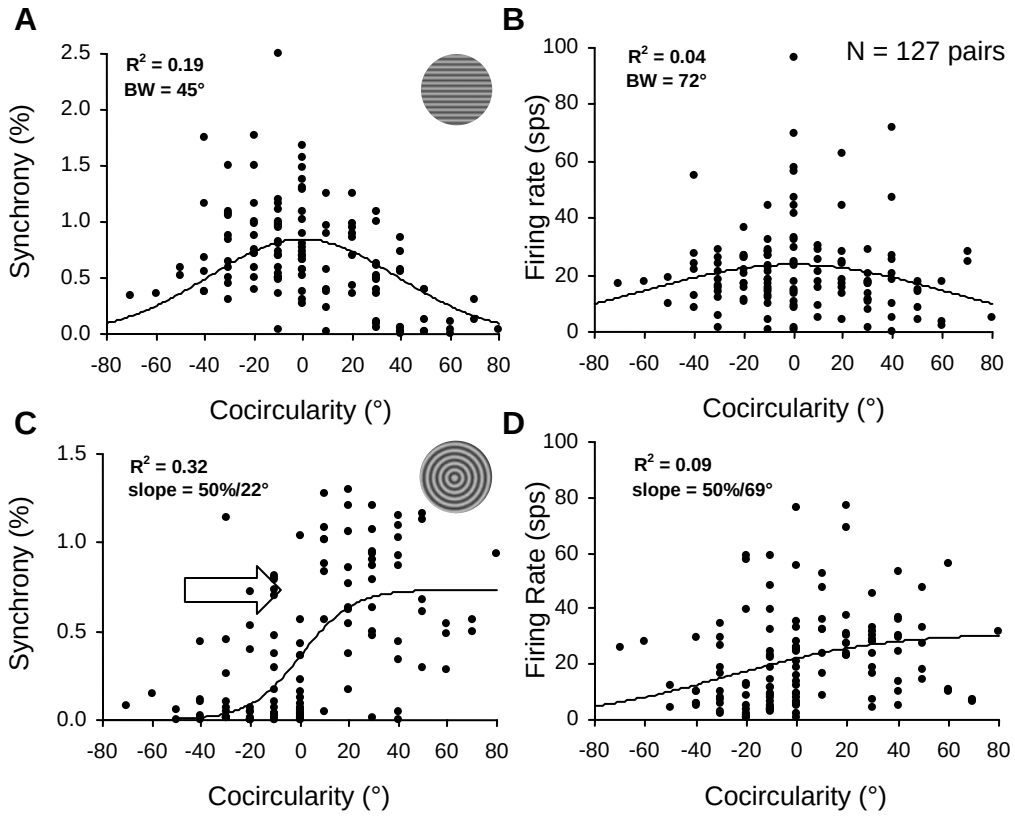

Figure 4-12: Synchrony Shifts to Higher Cocircularity for Concentric Rings (A) Synchrony measurements for *N* = 127 pairs during drifting grating stimulation. (B) Total average firing rate measurements for same data in (A). BW = half-height half-bandwidth. (C) Synchrony measurements for the same 127 pairs of cells during concentric rings stimulation. (D) Total average firing rate measurements for same data in (C). Measurement is slope at 50% magnitude.

average synchrony is weaker in Figure 4-12 C versus 12A). Again, synchrony is more selective and more reliable than firing rate at predicting the stimulus (Figure 4-12 C vs. 4-12 D; $\alpha<0.001$). The increased selectivity and reliability of the synchrony is not simply a multiplicative result of firing rate probabilities. The synchrony that we are measuring is above the chance level that is predicted by multiplying firing probabilities (which is in any case subtracted from the measurement; Aertsen et al. 1989). The Aertsen et al. (1989) rate-normalized synchrony we use, also termed *effective connectivity*, is clearly dynamic (i.e., not simply a fixed consequence of anatomical connections) and stimulus dependent with respect to contour configuration.

Lastly, we want to comment on the magnitude of the synchronous behavior we observe and its implications with respect to the decoding of contour information by higher visual areas. The synchrony peaks (1-ms bins) among visual cortical pairs are relatively weak (mean <1%; see Figure 4-12 A and 4-12 C). Integrated over a window of 10 ms, the average synchrony (correlation coefficient) is 6.2% (typically <20%). A hypothetical coincidence detector cannot distinguish between synchronous spikes that arise from chance and those that arise from network dynamics and connectivity (Shadlen and Movshon 1999). Based on our average firing rates, the synchronous spikes that arise from chance within a 10-ms window is on average 11.0% (and increases with increasing firing rates). Therefore, if we consider the synchrony we are measuring as the contour signal, the firing rate will add a considerable amount of noise. Whether or not this is detrimental to our interpretations described below cannot be determined from our data alone. First, the firing rate information is not all noise. Although more coarsely and with more errors, the firing rate still encodes some contour information (and with a

coincidence detector there is some improvement over summing firing rates). In addition, we cannot determine how the signal-to-noise will scale over larger numbers of cells although it seems likely that it would increase (Samonds et al. 2004).

Discussion

One of the fundamental presumptions about the role of V1 in visual processing is that single-cell orientation tuning forms the foundation for a system that detects edges or contours (e.g., Marr and Hildreth 1980). The association field theory provides rules about how orientation detectors might combine based on natural scene statistics and psychophysical tests of contour detection (Field et al. 1993; Polat and Sagi 1994; Pizlo et al. 1997; Pettet et al. 1998; Pettet 1999; Geisler et al. 2001; Sigman et al. 2001; Alais and Lorenceau 2002; Elder and Goldberg 2002). Lateral connections are thought to be critical in contour integration by enhancing responses to cells with collinear RFs driven by a single contour (Gilbert and Weisel 1989; Gilbert et al. 1996). Evidence of such enhancement (Kapadia et al., 1995) and the anatomical organization of horizontal connections in V1 (Gilbert and Weisel 1989; Malach et al. 1993; Bosking et al. 1997; Stettler et al. 2002; Lund et al. 2003) support this proposal and provide physiologic and anatomic links with the association field model.

Contextual Interactions and Contour Integration

The predominance of horizontal connections among cells with similar orientation preferences (Gilbert and Weisel 1989; Malach et al. 1993; Bosking et al. 1997; Lund et al. 2003) would predict greater firing rates for gratings (stimulation of similar

orientations) versus rings (stimulation of different orientations) if such connections are facilitatory. However, our results suggest that overall these lateral connections offer no advantage to responses from grating stimulation over concentric rings stimulation because the average firing rates are nearly the same in the two conditions. In addition, we find that aggregate V1 responses to gratings or rings stimulation are not easily predicted from the independent orientation tuning functions (Figure 4-9 B). The integrated firing rates are ambiguous and are therefore unreliable as encoders of the shape of the contour segment within the local RFs. Contour orientation must not be the only influence on firing rate (see also Hess et al. 2003).

This response ambiguity could result from contextual modulation of V1 responses by stimuli extending beyond the classical RF (CRF) (Fitzpatrick 2000). Although there are some systematic trends (e.g., Kapadia et al. 1995, 2000) for modulation of the CRF response by peripheral stimulation, there are also considerable inconsistencies (Jones et al. 2002). The reported effects include suppression, facilitation, and disinhibition with surround suppression being the most consistent result (Jones et al. 2002; Yao and Lee 2002; Cavanaugh et al. 2002; Guo et al. 2005). In most cases, suppression is strongest when the surround stimulus properties match the CRF stimulus properties, which is inconsistent with purely excitatory integration between cells with similar orientation preferences. Facilitation can occur when the surround orientation is orthogonal to CRF orientation, suggesting that contextual modulations might play a role in segmentation (Lamme 1995; Sillito and Jones 1996; Marcus and van Essen 2002). In limited cases (42%), the same orientation in the surround with collinear alignment results in facilitation, suggesting that contextual modulations support contour integration (Kapadia

et al. 1995). However, Cavanaugh et al. (2002) suggest that collinear facilitation might be overestimated in Kapadia et al. (1995) due to underestimating the extent of the classical RF. Lastly, surround effects have also been shown to support the integration of discontinuities such as junctions and corners (Sillito et al. 1995).

On the whole gratings are more likely than rings to cause surround suppression (Jones et al. 2002) because rings distribute energy across a variety of orientations in the surround. While an optimally orientated grating might generate a greater response from two collinear CRFs, it is reduced by suppression outside the CRF. Surround antagonism is likely less with rings stimulation. Thus while gratings are more effective for the CRF response, rings may ultimately generate an identical or larger firing rate, resulting in ambiguity about the local contour curvature. A similar response ambiguity would also arise with contrast changes (which minimally affect contour integration; see Hess et al. 2003). Synchronous integration again would preserve the contour information lost in the ambiguous firing rates because contrast leads to negligible changes in synchrony strength (Snider et al. 1998; Kohn and Smith 2005).

We believe that our sample of pairs and choice of stimuli generalize for the behavior of layers 2/3 of V1. Our comparison of firing rate versus synchrony was made when the local stimulus orientation was matched with the RFs of both cells. Our sample of cells was restricted to superficial layers, but the array dimensions (4×4 mm) provided us with a widespread sample across multiple orientation columns. Limiting our analysis to synchronous pairs does not appear to bias our sample significantly among this selection of cells. If our source of stimulation (gratings covering 16° of visual angle) biased our sample, it would be towards including more cells enhanced by elongated

contours (i.e., not including cells enhanced by discontinuities or cells with strong suppressive surrounds). Our choice of gratings is unlikely to influence our interpretations substantially because the predominance of suppressive surround effects has been found with bars, gratings, and natural scenes (Jones et al. 2002; Yao and Lee 2002; Cavanaugh et al. 2002; Guo et al. 2005).

Dynamic Contour Integration

We propose that contour integration is primarily driven by bottom-up synchronous integration via the diverging and converging anatomy in the earlier stages of visual processing (Alonso et al. 1996; Usrey and Reid 1999). Synchrony is more prominent and predictable than facilitation when tested over a diverse population of cells—i.e., synchrony occurs for >70% of our cocircular pairs (see also Tso et al. 1986; Gray et al. 1989; Samonds et al. 2004; >75% occurrence for similar orientations) while collinear facilitation occurs for less than half of V1 cells (Kapadia et al. 1995), and even that might be an overestimation (see above; Cavanaugh et al. 2002). Overall our data show that both the magnitude and probability of observing synchrony match the fundamental prediction of the association field model: segments are more likely to be part of the same contour when they are similarly oriented. Our analysis of electrode distance, RF overlap, and synchronous lag times all suggest that the synchrony we observe can most simply be explained by common and synchronous input from previous levels of the visual system. Specific afferent projections (100-300 μm) from layer 4 to layers 2/3 can span as much as 5 mm (Martin and Whitteridge 1984), which falls well within the range of all the synchrony we measure with the array (Figure 4-10).

Collinear contours would synchronize cells within and across different orientation columns that have the same orientation preference. The most acute curves would likely synchronize pairs located at orientation column discontinuities (i.e., pinwheel centers; Bonhoeffer and Grinvald 1992). Synchrony among cells with large orientation differences and discrete RFs can indeed be found near pinwheel centers (Das and Gilbert 1999).

Our data do not necessarily rule out a role for horizontal connections, but there is no clear evidence (e.g., lag times) to suggest that synchrony is driven by direct mono- or polysynaptic excitatory connections, at least among the population of V1 cell pairs that we observed. Nonetheless, the synchrony could be driven laterally by an intermediate common input that we were unable to observe. Horizontal connections within V1 suggest an appealing substrate for contour integration since 60-70% of these connections are between columns of similar orientation preferences (Malach et al. 1993; Bosking et al. 1997; Stettler et al. 2002; Lund et al. 2003) and therefore support the association field viewpoint (see Yen and Finkel 1998). However, Sperry et al. (1955) found virtually no change in performance for cats discriminating global contours and patterns after transecting horizontal connections throughout area 17 so this raises some doubt about their role in contour integration being critical. Broad integration might take place at higher levels, where RFs are larger.

Extent of V1 Contour Integration?

Although in general our synchrony data support the association field theory, we did not find clear evidence for its prediction of enhanced synchrony or higher probability of

observing synchrony with RF proximity (Figures 4-5 and 4-6; note however that any trends we did observe were in the right direction). This could be explained because the synchrony that we found was mainly limited to relatively local processing within the visual field. The total separation of contour segments that stimulated cell pairs was always less than 10º (≤ 3 complex cell RFs; Wilson and Sherman 1976) even though the total spread of RFs and stimulation spanned over 16º. The average RF overlap was 35% and only about 15% of our pairs were discrete or nearly discrete (<10% overlap). The term "local" must be tempered by the fact that in *all* cases we were still exploring stimulation extending beyond a single V1 classical RF and the cortical distances between electrodes (≥ 0.4 mm) suggest that the interactions were at least across different orientation columns.

Alternatively, the global aspects and proximity rule of contour integration might be implemented over multiple layers of the visual system hierarchy and possibly combined with inferential top-down mechanisms (e.g., Feldman 1997; Geisler et al. 2001; Elder and Goldberg 2002). This alternative view seems more likely if synchrony is supported by afferent inputs that limit integration within one layer to cell pairs with overlapping or nearby RFs. This limitation is suggested by the result that the majority of the synchrony we measure is within the cortical area of RF overlap (5 mm^2; Albus 1975; Figure 4-2 C) despite the array covering 16 mm^2 of cortex. Top-down connectivity could also be another source of the synchrony we measure (e.g., Sillito et al. 1994), but the connections between V2 to V1 appear to lack the necessary organization to support the association field model (Stettler et al. 2002). Nonetheless the flow of information

through the visual hierarchy could still support the association field proximity rules while the level of integration via synchronization in V1 guides the orientation rules.

Integration of V1 Responses in Extrastriate Cortex

Use of the contour information provided by synchrony in primary visual cortex requires that cells at higher levels of the visual system act as synchrony decoders or coincidence detectors. Softky and Koch (1993) have suggested that the irregular firing that is preserved from V1 to area MT is a result of the neurons acting as coincidence detectors. The changes in thresholding measured during normal activity also suggest that cortical cells are likely *only* to integrate synchronous spikes (Azouz and Gray 2003).

We suggest that the selective response of single cells in extrastriate regions of the Macaque monkey (the medial superior temporal area, V2, and V4) to curvature and cocircular spatiotemporal patterns (Saito et al. 1986; Tanaka and Saito 1989; Orban et al. 1992; Gallant et al. 1993; Gallant et al. 1996; Hegdé and Van Essen 2000; Pasupathy and Connor 2001) indicates recovery of information provided by synchronous spikes from striate cortex. The selectivity of V2 cells for corners and T-junctions (Hegdé and Van Essen 2000) might also reflect coincidence detection of synchrony driven by these features (Das and Gilbert 1999).

Wilson (1999) has suggested that extrastriate tuning for concentric rings and Glass patterns must originate from forms of integration of the responses from earlier levels of visual processing that are more complex than simple summation. Nonlinear integration via coincidence detection of synchronous spikes at least provides substantial improvement for detecting contour shape and has the capacity to resolve the contour

ambiguity present in firing rates. Because orientation discrimination improves substantially when considering the synchrony among larger groups of cells, the accuracy in representing contour configuration would likely continue to improve if we were able to examine more cells encoding the same contour (Samonds et al. 2004).

REFERENCES

Aertsen AMHJ, Gerstein GL, Habib MK, and Palm G. Dynamics of neuronal firing correlation: modulation of "effective connectivity." *J Neurophysiol* 61: 900-917, 1989.

Alais D and Lorenceau J. Perceptual grouping in the Ternus display: evidence for an 'association field' in apparent motion. *Vision Res* 42: 1005-1016, 2002.

Albus K. A quantitative study of the projection area of the central and the paracentral visual field in area 17 of the cat. *Exp Brain Res* 24: 159-179, 1975.

Alonso J-M, Usrey WM, and Reid RC. Precisely correlated firing in cells of the lateral geniculate nucleus. *Nature* 383: 815-819, 1996.

Azouz R and Gray CM. Adaptive coincidence detection and dynamic gain control in visual cortical neurons in vivo. *Neuron* 37: 513-523, 2003.

Beaudot WHA and Mullen KT. Processing time of contour integration: the role of colour, contrast, and curvature. *Perception* 30: 833-853, 2001.

Beaudot WHA and Mullen KT. How long range is contour integration in human color vision? *Visual Neurosci* 20: 51-64, 2003.

Bonhoeffer T and Grinvald A. Iso-orientation domains in cat visual cortex are arranged in pinwheel-like patterns. *Nature* 353: 429-431, 1992.

Bosking WH, Zhang Y, Schofield B, and Fitzpatrick D. Orientation selectivity and the arrangement of horizontal connections in tree shrew striate cortex. *J Neurosci* 17: 2112-2127, 1997.

Brody CD. Slow covariations in neuronal resting potentials can lead to artefactually fast cross-correlations in their spike trains. *J Neurophysiol* 80: 3345-3351, 1998.

Brody CD. Disambiguating different covariation types. *Neural Comp* 11: 1527-1535, 1999a.

Brody CD. Correlations without synchrony. *Neural Comp* 11: 1537-1551, 1999b.

Castelo-Branco M, Goebel R, Neuenschwander S, and Singer W. Neural synchrony correlates with surface segregation rules. *Nature* 405: 685-689, 2000.

Cavanaugh JR, Bair W, and Movshon JA. Nature and interaction of signals from the receptive field center and surround in macaque V1 neurons. *J Neurophysiol* 88: 2530-2546, 2002.

Das A and Gilbert CD. Topography of contextual modulations mediated by short-range interactions in primary visual cortex. *Nature* 399: 655-661, 1999.

Eckhorn R, Bauer R, Jordan W, Brosch M, Kruse W, Munk M, and Rietboeck HJ. Coherent oscillations: A mechanism of feature linking in the visual cortex? *Biol Cybern* 60: 121-130, 1988.

Efron B and Tibshirani R. *An introduction to the bootstrap*. London: Chapman & Hall, 1993.

Elder JH and Goldberg RM. Ecological statistics of Gestalt laws for the perceptual organization of contours. *J Vision* 2: 324-353, 2002.

Feldman J. Curvilinearity, covariance, and regularity in perceptual groups. *Vision Res* 37, 2835-2848, 1997.

Field DJ, Hayes A, and Hess RF. Contour integration by the human visual system: evidence for a local "association field". *Vision Res* 33: 173-193, 1993.

Fitzpatrick D. Seeing beyond the receptive field in primary visual cortex. *Curr Op Neurobiol* 10: 438-443, 2000.

Frien A, Eckhorn R, Bauer R, Woelbern T, and Gabriel A. Fast oscillations display sharper orientation tuning than slower components of the same recordings in striate cortex of the awake monkey. *Eur J Neurosci* 12: 1453-1465, 2000.

Gallant JL, Braun J, and Van Essen DC. Selectivity for polar, hyperbolic, and Cartesian gratings in macaque visual cortex. *Science* 259: 100-103, 1993.

Gallant JL, Connor CE, Rakshit S, Lewis JW, and Van Essen DC. Neural responses to polar, hyperbolic, and Cartesian gratings in area V4 of the Macaque monkey. *J Neurophysiol* 76: 2718-2739, 1996.

Geisler WS, Perry JS, Super BJ, and Gallogly DP. Edge co-occurrence in natural images predicts contour grouping performance. *Vision Res* 41: 711-724, 2001.

Gerstein GL and Kirkland KL. Neural assemblies: technical issues, analysis, and modeling. *Neural Netw* 14: 589-598, 2001.

Ghose GM, Ohzawa I, and Freeman RD. Receptive-field maps of correlated discharge between pairs of neurons in the cat's visual cortex. *J Neurophysiol* 71: 330-346, 1994.

Gilbert CD, Das A, Ito M, Kapadia M, and Westheimer G. Spatial integration and cortical dynamics. *Proc Nat Acad Sci USA* 93: 615-622, 1996.

Gilbert CD and Weisel TN. Columnar specificity of intrinsic horizontal and corticocortical connections in cat visual cortex. *J Neurosci* 9: 2432-2442, 1989.

Gray CM, König P, Engel AK, and Singer W. Oscillatory responses in cat visual cortex exhibit inter-columnar synchronization which reflects global stimulus properties. *Nature* 338: 334-337, 1989.

Guo K, Robertson RG, Mahmoodi S, and Young MP. Centre-surround interactions in response to natural scene stimulation in the primary visual cortex. *Eur J Neurosci* 21: 536-548, 2005.

Hedgé J and Van Essen DC. Selectivity for complex shapes in primate visual area V2. *J Neurosci* 20: RC61 (1-6), 2000.

Hess RF, Hayes A, and Field DJ. Contour integration and cortical processing. *J Physiol Paris* 97: 105-119, 2003.

Hubel DH and Wiesel TN. Receptive fields, binocular interaction and functional architecture in the cat's visual cortex. *J Physiol* 160: 106-154, 1962.

Ito H and Tsuji S. Model dependence in quantification of spike interdependence by joint peri-stimulus time histogram. *Neural Comp* 12: 195-217, 2000.

Jones HE, Wang W, and Sillito AM. Spatial organization and magnitude of orientation contrast interactions in primate V1. *J Neurophysiol* 88: 2796-2808, 2002.

Kapadia MK, Ito M, Gilbert CD, and Westheimer G. Improvement in visual sensitivity by changes in local context: parallel studies in human observers and in V1 of alert monkeys. *Neuron* 15: 843-856, 1995.

Kapadia MK, Westheimer G, and Gilbert CD. Spatial distribution of contextual interactions in primary visual cortex and in visual perception. *J Neurophysiol* 84: 2048-2062, 2000.

Kass RE, Ventura V, and Brown EN. Statistical issues in the analysis of neuronal data. *J Neurophysiol* 94: 8-25, 2005.

Kirkland KL, Sillito AM, Jones HE, West DC, and Gerstein GL. Oscillations and long-lasting correlations in a model of the lateral geniculate nucleus and visual cortex. *J Neurophysiol* 84: 1863-1868, 2000.

Kohn A and Smith MA. Stimulus dependence of neuronal correlation in primary visual cortex of the macaque. *J Neurosci* 25: 3661-3673, 2005.

Kovács I and Julesz B. A closed curve is much more than an incomplete one: Effect of closure in figure-ground segmentation. *Proc Nat Acad Sci USA* 90: 7495-7497, 1993.

Lamme VA. The neurophysiology of figure-ground segregation in primary visual cortex. *J Neurosci* 15: 1605-1615, 1995.

Lund JS, Angelucci A, and Bressloff PC. Anatomical substrates for functional columns in macaque monkey primary visual cortex. *Cereb Cortex* 13: 15-24, 2003.

Malach R, Amir Y, Harel M, and Grinvald A. Relationship between intrinsic connections and functional architecture revealed by optical imaging and in vivo targeted biocytin injections in primate striate cortex. *Proc Nat Acad Sci USA* 90: 10469-10473, 1993.

Marcus DS and Van Essen DC. Scene segmentation and attention in primate cortical areas V1 and V2. *J Neurophysiol* 88: 2648-2658, 2002.

Marr D and Hildreth E. Theory of edge detection. *Proc R Soc Lond B Biol Sci* 207: 187-217, 1980.

Martin KAC and Whitteridge D. Form, function, and intracortical projections of spiny neurones in the striate visual cortex of the cat. *J Physiol* 353: 463-504, 1984.

Moore GP, Segundo JP, Perkel DH, and Levitan H. Statistical signs of synaptic interaction in neurons. *Biophys J* 10: 876-900, 1970.

Orban GA, Lagae L, Verri A, Raiguel S, Xiao D, Maes H, and Torre V. First-order analysis of optical flow in monkey brain. *Proc Nat Acad Sci USA* 89: 2595-2599, 1992.

Palm G, Aertsen AMHJ, and Gerstein GL. On the significance of correlations among neuronal spike trains. *Biol Cybern* 59: 1-11, 1988.

Parent P and Zucker SW. Trace inference, curvature consistency, and curve detection. *IEEE Trans Pattern Anal Machine Intell* 11: 823-839, 1989.

Pasupathy A and Connor CE. Shape representation in area V4: position-specific tuning for boundary conformation. *J Neurophysiol* 86: 2505-2519, 2001.

Pettet MW. Shape and contour detection. *Vision Res* 39: 551-557, 1999.

Pettet MW, McKee SP, and Grzywacz NM. Constraints on long range interactions mediating contour detection. *Vision Res* 38: 865-879, 1998.

Pizlo Z, Salach-Golyska M, and Rosenfeld A. Curve detection in a noisy image. *Vision Res* 37: 1217-1241, 1997.

Polat U and Norcia AM. Elongated physiological summation pools in the human visual cortex. *Vision Res* 38: 3735-3741, 1998.

Polat U and Sagi D. The architecture of perceptual spatial interactions. *Vision Res* 34:73-78, 1994.

Polat U and Tyler CW. What pattern the eye sees best. *Vision Res* 39: 887-895, 1999.

Saito H, Yukie M, Tanaka K, Hikosaka K, Fukada Y, and Iwai E. Integration of direction signals of image motion in the superior temporal sulcus of the macaque monkey. *J Neurosci* 6: 145-157, 1986.

Samonds JM, Allison JD, Brown HA, and Bonds AB. Cooperation between area 17 neuron pairs enhances fine discrimination of orientation. *J Neurosci* 23: 2416-2425, 2003.

Samonds JM, Allison JD, Brown HA, and Bonds AB. Cooperative synchronized assemblies enhance orientation discrimination. *Proc Nat Acad Sci USA* 101: 6722-6727, 2004.

Samonds JM and Bonds AB. Gamma oscillation maintains stimulus structure-dependent synchronization in cat visual cortex. *J Neurophysiol* 93: 223-236, 2005.

Shadlen MN and Movshon JA. Synchrony unbound: a critical evaluation of the temporal binding hypothesis. *Neuron* 24: 67-77, 111-25, 1999.

Shoham S, Fellows MR, and Normann RA. Robust, automatic spike sorting using mixtures of multivariate t-distributions. *J Neurosci Meth* 127: 111-122, 2003.

Sigman M, Cecchi GA, Gilbert CD, and Magnasco MO. On a common circle: Natural scenes and Gestalt rules. *Proc Nat Acad Sci USA* 98: 1935-1940, 2001.

Sillito AM, Grieve KL, Jones HE, Cudeiro J, and Davis J. Visual cortical mechanisms detecting focal orientation discontinuities. *Nature* 378: 492-496, 1995.

Sillito AM and Jones HE. Context-dependent interactions and visual processing in V1. *J Physiol Paris* 90: 205-209, 1996.

Sillito AM, Jones HE, Gerstein GL, and West DC. Feature-linked synchronization of thalamic relay cell firing induced by feedback from the visual cortex. *Nature* 369: 479-482, 1994.

Singer W and Gray CM. Visual feature integration and the temporal correlation hypothesis. *Annu Rev Neurosci* 18: 555-586, 1995.

Skottun BC, De Valois RL, Movshon JA, Albrecht DG, and Bonds AB. Classifying simple and complex cells on the basis of response modulation. *Vision Res* 31: 1079-1086, 1991.

Snider RK, Kabara JK, Roig BR, and Bonds AB. Burst firing and modulation of functional connectivity in cat striate cortex. *J Neurophsyiol* 80: 730-744, 1998.

Softky WR and Koch C. The irregular firing of cortical cells is inconsistent with temporal integration of random EPSPs. *J Neurosci* 13: 334-350, 1993.

Solomon JA and Morgan MJ. Facilitation from collinear flanks is cancelled by non-collinear flanks. *Vision Res* 40: 279-286, 2000.

Sperry RW, Miner N, and Myers RE. Visual pattern perception following subpial slicing and tantalum wire implantations in the visual cortex. *J Compar Physiol Psychol* 48: 50-58, 1955.

Stettler DD, Das A, Bennett J, and Gilbert CD. Lateral connectivity and contextual interactions in macaque primary visual cortex. *Neuron* 36: 739-750, 2002.

Tanaka K and Saito H. Analysis of motion of the visual field by direction, expansion/contraction, and rotational cells clustered in the dorsal part of the medial superior temporal area of the Macaque monkey. *J Neurophysiol* 62: 626-641, 1989.

Ts'o DY, Gilbert CD, and Wiesel TN. Relationships between horizontal interactions and functional architecture in cat striate cortex as revealed by cross-correlation analysis. *J Neurosci* 6: 1160-1170, 1986.

Usrey WM and Reid RC. Synchronous activity in the visual system. *Annu Rev Physiol* 61: 435-456, 1999.

Victor JD and Purpura KP. Nature and precision of temporal coding in visual cortex: A metric-space analysis. *J Neurophysiol* 76: 1310-1326, 1996.

von der Malsburg C. The what and why of binding: the modeler's perspective. *Neuron* 24: 95-104, 111-25, 1999.

von der Malsburg C. (1981) *The correlation theory of brain function*. Internal Report. Goettingen, Germany: Max-Planck Institute for Biophysical Chemistry, 1981.

Wilson HR. Non-Fourier cortical processes in texture, form, and motion perception. In *Cerebral Cortex, vol. 13: Models of Cortical Circuitry*, PS Ulinski, and EG Jones, eds. New York: Plenum, pp. 445-477, 1999.

Wilson JR and Sherman SM. Receptive-field characteristics of neurons in cat striate cortex: changes with visual field eccentricity. *J Neurophysiol* 39: 512-533, 1976.

Yao H and Li CY. Clustered organization of neurons with similar extra-receptive field properties in the primary visual cortex. *Neuron* 35: 547-553, 2002.

Yen SC and Finkel LH. Extraction of perceptually salient contours by striate cortical networks. *Vision Res* 38:719-741, 1998.

CHAPTER V

INTERDEPENDENCE OF SPIKE TIMING AND OSCILLATION IN SYNCHRONIZED RESPONSES OF CAT VISUAL CORTEX

Zhiyi Zhou, Melanie R. Bernard, A. B. Bonds

Abstract

Synchronized neural responses, which often are accompanied by oscillations in the gamma frequency band (35 – 70 Hz), have been found extensively in the visual cortex and have been proposed as supporting perceptual mechanisms. We studied the correlated firing between cells recorded in cat primary visual cortex with both JPSTH and multi-taper coherence analyses. Linear regression analysis reveals strong correlation between neural synchrony and the corresponding coherence (R^2 = 0.63), which suggests that cross-correlation analysis and coherence analysis are internally related, though these two methods study neural cooperation from different perspectives. To explore the importance of the temporal structures of spike trains in maintaining the temporal and frequency correlation between neurons, we then randomly jittered the neural spikes over different time ranges (±5msec, ±10msec, ±20msec) to disturb the timing accuracy in neural responses. We found the strength of synchrony and coherence systematically dropped with the increase of jittering range, with the coherence in the gamma frequency band showing the greatest losses after spike trains were jittered. Dependency analysis shows that significant amounts of information are lost after correlation between neurons is disrupted by spike jittering.

Introduction

In the primary visual cortex, neurons give their strongest response, which is normally specified by the firing rate, to simple stimuli with defined spatial and temporal characteristics such as a moving light bar (Hubel and Wiesel, 1962; Albrecht et al., 1980; De Valois et al., 1982; Webster and De Valois, 1985; Bonds, 1989; Hubel, 1989). Cells located in the higher levels of the visual pathway, on the other hand, tend to respond to stimuli with more complicated features. For example, cells in area V4 of macaque monkey will show an elevated response rate if concentric rings or radial gratings are presented in their receptive fields (Gallant et al., 1996). A group of cells located in the inferior temporal cortex in macaque monkeys was reported to respond selectively to faces (Desimone et al., 1984). One common view is that discrimination of complexity is derived via a layered hierarchy in which information from cells in the lower level of the visual system converges upon cells in the higher levels. "Cardinal" cells located at the top of this hierarchy would have the ability to represent features that have the highest complexity (Barlow, 1972). However, the binding mechanism by which the higher level visual neurons selectively group and segment the convergent presynaptic inputs to form meaningful object(s) is not fully understood.

One proposed mechanism for detection of higher-order features is the so-called temporal binding theory, in which cells responding to combinations of lower-order features are grouped by temporal synchrony of either individual spikes or of periodic response structures (Milner, 1974; von der Malsburg, 1981; Eckhorn et al., 1988; Engel et al., 1992; Singer and Gray, 1995; Gray, 1999; Singer, 1999). With the aid of multi-electrode recording, synchronized activity has been found in multiple areas in the central

nervous system including the visual pathway (Mastronarde, 1989; Engel et al., 1991; Sillito et al., 1994; Alonso et al., 1996; Kreiter and Singer, 1996; Riehle et al., 1997; Dan et al., 1998; Oertel, 1999; Aksay et al., 2003). Synchrony is dependent on visual stimuli (Ts'o et al., 1986; Gray et al., 1989; Engel et al., 1991; Kreiter and Singer, 1996; Castelo-Branco et al., 2000; Kohn and Smith, 2005; Samonds et al., 2006) and there is some evidence to suggest that it could act as a binding mechanism signaling the integrity of visual structures (Gray et al., 1989; Singer and Gray, 1995; Neuenschwander and Singer, 1996; Castelo-Branco et al., 2000; Gail et al., 2000), though the validity of this proposal is still under debate (Lamme and Spekreijse, 1998; Shadlen and Movshon, 1999; Thiele and Stoner, 2003; Palanca and DeAngelis, 2005).

Spike timing synchronization between neurons is traditionally assessed by means of the normalized cross-correlation histogram (CCH), which measures the temporal proximity of firing events between two neurons. Generally, a peak in the normalized CCH indicates that cells are firing synchronously with or without time lag (Perkel et al., 1967; Aertsen et al., 1989). Another approach to assessing the association of neural firing patterns is to estimate the dependence between spike trains in the frequency domain, which is quantified by coherence. Coherence is mathematically defined as the Fourier transform of the autocovariance function and estimates the frequency association between spike trains by computing the spectrum of individual spike trains and the cross-spectrum between spike trains (Thomson, 1982; Mitra and Pesaran, 1999; Jarvis and Mitra, 2001; Brown et al., 2004; Henrie and Shapley, 2005). Cross-correlation and coherence analysis both evaluate the association between neural spike events, but to date there has been no systematic study of the direct relationship between the two approaches. There are also

questions of possible artifact in the application of the JPSTH due to effects of latency and nonstationarity (Brody, 1999a; Brody, 1999b) as well as inadequate normalization (Ito and Tsuji, 2000). Coherence analysis is much less sensitive to these factors. Here we analyze synchronized neural response by using both the joint peri-stimulus time histogram (JPSTH) and coherence analysis. Linear regression shows that the results from JPSTH and coherence analysis are highly correlated, which suggests that the JPSTH is a reasonable estimate of cooperativity and that the processes detected by both cross-correlation analysis and coherence analysis are internally related.

Previous studies have shown that the temporal structures in correlated neural response may carry information that is not delivered by the average response rate (Reinagel and Reid, 2000; Samonds and Bonds, 2004). We are interested in the importance of the fine temporal structure in maintaining the association between neural responses and whether breaking the temporal correlation between neurons can cause any information loss. We randomly jittered the spike timing in our collected signals with different time ranges (±5msec, ±10msec, ±20msec) and then analyzed the association between neural responses by conducting cross-correlation and coherence analysis on jittered spike trains. Our jitter method does not change either the average firing rate or the overall response dynamics of individual cells (see *Results*), but the fine temporal structure is systematically perturbed. We found the strength of synchrony and coherence systematically decreased with increase of jitter range. We defined the average coherence of spike trains that were jittered with the largest time range (±20msec) as the "baseline" coherence, and derived modulation functions. The coherence of the unjittered spike trains in the gamma frequency band showed the greatest losses after spike trains were jittered.

We last estimated the transneural correlation by calculating the functional dependency of synchronized pairs. We found the tuning response of dependency progressively was systematically degraded with the increase of spike jittering range. We propose that the fine temporal structures in spike trains are important in maintaining the temporal and frequency dependence between neurons, and perturbing spike timing accuracy can cause loss of information that is contained in the correlated neural response.

Materials and Methods

Physiological Preparation

Two adult cats (2.3 and 2.5 kg) were prepared for electrophysiological studies under the guidelines of the American Physiological Society and Vanderbilt University's Animal Care and Use Committee. Before surgery, each cat was injected intramuscularly with 0.5ml acepromazine maleate and 0.5ml atropine sulfate. After cannulating two forelimb veins, anesthesia was induced with 5% halothane in O_2 and maintained with intravenous injection of 0.3 $mg \cdot kg^{-1} \cdot hr^{-1}$ propofol. The trachea was then cannulated and the cats were mounted in a stereotaxic device. A small craniotomy (8 × 8 mm) was performed over the area centralis representation (Horsley-Clark coordinates P4-L2). The electrode array was inserted after the dura was incised, and the hole was covered with agar mixed in mammalian Ringer solution.

During recording, paralysis was induced with a loading dose of 6mg and maintained with 0.3 $mg \cdot kg^{-1} \cdot hr^{-1}$ pancuronium bromide via the second cannula. The cats were respirated at 30 breaths/min with a mixture of N_2O:O_2:CO_2 (75:23.5:1.5), and pCO_2 was held at 3.9%. The cats' body temperature was maintained at 37.5ºC with a

servo-controlled heat pad and the rectal temperature was monitored throughout the recording. Anesthetic stability was ensured by monitoring the brain activity and heart rate via the electroencephalogram and electrocardiogram respectively. The cats' nictitating membranes were retracted with 10% phenylephrine hydrochloride and the pupils were dilated with 1% atropine sulfate. Contact lenses with 4mm artificial pupils and auxiliary lenses were applied to render the retina conjugate with a screen at a viewing distance of 57 cm.

Visual Stimuli

After mapping individual cell's receptive field location with rear-projected light bars, we determined the center and size of the aggregated area that would be simultaneously covered by the visual stimuli. Drifting sinusoid gratings were generated with Cambridge Research System (Rochester, UK) VSG2/4 controller board and displayed on a gamma-corrected 21-inch Sony Trinitron monitor at a distance of 57 cm. The monitor was set to have a frame rate of 120 Hz and a mean luminance of 73 cd/m^2. For each presentation, gratings were displayed within a circular aperture (diameter = 14º or 18º) for 2 seconds. The orientation and direction of the gratings varied from 10 to 180º in 10º increment or 0 to 340º in 20º increments, while other parameters were fixed (contrast = 50%, spatial frequency = 0.5 c/º, and temporal frequency = 2.0 Hz). Gratings were randomly displayed at each orientation for 75 to 100 trials to ensure the reliability of the results. A blank window lasting 1 second was interleaved between stimulus presentations to avoid adaptation.

Recording

A Cyberkinetics 10 × 10 microelectrode array (4 x 4 mm) was pneumatically inserted to a fixed depth of 600 μm in cat areas 17 and 18 based on Horsley-Clark coordinates. Single or multiunit activities were recorded with this electrode array. The raw data was processed offline with a spike sorting procedure to remove noise and artifact on each channel (Shoham et al., 2003). We only included channels that recorded single unit activity, thus all single units reported in this study were resolved from different channels. We isolated single units (cells) that showed reliable orientation selectivity (i.e., firing rate at the preferred orientation was at least twice that at the worst orientation), and we only studied units with a stable firing rate of at least 8 spikes/sec for reliable spectral analysis. A total of 66 cells (32 and 34 cells from each cat), which provided 1057 pairs of cells, were finally chosen for analysis in this report. All cells we studied were classified as complex (Skottun et al., 1991).

Synchrony and Coherence

The cross-correlation histograms (CCHs) between cells were derived from the JPSTHs (Aertsen et al., 1989). The cross-product of PSTHs (expected correlation) is subtracted from the raw JPSTH (observed correlation), and the difference is then divided by the standard deviation of the PSTH predictor to create the normalized JPSTH (Aertsen et al., 1989; Sillito et al., 1994; Snider et al., 1998; Samonds et al., 2003). The normalized CCH is then created by integrating along the principle diagonal of the normalized JPSTH, which Aertsen et al. (1989) refer as *effective connectivity*. A pair of cells is considered to fire synchronously when their CCH shows a discernable central peak located at around 0

msec time delay, and we consider synchrony significant if the peak value is at least twice the random fluctuations or noise in the CCH. The normalization procedure applied in JPSTH analysis is statistically equivalent to the method of the shift predictor (Perkel et al., 1967; Gerstein and Perkel, 1972; Aertsen et al., 1989) to remove the contribution from the joint elevation of firing rates, except that the method of JPSTH produces smoother results because the PSTHs are averaged over all trials (Aertsen et al., 1989).

Coherency measures the frequency dependence between spike trains (Brown et al., 2004), which is defined by the following equation:

$$\gamma(f) = \frac{S_{12}(f)}{\sqrt{S_{11}(f)S_{22}(f)}} \tag{5-1}$$

in which $S_{11}(f)$ and $S_{22}(f)$ are the power spectra of two neural spike trains, and $S_{12}(f)$ is the cross spectrum between these two spike trains (Thomson, 1982; Percival and Walden, 1993; Mitra and Pesaran, 1999; Jarvis and Mitra, 2001). Coherency is a complex value, while coherence is the modulus of the coherency (Jarvis and Mitra, 2001; Henrie and Shapley, 2005). Normally, the spectrum is estimated by multiplying the Fourier transform of the data with a taper (windowing) to reduce the leakage errors. However, this single taper method also causes the loss of information (Percival and Walden, 1993; Mitra and Pesaran, 1999). Fortunately, this information loss can be recovered by introducing multiple orthogonal tapers during the procedure of spectral estimation. The final spectral estimate is the average quantity over individual tapered spectral estimates, which can effectively reduced the bias (Percival and Walden, 1993; Mitra and Pesaran, 1999; Jarvis and Mitra, 2001). The multi-taper method also provides some other computational advantages over single tapering, including supplying variance estimate by "jackknifing" (Thomson and Chave, 1991; Percival and Walden, 1993).

We used the Chronux package 1.0 (Chronux.org) to calculate the coherence spectra in cell pairs that showed synchronous firing based on the observation of peaks in the CCHs. Neural spike trains were computed within a 2 second window and sampled at a rate of 500 Hz. Coherence was estimated with the multi-taper method with five Slepian tapers. Each spectrum was calculated for a frequency range from 2 to 100 Hz and averaged by trials to reduce variance (Jarvis and Mitra, 2001), and 95% confidence intervals of the coherence, which measure the variance of the estimator, were calculated with the jackknifing method. The theoretical 95% confidence limits for the coherence were also established with multivariate statistics to examine whether the coherence is significant in certain frequency band(s) (Hannan, 1970; Jarvis and Mitra, 2001).

We smoothed the original normalized CCHs with a 5 msec moving average window. The time interval located between the two local minima on each side of the central peak on CCH defined the maximum time delay ($\Delta\tau$) of the synchronized spikes, which can be transformed into a critical phase interval (ϕ) by following equation (Jarvis and Mitra, 2001):

$$\phi(f) = 2\pi f \Delta\tau \tag{5-2}$$

We quantified the synchrony strength by integrating the area under the central peak on the smoothed CCH as a measure of the percentage of all synchronized spikes from the two spike trains. We further quantified the frequency dependence across a broad band (5-100 Hz) between two spike trains by integrating the areas underneath the coherence trace where the value of coherence exceeded the 95% confidence interval and the corresponding phase value was within the phase range derived from the above maximum time delay. Note that because we use an integrated value derived from the coherence plot

instead of a single peak value, the coherence strength is an arbitrary quantity which no longer ranges from 0 to 1.

We also applied a spike jitter method (Hatsopoulos et al., 2003) to evaluate how the frequency dependence between spike trains is affected by the spike timing accuracy. In this study, we defined three different jitter ranges, ± 5msec, ± 10msec, ± 20msec, and randomly jittered all the spikes uniformly within the different ranges. The spike jitter method will not change the average response rate or overall response statistics, but the fine temporal structure and the frequency components contained in the neural spike trains will be modified. Jittering with ± 20msec time range flattened the coherence spectra across the mid and high frequency ranges. To explore how coherence is affected by different ranges of jittering, we defined the coherence estimate with ± 20msec spike jittering as the "baseline" coherence. Following the method defined by Henrie and Shapley (2005), spectral modulation relative to the "baseline" was derived, frequency by frequency, as

$$M(f) = C(f) / C_{bl}(f) \tag{5-3}$$

while $M(f)$ was further transformed to a percentage change from "baseline" by

$$\Delta M(f) = (M - 1) \times 100\% \tag{5-4}$$

We recalculated the temporal correlation (normalized CCHs) and the coherence between cells after spikes were jittered, and observed that association between cells was changed in both the time and frequency domains.

Dependency Analysis

Besides evaluating the effect of perturbing spike timings on neural correlation with cross-correlation and coherence analysis, we further analyzed the functional dependency of synchronized pairs before and after spike jittering. The dependency analysis, which is originally derived from type analysis, measures the transneural correlation (Samonds et al., 2003). Type analysis and dependency analysis have been described in detail by Johnson et al. (2001) and Samonds et al. (2003). Briefly, spike trains were first translated into binary representations depending on whether or not a spike occurs within a time bin. The joint firing pattern of a pair of spike trains was then described by a temporal sequence of numbers based on the binary representation from the first step. Since we only studied dependency between cell pairs, these numbers ranged from 0 to 3. We calculated the observed firing/nonfiring probabilities of each neuron. The forced-independent firing/nonfiring probabilities between neurons were also estimated under the assumption that neurons are firing independently (Samonds et al., 2003). The Kullback-Leibler (KL) distance between the observed type and forced-independent type is calculated as:

$$d(P_1 \parallel P_2) = \sum_{b=1}^{B} \sum_{k=0}^{3} P_1(k_b) \times \log_2 \frac{P_1(k_b)}{P_2(k_b)} \tag{5-5}$$

in which P_1 indicates the observed firing/nonfiring probability while P_2 indicates the forced-independent firing/nonfiring probability. The letter B in Eq. 5-5 represents the index of bins. The dependency of neurons is then created by calculating the resistor average of the KL distances between the observed and force-independent types:

$$r(P_1, P_2) = \frac{d(P_1 \parallel P_2) \times d(P_2 \parallel P_1)}{d(P_1 \parallel P_2) + d(P_2 \parallel P_1)} \tag{5-6}$$

Results

We recorded a total of 66 cells in areas 17 and 18 of two anesthetized and paralyzed cats with a 10x10 Cyberkinetics microelectrode array. Traditional drifting sinusoidal gratings with fixed temporal and spatial frequency but varied orientations were used as visual stimuli. We first conducted cross-correlation analysis to identify synchronized cell samples. Coherence analysis was then applied with the multi-taper method on those synchronized cell pairs and linear regression analysis was performed between synchrony and coherence to reveal the correlation between the two quantities, derived from temporal and frequency domain analysis respectively. We also jittered the spike trains in our sampled data in order to assess the dependence of these two properties on timing accuracy and observed that both synchrony and coherence were significantly affected.

Synchrony Analysis

Temporal correlation between neural spike trains was measured by conducting cross-correlation analysis with the JPSTH method (Aertsen et al., 1989) on all possible 1057 cell pairs. Among these pairs we identified 694 (65.7% of total sampled pairs) that showed synchronized firing. Since 152 pairs (of 694) showed only moderate synchrony strength (lower than the level of significance defined in *Methods*), we only included data from the remaining 542 pairs. Our data set contains 1569 samples because 361 cell pairs synchronized their firing for more than one stimulus condition. The reason that we focused on cell pairs having stronger synchrony strength is because the better signal-to-noise ratio provides a clearer relationship between the analysis results in the time and frequency domains. Consistent with the previous findings (Ts'o et al., 1986; Eckhorn et

al., 1988; Gray et al., 1989; Engel et al., 1991; Kreiter and Singer, 1996; Kohn and Smith, 2005), we found that most synchronized cell pairs had some level of receptive field overlap (mean = 43%) while only 31 cell pairs (5.7%) had entirely separate receptive fields. The locations of our sampled cells were spread broadly in the visual cortex (distance between recording channels ranged from 0.4 to 4 mm). The mean distance between synchronized cells (interelectrode distance) was 1.77mm and the probability of neural synchrony decreased with the increasing distance between cells (Figure 5-1 A).

We also studied the influence of difference in cells' preferred orientations on synchrony strength from all synchronized cell pairs (N= 319) in one cat on which we tested the full range of orientations with 20^{o} increments. A drifting sinewave grating is effective in synchronizing the firing of a pair of cells only if this stimulus is drifting at an orientation that can drive both cells to reasonably high firing rates. More than half of the synchronized pairs showed synchrony for more than one stimulus orientation. If cells had the same orientation preference, the strongest synchrony was usually induced by gratings presented at this orientation. If cells had different orientation preferences, the stimulus orientation that induced the strongest synchrony was usually intermediate between the cells' preferred orientations (Kohn and Smith, 2005). Figure 5-1 B shows that cell pairs with smaller orientation differences tended to have stronger synchrony than cell pairs with larger differences in their preferred orientations. This was not simply a consequence of lower firing rate at non-optimal orientations, since the JPSTH is normalized for firing rate. Our result is in general agreement with previous reports that synchrony is dependent on the similarity of receptive field properties (Ts'o et al., 1986; Eckhorn et al., 1988; Gray et al., 1989; Engel et al., 1991). However, this result should be carefully interpreted. We

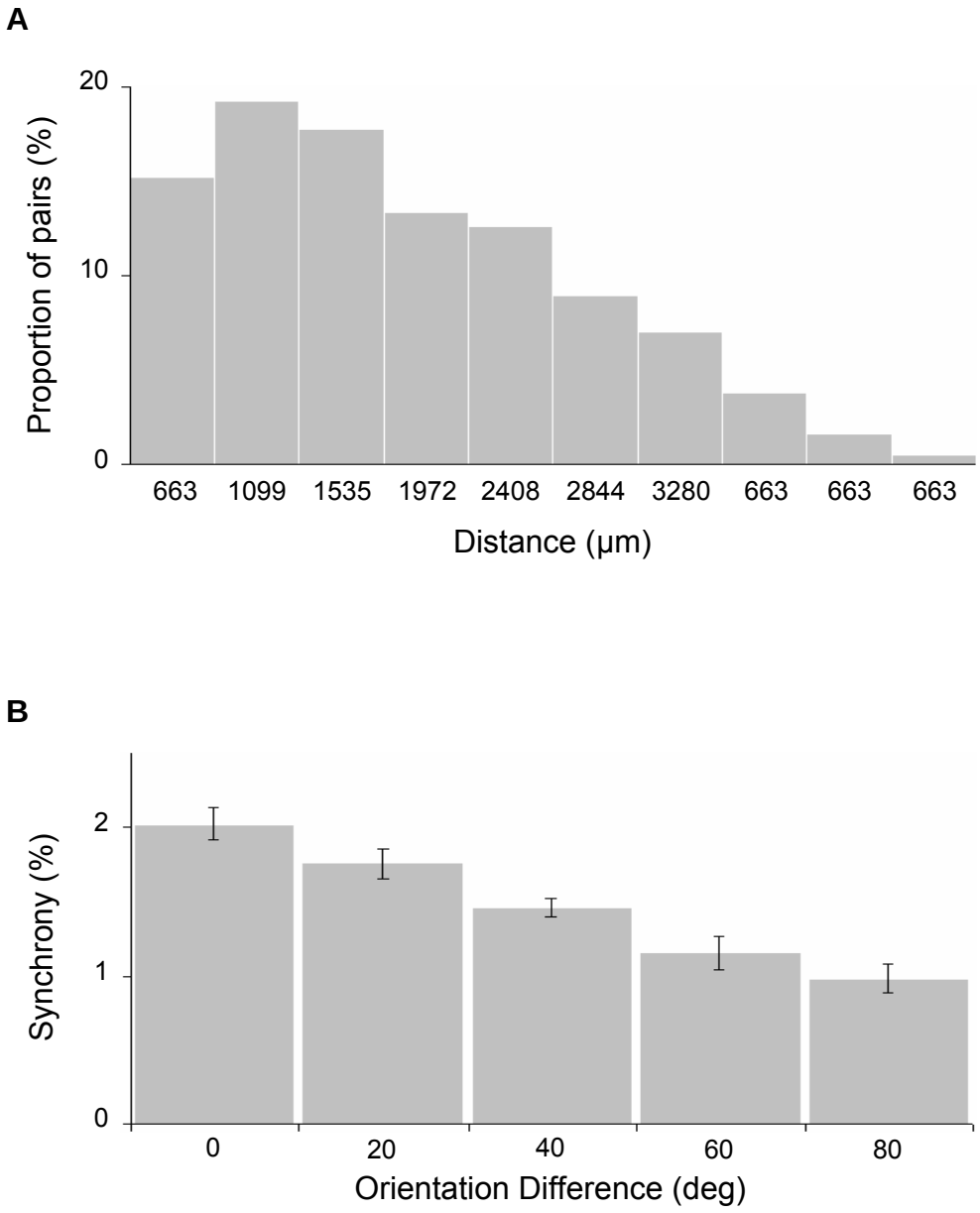

Figure 5-1: Relationship between synchrony and RF properties (A) Cells that are located closer to each other are more likely to synchronize their firing. (B) Cells pairs with less orientation difference tend to have stronger synchrony. Error bars indicate SEM.

only stimulated our cells with simple oriented gratings in this study, which may not adequately explore the role of synchrony in transmission of visual information. One-dimensional stimuli are only effective for cells with similar orientations, and we have found with two-dimensional stimuli that synchronization is primarily determined by the effectiveness of a stimulus in driving both cells simultaneously, as opposed to orientation similarities between the cells (Samonds et al., 2006).

Spectral Analysis

To explore the frequency components in neural spike trains that may contribute to neural synchrony, we conducted coherence analysis with the multi-taper method in cell pairs that showed significant synchrony under grating stimulation. Spectra were estimated across the frequency band from 2 to 100 Hz. All the cells we recorded were of complex type with a mean of $F1/F0 = 0.24 \pm 0.22$ (Hubel and Wiesel, 1962; Skottun et al., 1991). We consider that coherence at the lowest frequencies (ie. < 4 Hz) reflects response covariation corresponding to grating drift (2Hz) rather than originating from the network interactions. Therefore, we focused our analysis on the frequencies from 5 to 100 Hz. To examine if our coherence result is significant, we compare the coherence values estimated via jackknifing method with the theoretical confidence limits derived by multivariate statistical distribution (see *Methods*). Among all data samples, we found that 1542 (98.3%) showed a coherence value higher than the theoretical 95% confidence interval at certain frequency band(s), and the lower bounds of the coherence in 791 samples (51.2%) reached the theoretical 95% confidence interval.

As with the JPSTH analysis, we found that the strength of coherence decreases with the increase of distance between cells (recording sites). We divided our cell pairs into three subsets, short (<1500 μm), medium (1500 ~ 3000 μm) and long (>3000 μm) separation between cell pairs, and grouped our coherence results into three bins with coherence strengths based on the integrated area underneath the coherence curve and beyond the theoretical 95% confidence interval (see *Methods*). Histograms in Figure 5-2 show the relative proportion of cell pairs in every coherence strength category for each cell separation subset. For the subset with short distance between cells, a relatively large portion (61.7%) of pairs showed medium to strong coherence (integrated coherence ≥ 1.5). For cell pairs with medium and long separations, coherence is biased towards low coherence strengths.

In our analysis, we did not find any obvious relationship between the peaks in the spike spectra and the peaks of the coherence functions. In other words, the frequency bands of peaks in the individual cells' response spectra do not necessarily determine the frequency band in which the two spike trains show correlated firing. Figure 5-3 A shows an example in which two cells both exhibit elevated power around 30 Hz in their spike spectra, and the coherence has the highest peak at 31 Hz. The two cells in Figure 5-3 B have highest peaks at the frequency lower than 20 Hz, but the peak on their coherence curve is located at 42 Hz. Figure 5-3 C shows two cells have clear peaks in spike spectra in 40-50 Hz frequency bands, but their greatest coherence is located at 16 Hz .

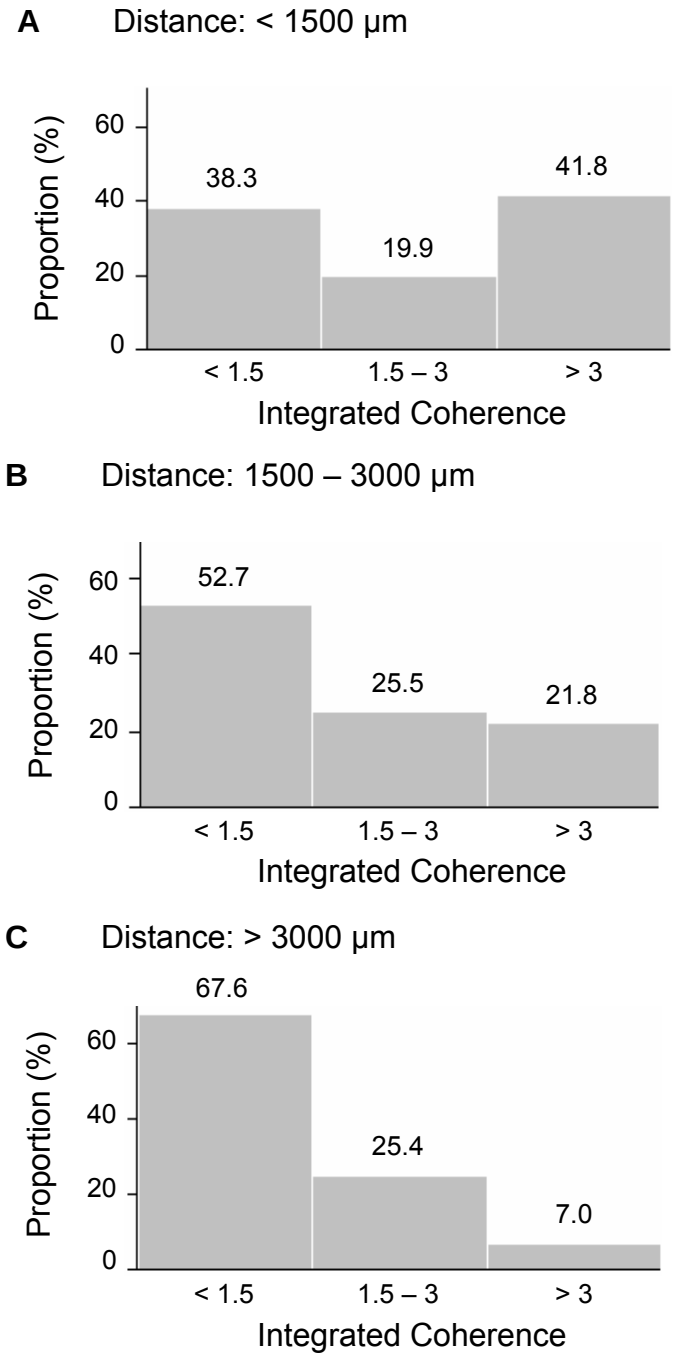

Figure 5-2: We divide our data samples into three subsets based on the distance between recording sites (A: less than 1500 µm; B: 1500 to 3000 µm; and longer than 3000 µm). We further binned our samples into three categories according to the integrated coherence (weak coherence: less than 1.5; medium coherence: 1.5 to 3; strong coherence: higher than 3). Histograms show coherence is stronger in cells with shorter distance between receptive fields than in cells with longer distance.

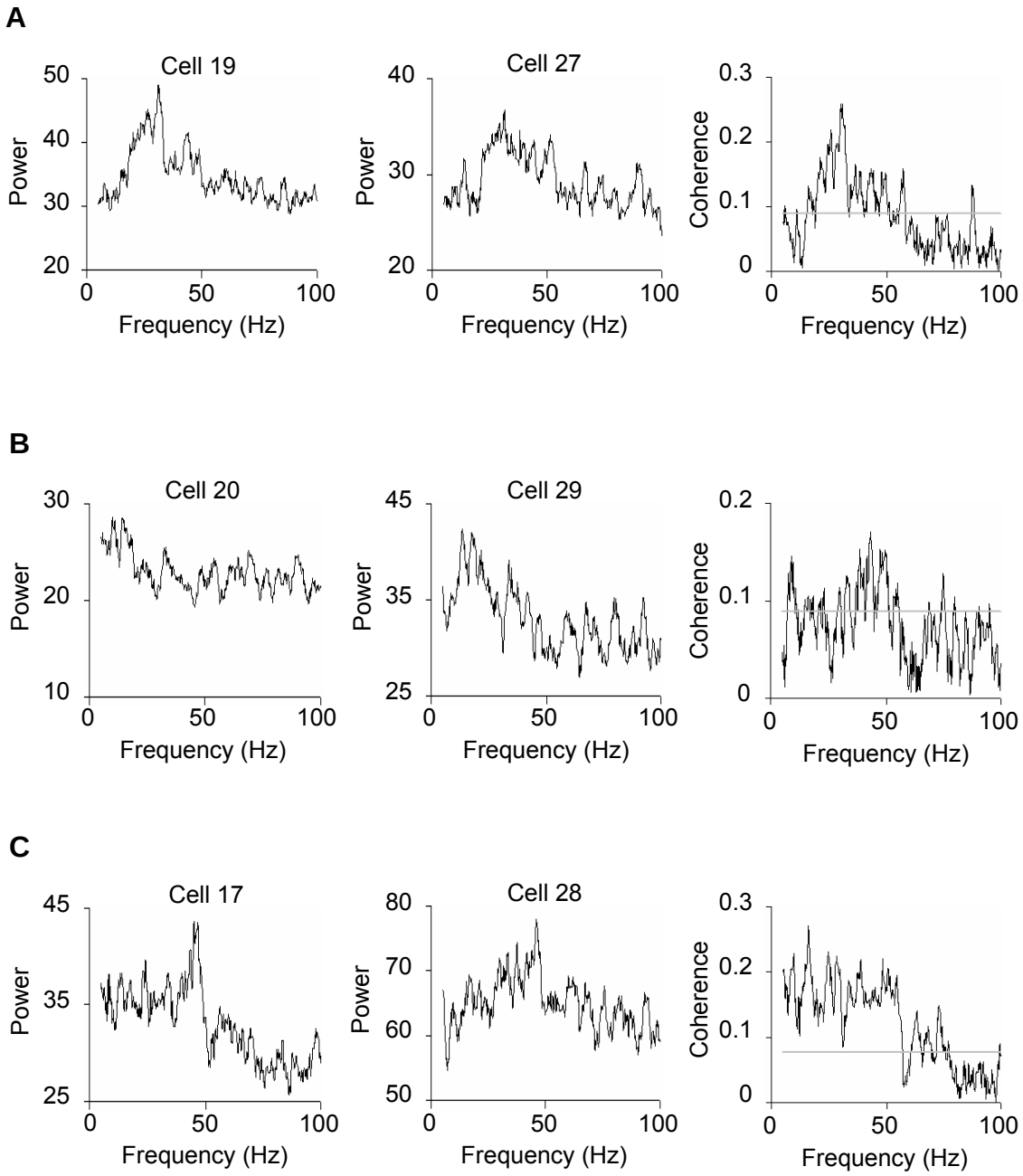

Figure 5-3: Examples of spectral analysis (A) cells 19 and 27 both showed elevated power around 30 Hz (left and middle plots), and the coherence between these two cells is highest at 31 Hz (right plot). (B) The highest coherence for cells 20 and 29 is found at 42 Hz (right plot), though the highest peaks on the power spectra for both cells are located at the frequency band lower than 20 Hz (left and middle plots). (C) Cells 17 and 28 both showed peaks in 40 to 50 Hz range on their power spectra (left and middle plots), but the highest coherence is located at 16 Hz. The gray horizontal lines in the coherence plots indicate the 95% confident limit.

Correlation between JPSTH and Coherence Analysis

We conducted linear regression analysis between coherence and synchrony to observe whether the two estimates, derived from the time and frequency domains, showed any systematic correlation in the context of biological signals. The appearance of a central peak in the CCH indicates that two cells synchronize a certain percentage of their spikes (Perkel et al., 1967; Aertsen et al., 1989). The area underneath this central peak was thus treated as the total accumulation of synchronized spikes (with slightly different time delays) from the two spike trains. With coherence analysis, frequency-dependent correlation between two signals is implied by a coherence value beyond a certain confidence limit (Jarvis and Mitra, 2001; Brown et al., 2004). For each pair of cells, we quantified total coherence by integrating the area between the coherence curve and the 95% confidence limit over a frequency range of 5 to 100 Hz. Coherence may not be directly related to synchrony unless the time offset translated from the phase of the coherency (see *Methods*) is within a time range that corresponds to the width of the central peak of the CCH, so we ignored the area under the coherence curve where the phase of the coherency fell out of the range defined by the width of the peak of the CCH. The scatter plot in figure 5-4 shows the relationship between these integrated quantities for each data sample (N = 1569). The location of a large number of data points close to the zero coordinates is not surprising. Our data set contains cell pairs that show synchronized firing for both optimal and non-optimal orientations, and the latter drive synchronous responses less effectively. Overall coherence is strongly correlated with synchrony ($R^2 = 0.63$), which suggests that these two quantitative methods of analysis reflect fundamentally the same neurological response properties.

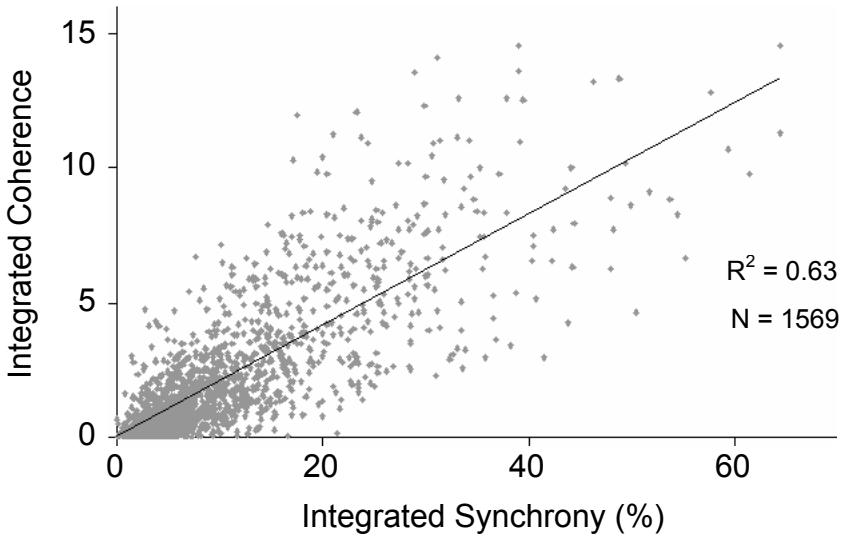

Figure 5-4: Linear regression analysis between synchrony and coherence. Strong correlation was found between results from coherence and JPSTH analysis.

Temporal Structure and Neural Correlation

The fine temporal structure in neural spikes cooperates with the average response rate of visual neurons to provide visual information, though these two variables have different roles in coding specific properties (Cattaneo et al., 1981; Debusk et al., 1997; Snider et al., 1998; Castelo-Branco et al., 2000; Samonds et al., 2003, 2004; Samonds et al., 2006). We applied a spike jittering method with different time ranges (±5msec, ±10msec, and ±20msec) to perturb the timing accuracy in the spike trains systematically at different levels to see how both synchrony and coherence depend on fine structure, as opposed to general response organization or chance. We are trying to clarify that correlation between neural responses is induced specifically instead of resulting accidentally from spike rate modulation.

We also studied the response distribution of the spike trains before and after jittering to ensure that the jittering procedure does not change the overall statistics of the response. One characteristic feature in visual cortical responses is the high variability exhibited in the discharge pattern (Softky and Koch, 1993; Shadlen and Newsome, 1998), which is also found in our data. We examined the response variation of all the spike trains (N = 596) in our sampled data. The variation coefficient ($C_{V_{ISI}} = SD_{ISI} / mean_{ISI}$) of interspike intervals (ISIs) in the unperturbed spike trains ranges from 0.5 to 1.17 while the variation coefficient of response rate ($C_{V_{FR}} = SD_{FR} / mean_{FR}$) ranges from 0.17 to 2.37. Our result (mean of $C_{V_{ISI}}$ = 0.64; mean of $C_{V_{FR}}$ = 0.69) is in agreement with the previous reports that neural response has high variability even for the exactly same stimulus (Softky and Koch, 1993; Shadlen and Newsome, 1998). We compared ISI and PSTH distributions derived from the original spikes trains with the ISI and PSTH distributions

after spike jittering at different jittering ranges (Figures 5-5 & 5-6). After spike jittering, 5 percent of spike trains (30/596) changed the ISI distribution significantly (two-tailed Kolmogorov-Smirnov test, $\alpha = 0.05$) while only one of the spike trains showed significant changes in its PSTH distribution (two-tailed Kolmogorov-Smirnov test, $\alpha = 0.05$). Thus, the jitter procedure not only keeps the firing rate constant but also maintains statistical characteristics of the overall response.

We then refined our study to include only data samples (N = 1280) that did not show significant change in either ISI or PSTH distribution. In the refined data sample, we found both the amplitude of synchrony and the integrated coherence derived from the unperturbed spike trains are significantly higher than those derived from the spike trains jittered with different ranges (paired student's t-test, $p<10^{-10}$). Figure 5-7 shows an example of synchrony and coherence analysis results from one cell pair. These two cells have similar orientation preferences (110º and 150º) and show synchronized firing with stimulation by a moving grating (orientation = 140º) that is effective in driving both cells. Strong frequency dependence between these two cells was mainly focused in the gamma band with the highest coherence value (coherence = 0.26) located at 52 Hz. After the spikes of both cells were randomly jittered across a ±5msec range, synchrony and the coherence strength reduced dramatically. When the two spike trains were jittered across broader time ranges (±10msec and ±20msec), the central peaks on the CCHs were nearly extinguished and the frequency dependence between these two cells was almost destroyed completely.

The reduction of temporal and frequency dependence after spike jittering also applies to our entire population. We averaged the synchrony and coherence curves for all

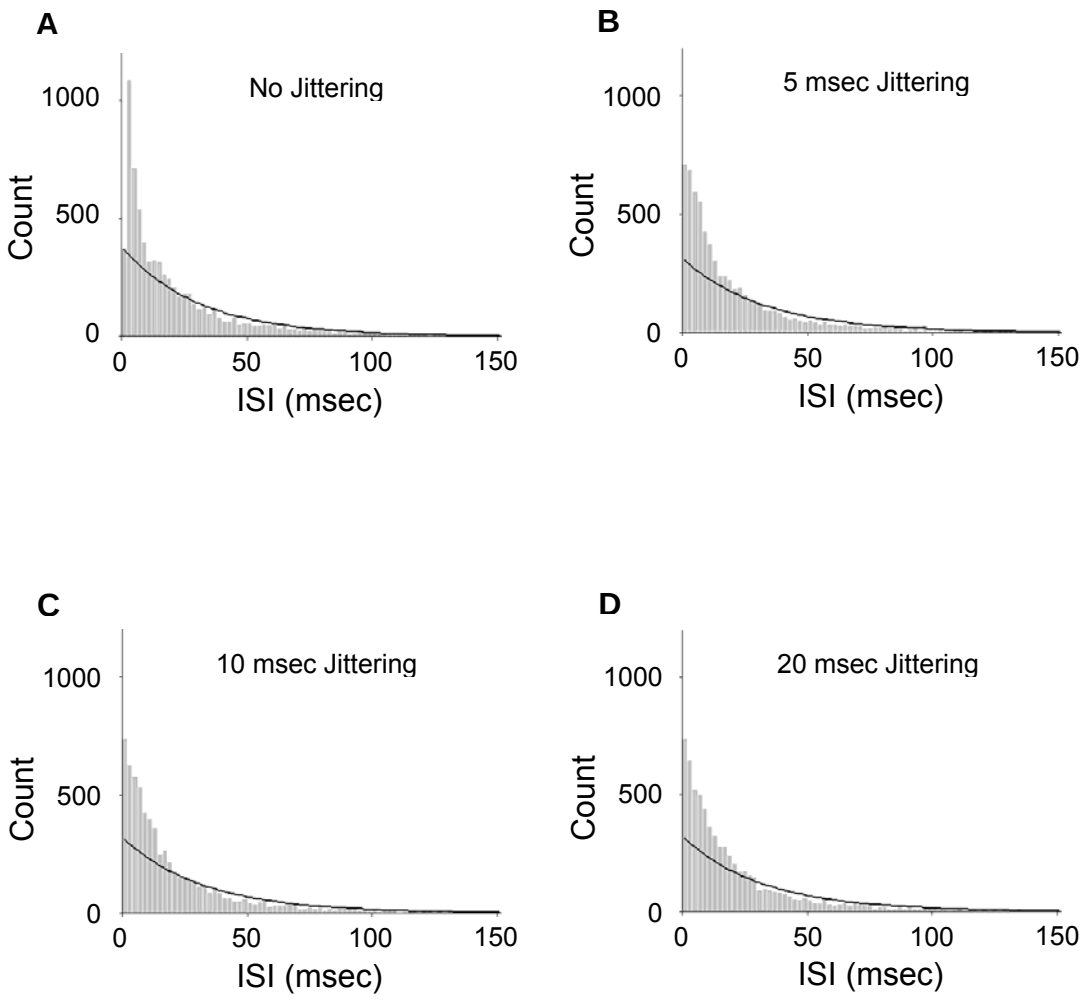

Figure 5-5: Example histograms of ISI before and after spike jittering (A) ISI histogram without spike jittering. (B) ISI histogram with spikes jittered over ±5 msec time interval. (C) ISI histogram with spikes jittered over ±10 msec time interval. (D) ISI histogram with spikes jittered over ±20 msec time interval.

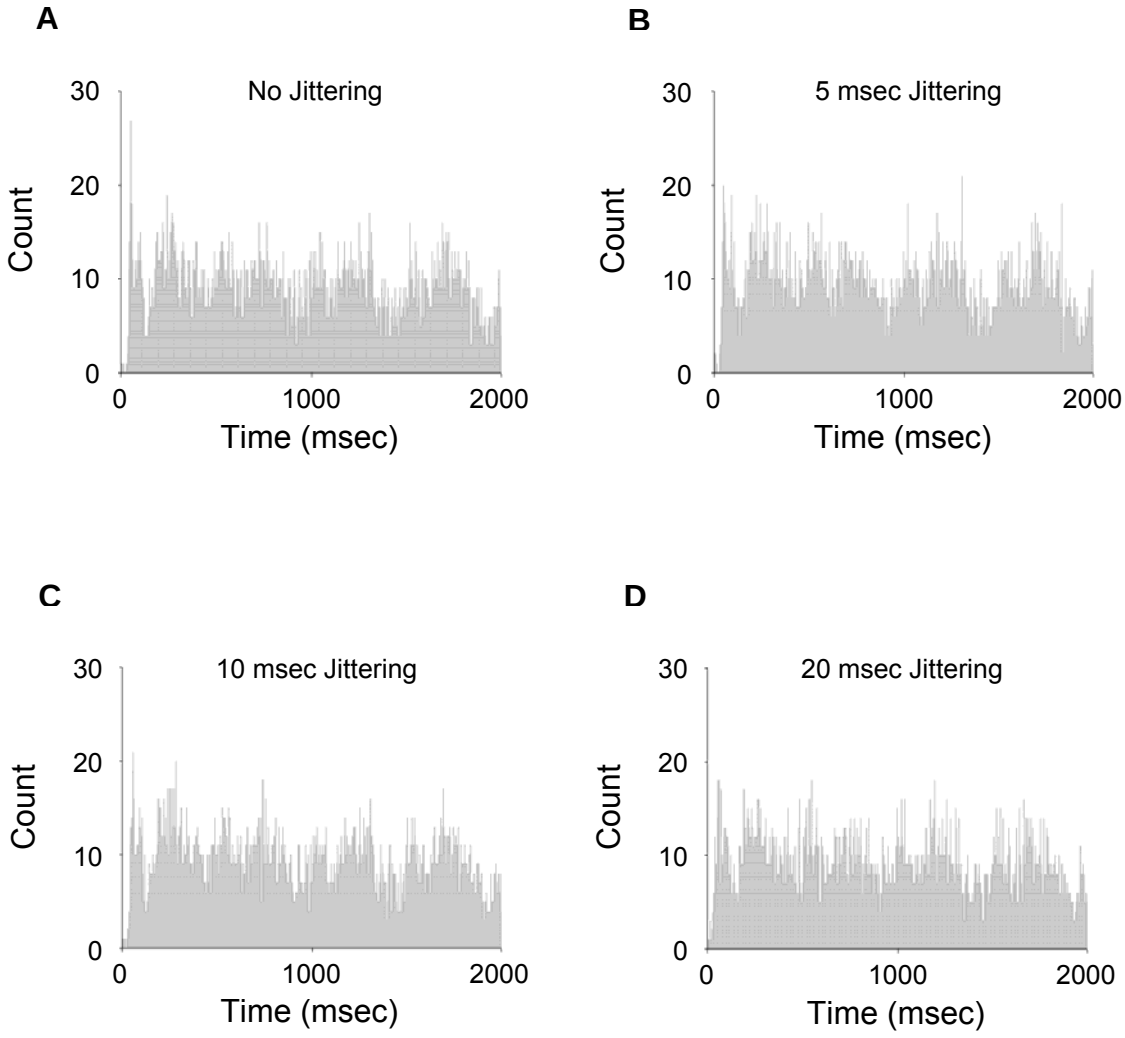

Figure 5-6: Example histograms of PSTH before and after spike jittering (A) PSTH histogram without spike jittering. (B) PSTH histogram with spikes jittered over ±5 msec time interval. (C) PSTH histogram with spikes jittered over ±10 msec time interval. (D) PSTH histogram with spikes jittered over ±20 msec time interval.

Figure 5-7: Example of synchrony and coherence modulate systematically with the increase of spike jittering range (A) The CCH (left) and coherence (right) plots for the original spike trains show two cells having strong correlation in both time and frequency domains. The gray area around the coherence curve represents the upper and lower bounds of the coherence estimate. The gray horizontal line in the coherence plot indicates the 95% confident limit. (B) Synchrony and coherence both reduced after the spike trains were jittered in ±5msec range. (C) Synchrony and coherence both reduced further after the spike trains were jittered in ±10msec range. (D) After the spike trains were jittered in ±20msec range, the peak on CCH is hardly detectable, and the area between coherence curve and 95% confidence limit almost disappears.

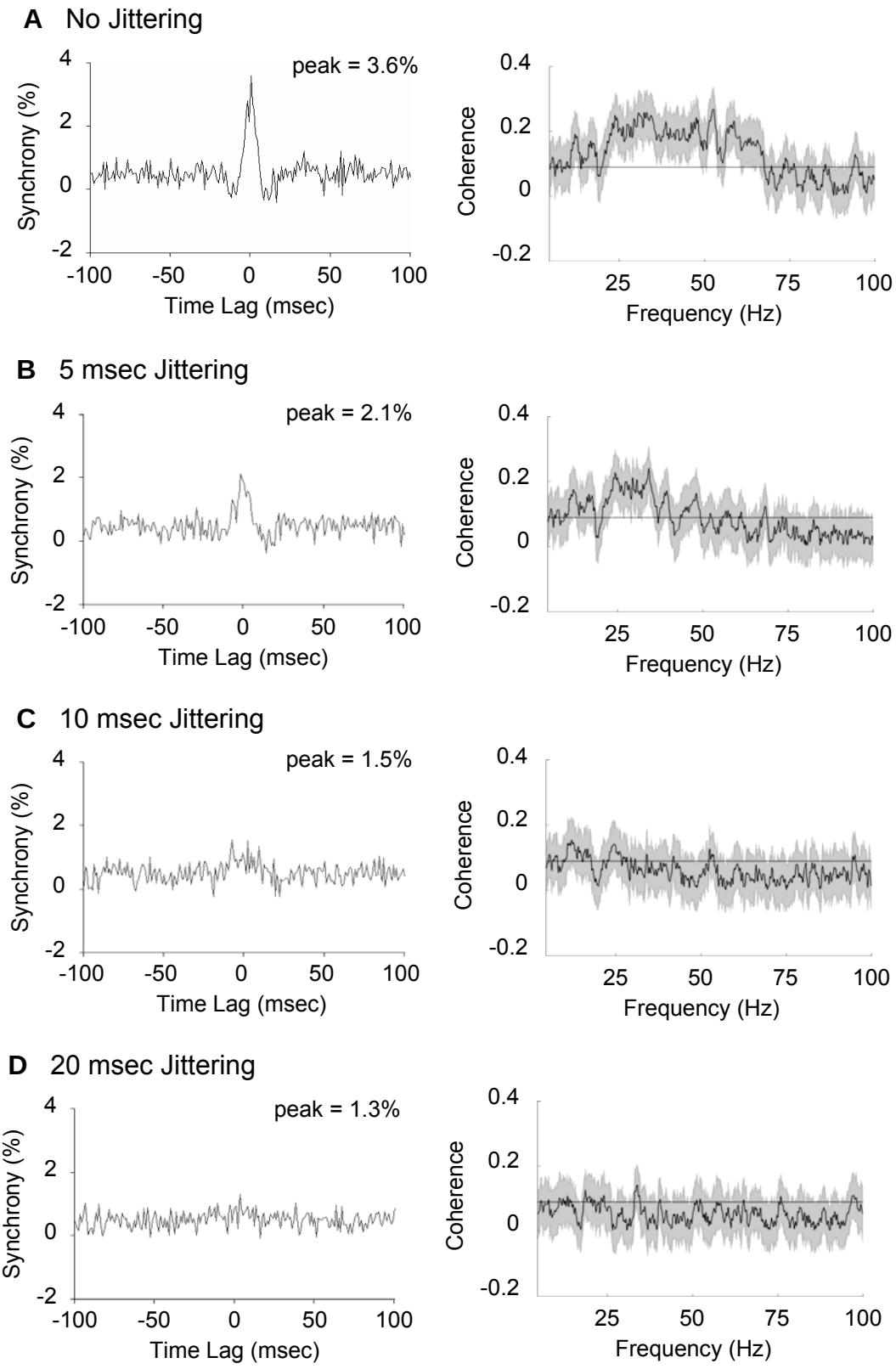
A No Jittering
peak = 3.6%
Synchrony (%)
Time Lag (msec)
Coherence
Frequency (Hz)
B 5 msec Jittering
peak = 2.1%
Synchrony (%)
Time Lag (msec)
Coherence
Frequency (Hz)
C 10 msec Jittering
peak = 1.5%
Synchrony (%)
Time Lag (msec)
Coherence
Frequency (Hz)
D 20 msec Jittering
peak = 1.3%
Synchrony (%)
Time Lag (msec)
Coherence
Frequency (Hz)

synchronized pairs we identified, with results shown in Figures 5-8 and 5-9. The average synchrony is highest before spike trains were jittered. On the averaged CCH, the peak amplitude is 1.16% and is located at 0 msec delay. After the spikes were jittered randomly with increased time ranges (±5 msec, ±10 msec, and ±20 msec), synchrony gradually reduced to 0.82%, 0.66%, 0.56% respectively with statistical significance (paired student's t-test, $p<10^{-10}$). Meanwhile, the width of the central peak on the averaged CCHs also increased when the spikes were jittered across a broader time range, indicating a disruption of the temporal relationship between cells.

We find that the average coherence spectrum for the unperturbed spike trains has its greatest power in the lower frequency bands and a second peak on the coherence curve is found in the gamma range, around 45 Hz (Figure 5-9 A). As expected, the power in the coherence spectrum gradually decreases with the increase of the spike jittering range. When spikes were jittered in the ±5msec range, the second coherence peak disappeared, and when spikes were jittered in the ±10 or ±20msec range, the coherence trace in the gamma range flattened. To explore how much frequency dependence is embedded in the fine temporal structure, we derived a figure for coherence modulation with respect to the "baseline" coherence (i.e., coherence expected in the absence of fine coordination), which is defined by the average coherence for spike trains jittered in the ±20msec range (see *Methods*). Figure 5-9 B shows, for the average coherence from the original spike trains, the coherence modulation is highest at 46 Hz and falls off gradually towards the lower and higher frequency bands. For the average coherence from spike trains jittered in ±5 and ±10msec ranges, modulations are lower than that from the "raw" spike trains and the modulation peaks shift towards the lower frequency (peaks locate at 20 and 13 Hz

respectively). We compared the modulation loss among alpha (5 – 15 Hz), beta (15 – 35 Hz), and gamma bands. For each band, we integrate the areas below the modulation curves with different jittering ranges (no jittering, ±5 msec jittering, or ±10 msec jittering). In the alpha band, the integrated area was reduced by 9.1% or 34.1% respectively after ±5 msec or ±10 msec jittering. In the beta band, reduction was 29.6% or 75.9% respectively after ±5 msec or ±10 msec jittering. In the gamma band, however, the reduction was 76.4% or 100% after ±5 msec or ±10 msec jittering. Our results suggest that the fine temporal structure in neural spike trains is critical in maintaining the frequency dependence between neurons, and that the frequency band that is most sensitive to the integrity of the temporal structures in the neural spike trains is the gamma band.

We last explored if there is any information loss due to spike jittering by calculating the functional dependency (resistor averaged KL distance between observed type and forced-independent type). The dependency tuning was calculated on 51 cell pairs, for which the orientation preference was the same within each pair. Dependency was calculated for both original and jittered spike trains with temporal resolutions from 1 to 10 msec and the result at the temporal resolution yielding the maximum dependency was chosen to build the dependency tuning. The example in figure 5-10 A shows that tuning response was systematically reduced with the increase the jittering range. Dependency was further quantified for different jittering ranges by integrating the area underneath the corresponding tuning curves and average across sampled pairs. We found the mean dependency to be highest (7.16 bits) with the original spike trains and drops to 5.93, 5.00, and 4.52 bits respectively with spikes jittered in ±5, ±10, and ±20 msec ranges

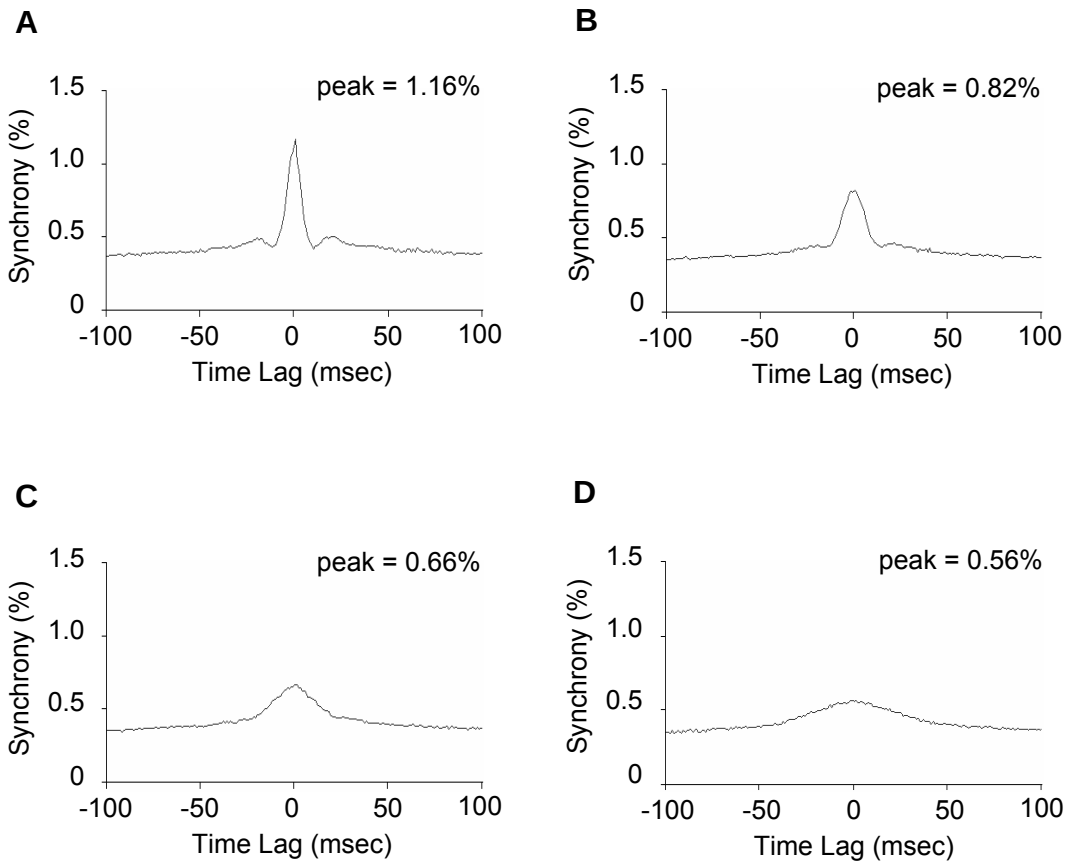

Figure 5-8: The population averaged synchrony estimates with spike jittering (A) The average CCH from the original spike trains shows a sharp peak centered at 0msec delay. (B-D) After the spike trains were jittered in ±5msec, ±10msec, and ±20msec ranges, the peak of the averaged CCH reduced and the peak width increased systematically.

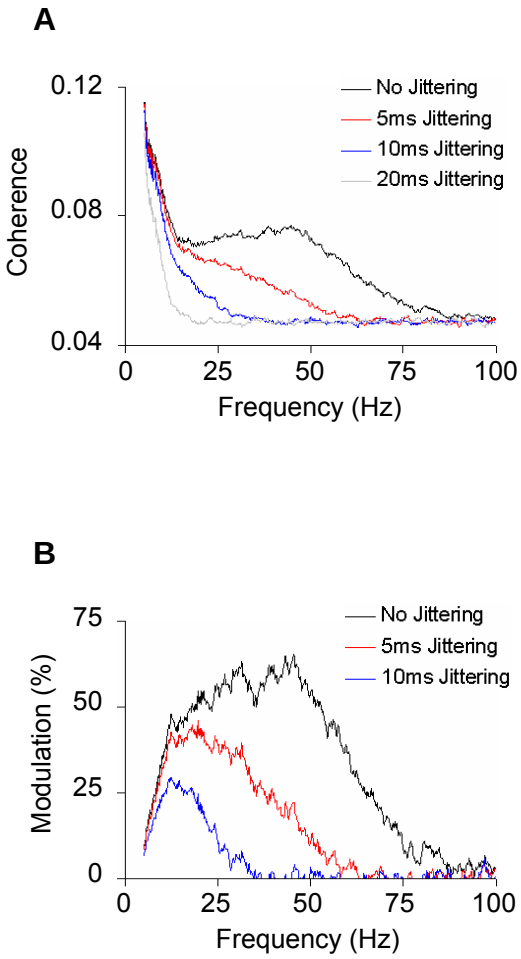

Figure 5-9: The population averaged coherence estimates with spike jittering (A) The average coherence of the "raw" spike trains (black curve) shows the greatest power in low frequency band and displays a second peak at 45 Hz. After the spike trains were jittered in ±5msec range, the second peak on the averaged coherence (red curve) disappeared. After the spikes were jittered in ±10msec and ±20msec ranges, the average coherence (blue and gray curves) became flat lines in gamma range. (B) With the average coherence of spike trains jittered in ±20msec range defined as the "baseline" coherence, the coherence from the "raw" spike trains shows greatest modulation (black curve) with a peak located at 46 Hz. When spikes trains were jittered in ±10msec and ±20msec ranges, coherence modulation (red and blue curves) reduced and the peak of the modulation shifted to frequency band lower than gamma band.

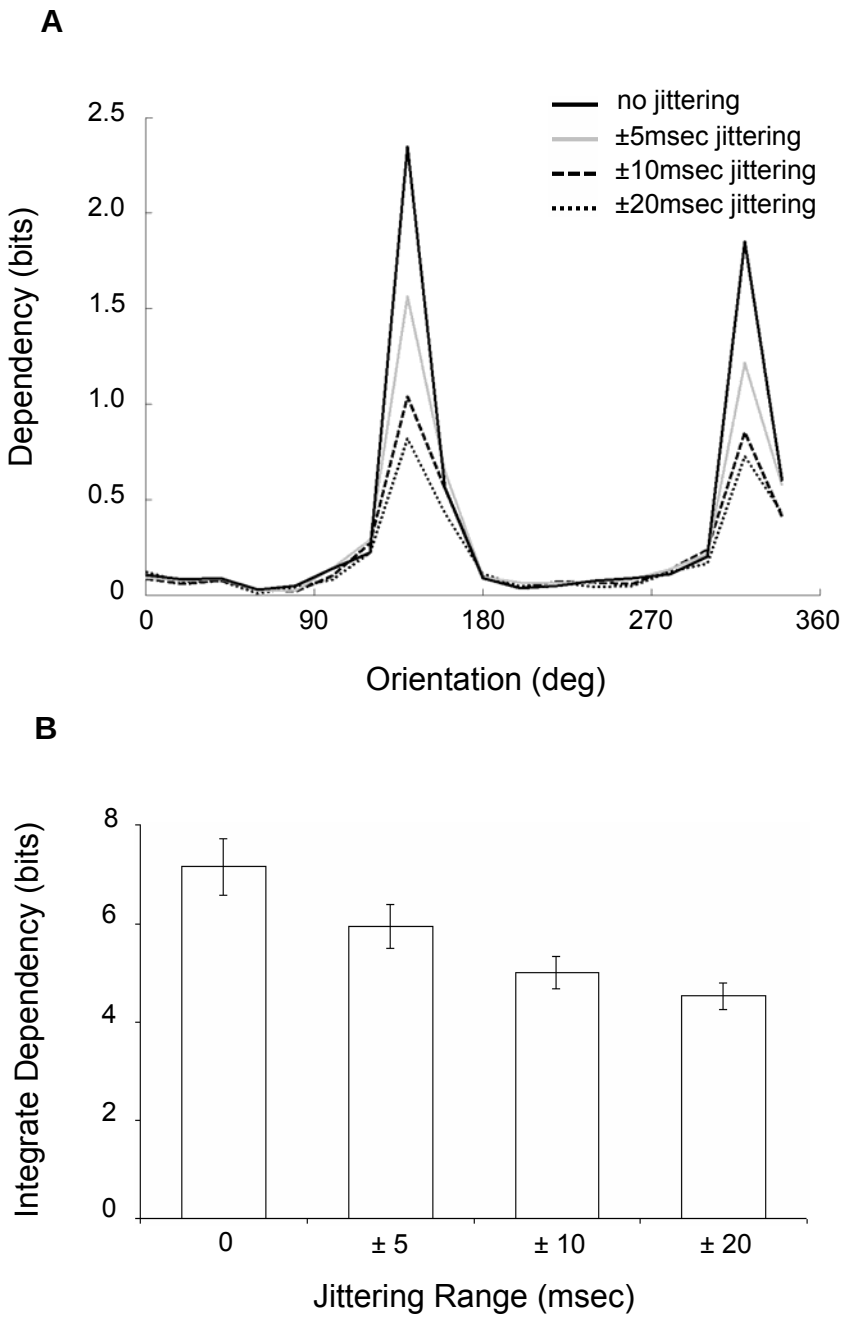

Figure 5-10: Dependency analysis (A) An example of dependency tunings for the original and jittered spike trains. (B) Mean integrated dependency systematically reduced with the increase of jittering range. Error bars indicate SEM.

(Figure 5-10 B), indicating significant information loss (One-way ANOVA test, $p<0.0001$) after the spike timing was perturbed.

Discussion

In cat visual cortical cells (areas V1 and V2) stimulated with sinewave gratings, coherence analysis and the CCHs derived from JPSTHs showed high correlation. This consistency validates both analytical approaches for studying the associative relationship between neural spike trains. We also perturbed the timing accuracy of the original neural spike trains by jittering the spike timing. We found that synchrony and coherence both systematically decrease with the increase of the jittering time range while the coherence in the gamma frequency band exhibits the greatest loss.

Temporal and Spectral Analysis of Neural Cooperation

The most commonly used methods for investigating the association between neural firing include time domain and frequency domain analysis. With the development of multi-electrode recordings, cross-correlation analysis (Perkel et al., 1967; Aertsen et al., 1989) has been extensively used to study the role of neural synchrony in visual perception. A shift predictor is generally subtracted from the raw CCHs to remove the expected synchrony from chance (Perkel et al., 1967; Aertsen et al., 1989). However, its application for studying associations between neural responses has been challenged by the proposal that peaks in the CCH may be induced by trial by trial latency and excitability covariations, which confound the estimation of spike timing synchronization (Brody, 1999a; Brody, 1999b; Brown et al., 2004). Meanwhile, because factors such as

ISI and spike count in the discharge pattern are highly irregular, the temporal structures embedded in the neural spike trains have been considered to merely reflect noise and contain little meaningful information (Shadlen and Newsome, 1998). The spike jittering process applied in our study preserved both the mean firing rate and the overall response dynamics (ISI and PSTH distributions derived over multiple trials). What has been interrupted is the common fine temporal structure contained in the synchronized spike trains. The attenuation of neural synchrony and coherence after spike jittering indicates that the correlation between neurons in both time and frequency domains is not a trivial consequence of response rate statistics but rather results from some causal mechanisms, arising from stimuli and/or brain network interactions.

The method of normalization of the JPSTH has also been criticized as inadequate, especially in cases of higher firing rates (Ito and Tsuji, 2000). To examine the validity of the normalization implemented in the JPSTH on real data, we compared the results between time and frequency domain analysis. Coherence analysis has several advantages over time domain analysis, which include insensitivity to nonstationarity in the discharge history and more effective normalization than time domain correlation analysis (Jarvis and Mitra, 2001). Initial studies based on computer simulated data suggest that coherence analysis and cross-correlation analysis are complimentary to each other. Moritz et al. (2005) reported that synchronized neural discharges in simulated motor neurons can induce a peak between 16 – 32Hz in the coherence spectrum. The amplitude and the area of the coherence peak are strongly correlated with the strength of synchrony. Here we report that regression analysis between JPSTH analysis and coherence analysis on responses from visual cortical cells is consistent with Moritz's finding. The strong

correlation between the results from both methods not only implies that the coherence analysis and JPSTH method are internally related, but also supports the validity of the normalization procedure applied in JPSTH analysis.

Temporal Structure and Neural Cooperation

Earlier studies have described emergent information in visual cortical neurons that is independent of the average response rate. Cattaneo et al. (1981) reported that spikes within bursts ("clustered spikes", with intervals of 8 msec or less) and outside bursts ("isolated spikes") have detection sensitivities to different attributes of the stimulus. Clustered spikes are more finely tuned for orientation and spatial frequency while both the isolated and clustered spikes are sensitive to contrast change. DeBusk et al. (1997) also found that, at a given firing rate, optimal orientations can induce bursts with greater length than nonoptimal orientations. With information-theoretic analysis, Dan et al. (1998) found that more information can be extracted from the activity of LGN neurons if temporal correlations between neurons are considered. The percentage increase can be as high as 20% in strongly synchronized pairs. The information carried by cooperative responses in neural ensemble is restricted within a limited time interval. By applying type analysis, Samonds et al. (2003) found that cooperativity between synchronized complex cells in cat area 17 enhances fine orientation discrimination beyond the coding of the firing rate, and that the information is primarily contained within 10 msec time window.

The question remains as to whether this information is useful. Any candidate mechanism for coding neural information requires a means for discriminating the code. In the case of neural synchrony, this is readily provided by spatial summation:

synchronized inputs are more efficient than isolated spikes in eliciting action potentials on postsynaptic neurons (Alonso et al., 1996; Usrey et al., 1998). The effective window for temporal summation of synchronized inputs is generally considered to be about 10 msec (Softky and Koch, 1993; Diesmann et al., 1999; Larkum et al., 1999). This summation may be more than simply linear, since rapid depolarization lowers the voltage threshold for spiking in postsynaptic cells (Azouz and Gray, 2000). Here we have confirmed by systematic disruption of the fine structure within the spike trains that timing on a scale of 10 msec is critical for maintaining the information contained in both the cross-correlation as well as the spectrally-organized cooperation (gamma oscillation). Whether the "tuning" of the post-synaptic membrane to be specifically sensitive to timing on this scale validates the concept that this is a functionally significant means of transmitting visual information remains open to debate, but it is certainly both supportive and suggestive.

Source of Oscillation

Frequency dependence of cooperative neural firing is thought to result from common excitatory or inhibitory inputs (Rosenberg et al., 1998). A presynaptic cell is likely to transmit any periodicity in its firing pattern to common recipient cells, which would result in coherence at the corresponding frequency band. Although coherence between two cells can display a prominent elevation at a particular frequency, here we often found that the power spectra of the individual cells may have no relationship to this peak. Therefore, common oscillatory input is not necessary to produce periodically associated firing between single cells, though the synchrony is stronger in cell pairs with oscillation

than in cells with no oscillation (Samonds and Bonds, 2005). Gray and Singer proposed that the oscillation around 40 Hz found in the visual cortex originates from intracortical mechanisms, since no similar oscillation was found in the thalamic input to visual cortex (Gray and Singer, 1989). Ghose and Freeman showed, however, that intracortical connections are not necessary to produce cortical oscillations, while lateral geniculate nucleus (LGN) oscillation combined with intrinsic cortical oscillators maybe induce oscillation in visual cortex.

The spectral analysis in our study shows that oscillation in the cat's primary visual cortex is not a simple harmonic of the temporal and spatial frequency features in the visual stimuli. However, neurons with receptive fields being co-activated by the sustained stimulation of the coherent structures in the visual stimulus could synchronize their responses as a consequence of similar response latencies (Fries et al., 2001; Samonds and Bonds, 2005; Samonds et al., 2006).

REFERENCES

Aertsen AM, Gerstein GL, Habib MK, Palm G (1989) Dynamics of neuronal firing correlation: modulation of "effective connectivity". J Neurophysiol 61:900-917.

Aksay E, Baker R, Seung HS, Tank DW (2003) Correlated discharge among cell pairs within the oculomotor horizontal velocity-to-position integrator. J Neurosci 23:10852-10858.

Albrecht DG, De Valois RL, Thorell LG (1980) Visual cortical neurons: are bars or gratings the optimal stimuli? Science 207:88-90.

Alonso J-M, Usrey WM, Reid RC (1996) Precisely correlated firing in cells of the lateral geniculate nucleus. Nature 383:815-819.

Azouz R, Gray CM (2000) Dynamic spike threshold reveals a mechanism for synaptic coincidence detection in cortical neurons in vivo. Proc Natl Acad Sci USA 97:8110-8115.

Barlow HB (1972) Single units and sensation: a neuron doctrine for perceptual psychology? Perception 1:371-394.

Bonds AB (1989) Role of inhibition in the specification of orientation selectivity of cells in the cat striate cortex. Vis Neurosci 2:41-55.

Brody CD (1999a) Correlations without synchrony. Neural Comput 11:1537-1551.

Brody CD (1999b) Disambiguating different covariation types Neural Comput 11:1527-1535.

Brown EN, Kass RE, Mitra PP (2004) Multiple neural spike train data analysis: state-of-the-art and future challenges. Nat Neurosci 7:456-461.

Castelo-Branco M, Goebel R, Neuenschwander S, Singer W (2000) Neural synchrony correlates with surface segregation rules. Nature 405:685-689.

Cattaneo A, Maffei L, Morrone C (1981) Two firing patterns in the discharge of complex cells encoding different attributes of the visual stimulus. Exp Brain Res V43:115-118.

Dan Y, Alonso J-M, Usrey WM, Reid RC (1998) Coding of visual information by precisely correlated spikes in the lateral geniculate nucleus. Nat Neurosci 1:501-507.

De Valois RL, Albrecht DG, Thorell LG (1982) Spatial frequency selectivity of cells in macaque visual cortex. Vision Res 22:545-559.

Debusk BC, Debruyn EJ, Snider RK, Kabara JF, Bonds AB (1997) Stimulus-Dependent Modulation of Spike Burst Length in Cat Striate Cortical Cells. J Neurophysiol 78:199-213.

Desimone R, Albright TD, Gross CG, Bruce C (1984) Stimulus-selective properties of inferior temporal neurons in the macaque. J Neurophysiol 4:2051-2062.

Diesmann M, Gewaltig M-O, Aertsen A (1999) Stable propagation of synchronous spiking in cortical neural networks. Nature 402:529-533.

Eckhorn R, Bauer R, Jordan W, Brosch M, Kruse W, Munk M, Reitboeck HJ (1988) Coherent oscillations: A mechanism of feature linking in the visual cortex? Biological Cybernetics V60:121-130.

Engel AK, Kreiter AK, Konig P, Singer W (1991) Synchronization of oscillatory neuronal responses between striate and extrastriate visual cortical areas of the cat. Proc Natl Acad Sci USA 88:6048-6052.

Engel AK, Konig P, Kreiter AK, Schillen TB, Singer W (1992) Temporal coding in the visual cortex: new vistas on integration in the nervous system. Trends in Neurosciences 15:218-226.

Fries P, Neuenschwander S, Engel AK, Goebel R, Singer W (2001) Rapid feature selective neuronal synchronization through correlated latency shifting. Nat Neurosci 4:194-200.

Gail A, Brinksmeyer HJ, Eckhorn R (2000) Contour Decouples Gamma Activity Across Texture Representation in Monkey Striate Cortex. Cereb Cortex 10:840-850.

Gallant JL, Connor CE, Rakshit S, Lewis JW, Van Essen DC (1996) Neural responses to polar, hyperbolic, and Cartesian gratings in area V4 of the macaque monkey. J Neurophysiol 76:2718-2739.

Gerstein GL, Perkel DH (1972) Mutual temporal relationships among neuronal spike trains. Biophys J 12:453–473.

Gray CM (1999) The Temporal Correlation Hypothesis of Visual Feature Integration: Still Alive and Well. Neuron 24:31-47.

Gray CM, Singer W (1989) Stimulus-Specific Neuronal Oscillations in Orientation Columns of Cat Visual Cortex. Proc Natl Acad Sci USA 86:1698-1702.

Gray CM, Konig P, Engel AK, Singer W (1989) Oscillatory responses in cat visual cortex exhibit inter-columnar synchronization which reflects global stimulus properties. Nature 338:334-337.

Hannan EJ (1970) Multiple time series. New York: Wiley.

Hatsopoulos N, Geman S, Amarasingham A, Bienenstock E (2003) At what time scale does the nervous system operate? Neurocomputing 52-54:25-29.

Henrie JA, Shapley R (2005) LFP Power Spectra in V1 Cortex: The Graded Effect of Stimulus Contrast. J Neurophysiol 94:479-490.

Hubel DH (1989) Eye, Brain, and Vision. New York : Scientific American Library.

Hubel DH, Wiesel TN (1962) Receptive fields, binocular interaction and functional architecture in the cat's visual cortex. J Physiol 160:106-154.

Ito H, Tsuji S (2000) Model dependence in quantification of spike interdependence by joint peri-stimulus time histogram. Neural Comput 12:195-217.

Jarvis MR, Mitra PP (2001) Sampling properties of the spectrum and coherency of sequences of action potentials. Neural Comput 13:717-749.

Kohn A, Smith MA (2005) Stimulus Dependence of Neuronal Correlation in Primary Visual Cortex of the Macaque. J Neurosci 25:3661-3673.

Kreiter AK, Singer W (1996) Stimulus-dependent synchronization of neuronal responses in the visual cortex of the awake macaque monkey. Journal of Neuroscience 16:2381-2396.

Lamme VAF, Spekreijse H (1998) Neuronal synchrony does not represent texture segregation. Nature 396:362-366.

Larkum ME, Zhu JJ, Sakmann B (1999) A new cellular mechanism for coupling inputs arriving at different cortical layers. Nature 398:338-341.

Mastronarde DN (1989) Correlated firing of retinal ganglion cells. Trends in Neurosciences 12:75-80.

Milner PM (1974) A model for visual shape recognition. Psychol Rev 81:521-535.

Mitra PP, Pesaran B (1999) Analysis of Dynamic Brain Imaging Data. Biophys J 76:691-708.

Moritz CT, Christou EA, Meyer FG, Enoka RM (2005) Coherence at 16-32 Hz Can Be Caused by Short-Term Synchrony of Motor Units. J Neurophysiol 94:105-118.

Neuenschwander S, Singer W (1996) Long-range synchronization of oscillatory light responses in the cat retina and lateral geniculate nucleus. Nature 379:728-733.

Oertel D (1999) The role of timing in the brain stem auditory nuclei of vertebrates. Annu Rev Physiol 61:497-519.

Palanca BJA, DeAngelis GC (2005) Does Neuronal Synchrony Underlie Visual Feature Grouping? Neuron 46:333-346.

Percival DB, Walden AT (1993) Spectral Analysis for Physical Applications, Multitaper and Conventional Univariate Techniques: Cambridge University Press.

Perkel DH, Gerstein GL, Moore GP (1967) Neuronal spike trains and stochastic point processes. II. Simultaneous spike trains. Biophys J 7:419–440.

Reinagel P, Reid RC (2000) Temporal coding of visual information in the thalamus. J Neurosci 20:5392-5400.

Riehle A, Grun S, Diesmann M, Aertsen A (1997) Spike synchronization and rate modulation differentially involved in motor cortical function. Science 278:1950-1953.

Rosenberg JR, Halliday DM, Breeze P, Conway BA (1998) Identification of patterns of neuronal connectivity--partial spectra, partial coherence, and neuronal interactions. Journal of Neuroscience Methods 83:57-72.

Samonds JM, Bonds AB (2004) From Another Angle: Differences in Cortical Coding Between Fine and Coarse Discrimination of Orientation. J Neurophysiol 91:1193-1202.

Samonds JM, Bonds AB (2005) Gamma Oscillation Maintains Stimulus Structure-Dependent Synchronization in Cat Visual Cortex. J Neurophysiol 93:223-236.

Samonds JM, Allison JD, Brown HA, Bonds AB (2003) Cooperation between Area 17 Neuron Pairs Enhances Fine Discrimination of Orientation. J Neurosci 23:2416-2425.

Samonds JM, Allison JD, Brown HA, Bonds AB (2004) Cooperative synchronized assemblies enhance orientation discrimination. Proc Natl Acad Sci USA 101:6722-6727.

Samonds JM, Zhou Z, Bernard MR, Bonds AB (2006) Synchronous Activity in Cat Visual Cortex Encodes Collinear and Cocircular Contours. J Neurophysiol 95:2602-2616.

Shadlen MN, Newsome WT (1998) The variable discharge of cortical neurons: implications for connectivity, computation, and information coding. J Neurosci 18:3870-3896.

Shadlen MN, Movshon JA (1999) Synchrony Unbound: A Critical Evaluation of the Temporal Binding Hypothesis. Neuron 24:67-77.

Shoham S, Fellows MR, Normann RA (2003) Robust, automatic spike sorting using mixtures of multivariate t-distributions. J Neurosci Methods 127:111-122.

Sillito AM, Jones HE, Gerstein GL, West DC (1994) Feature-linked synchronization of thalamic relay cell firing induced by feedback from the visual cortex. Nature 369:479-482.

Singer W (1999) Neuronal synchrony: a versatile code for the definition of relations? Neuron 24:49-65.

Singer W, Gray CM (1995) Visual Feature Integration and the Temporal Correlation Hypothesis. Annu Rev Neurosci 18:555-586.

Skottun BC, De Valois RL, Grosof DH, Movshon JA, Albrecht DG, Bonds AB (1991) Classifying simple and complex cells on the basis of response modulation. Vision Research 31:1079-1086.

Snider RK, Kabara JF, Roig BR, Bonds AB (1998) Burst Firing and Modulation of Functional Connectivity in Cat Striate Cortex. J Neurophysiol 80:730-744.

Softky WR, Koch C (1993) The highly irregular firing of cortical cells is inconsistent with temporal integration of random EPSPs. J Neurosci 13:334-350.

Thiele A, Stoner G (2003) Neuronal synchrony does not correlate with motion coherence in cortical area MT. Nature 421:366-370.

Thomson DJ (1982) Spectrum estimation and harmonic analysis. Proceedings of the IEEE 70:1055-1096.

Thomson DJ, Chave AD (1991) Jackknifed error estimates for spectra, coherences, and transfer functions. In: Advances in spectrum analysis and array processing, pp 58-113. Englewood Cliffs, New Jersey: Prentice Hall.

Ts'o DY, Gilbert CD, Wiesel TN (1986) Relationships between horizontal interactions and functional architecture in cat striate cortex as revealed by cross-correlation analysis. J Neurosci 6:1160-1170.

Usrey WM, Reppas JB, Reid RC (1998) Paired-spike interactions and synaptic efficacy of retinal inputs to the thalamus. Nature 395:384-387.

von der Malsburg C (1981) The correlation theory of brain function. In. Goettingen, Germany: Max-Planck-Institute for Biophysical Chemistry.

Webster MA, De Valois RL (1985) Relationship between spatial-frequency and orientation tuning of striate-cortex cells. J Opt Soc Am A 2:1124-1132.

CHAPTER VI

DECONSTRUCTION OF SPATIAL INTEGRITY IN VISUAL STIMULUS DETECTED BY MODULATION OF SYNCHRONIZED ACTIVITY IN CAT VISUAL CORTEX

Zhiyi Zhou, Melanie R. Bernard, A. B. Bonds

Abstract

Spatiotemporal relationships among contour segments can influence synchronization of neural responses in the primary visual cortex. We have carried out a systematic study to dissociate the impact of spatial and temporal factors in the signaling of contour integration via synchrony. In addition, we characterized the temporal evolution of this process to clarify potential underlying mechanisms. With a 10x10 microelectrode array, we recorded the simultaneous activity of multiple cells in the cat primary visual cortex while stimulating with drifting sinewave gratings. We preserved temporal integrity and systematically degraded spatial integrity of the sinewave gratings by adding spatial noise. Neural synchronization was analyzed in the time and frequency domains by conducting cross-correlation and coherence analyses. The general association between neural spike trains depends strongly on spatial integrity, with coherence in the gamma band (35 – 70 Hz) showing greater sensitivity to the change of spatial structure than other frequency bands. Analysis of the temporal dynamics of synchronization in both time and frequency domains suggests that spike timing synchronization is triggered nearly instantaneously by coherent structure in the stimuli while frequency-specific oscillatory components develop

more slowly, presumably through network interactions. Our results suggest that while temporal integrity is required for the generation of synchrony; spatial integrity is critical in triggering subsequent gamma band synchronization.

Introduction

While mechanisms of visual perception are generally accepted as resulting from changes in the response rate of neurons (Barlow, 1972), cooperative neural firing may also serve as a versatile coding mechanism that extends the information capacity of the visual system (Milner, 1974; von der Malsburg, 1981; Singer and Gray, 1995; Gray, 1999; Singer, 1999; von der Malsburg, 1999). Earlier studies have focused either on the tight (<10 msec) synchronization of spike timing or phase-locked oscillation at particular frequencies, most notably gamma (35 – 70 Hz; Alonso et al. 1996; Dan et al. 1998; Eckhorn et al. 1988; Engel et al. 1991; Frien et al. 2000; Fries et al. 2001; Gray et al. 1989; Gray and Singer 1989; Kohn and Smith 2005; Samonds et al. 2004; Samonds et al. 2006; Usrey et al. 1998). Analysis of single or multiunit activity (MUA) and local field potentials (LFPs) responding to stimulation by coherent structures such as moving light bars or drifting gratings reveals that neural synchronization is stimulus-dependent and may occur within or between cortical columns or even across different cortical areas (Eckhorn et al., 1988; Gray et al., 1989; Gray and Singer, 1989; Engel et al., 1991). Evaluation of synchronization modulation by spatial and/or temporal changes in visual stimulation has led to the suggestion that neural cooperation may play a role in visual binding (Castelo-Branco et al. 2000; Engel et al. 1991a; Gail et al. 2000; Gray et al. 1989), though the generality of this proposal has been challenged by several negative results (Lamme and Spekreijse, 1998; Thiele and Stoner, 2003; Palanca and DeAngelis, 2005).

The functional significance and exact behavior of gamma-band oscillation also remains unclear. It can be found over considerable cortical distance and is enhanced by

coherent stimuli and destroyed by incoherent stimuli (Gray et al., 1989; Engel et al., 1991; Konig et al., 1995; Castelo-Branco et al., 2000; Gail et al., 2000). Though oscillation is not necessary for generating synchrony, synchrony can be strengthened or sustained if oscillation exists (Samonds and Bonds, 2005).

Spike timing synchronization, which in this paper is generally referred to as synchrony, and frequency coherence reflect neural cooperation from different perspectives, though the analyses in the time and frequency domains are correlated (Zhou et al., 2007). We consider that synchrony is triggered by coherent spatial and temporal structures in the visual input which simultaneously activate populations of retinal cells (Samonds and Bonds, 2005). The timing synchronization between neural spike trains is then propagated through the visual pathway via divergent and convergent transmission (Usrey and Reid, 1999). Neural synchronization may provide emergent information that is not carried by independent firing rates (Dan et al., 1998; Kohn and Smith, 2005; Samonds et al., 2006; Montani et al., 2007). For example, synchronized responses in neural ensembles permit the discrimination of fine differences of orientation that are not evident from independent firing rates (Samonds et al., 2003, 2004). The present study tests the specific image qualities that encourage synchrony, with a view towards describing the *nature* of the visual information carried by synchrony. While we agree that synchrony arises from coherent spatiotemporal structures in the retinal image, here we try to disambiguate the two variables by investigating how synchrony and oscillation depend on the degree of spatial integrity in the stimulus, without changing global temporal structure (drift rate). More specifically, we systematically deconstructed the contour integrity of drifting sinewave gratings by progressively adding spatial noise,

while maintaining the coherent motion of both noise and gratings. Single unit recordings were made simultaneously with a 10x10 microelectrode array from large numbers of cells in areas 17 and 18 of three anesthetized and paralyzed cats. We analyzed spike timing synchronization and frequency association between neural spike trains with cross-correlation and coherence analyses and found that the synchronization between neural responses in the time and frequency domains both modulated systematically with the change of spatial integrity in the visual stimuli. We also discovered that coherence in the gamma frequency band is more sensitive to changes in spatial integrity than either lower frequency bands or general spike synchrony as revealed by the JPSTH. Coherence in the lower (alpha and beta) frequency bands dropped only moderately even after large amounts of spatial noise (i.e. 55%) were added to the image. We suspect that low frequency coherence may be driven mainly by the temporal structure in the stimulus, though additional study is needed to confirm this conjecture. To further explore the relationship between synchrony and gamma coherence, we analyzed the temporal dynamics of synchronization in both the time and frequency domains. Our result suggests that spike timing synchronization is triggered nearly instantaneously by coherent structure in the stimuli while the frequency-specific oscillatory components evolve more slowly, presumably through network interactions.

Materials and Methods

Physiological Preparation

Electrophysiological recordings were made in three adult (2.5- 3.5 kg) cats. All experimental procedures were performed under the guidelines of the American

Physiological Society and Vanderbilt University's Animal Care and Use Committee. Each cat initially received intramuscular injections of 2mg dexamethasone about 20 hours before surgery and 0.5ml acepromazine maleate and 0.5ml atropine sulfate about 2 hours before surgery. General anesthesia was induced by inhalation of 5% halothane in O_2. One of the forelimb veins was cannulated for intravenous injection of 0.3 $mg \cdot kg^{-1} \cdot hr^{-1}$ propofol to maintain anesthesia. After a tracheal cannula was inserted, cats were mounted in a stereotaxic device. Paralysis was induced with 6mg and maintained with 0.3 $mg \cdot kg^{-1} \cdot hr^{-1}$ pancuronium bromide through another cannulated forelimb vein. Cats were ventilated at the rate of 30 breaths per minute with a mixture of N_2O:O_2:CO_2 (75:23.5:1.5), and the expired pCO_2 was maintained at 3.9%. An 8 × 8 mm craniotomy was performed over the area centralis representation in area 17 (Horsley-Clark coordinates P4-L2). After the electrode array was inserted, the hole was covered with agar mixed in mammalian Ringer's solution.

During recording, we maintained cats' body temperature at 37.5ºC with a servo-controlled heat pad. The brain activity and heart rate were monitored with electroencephalograms and electrocardiograms to ensure anesthetic stability. Phenylephrine hydrochloride (10%) was dropped into both eyes to retract the nictitating membranes, and the pupils were dilated with 1% atropine sulfate. The corneas were protected by adding contact lenses with 4mm artificial pupils, and auxiliary lenses were applied to ensure the eyes were focused on the stimulus plane.

Stimulation

The location of the receptive fields of individual cells was first mapped with rear-projected light bars, then the center and size of the aggregate area were determined so that multiple receptive fields could be simultaneously covered by the visual stimulus. A 21-inch gamma-corrected Sony Trinitron monitor (mean luminance 73 cd/m^2) was positioned at a viewing distance of 57 cm to display visual stimuli. The monitor was set to a refresh rate of 120 Hz and each frame was presented twice.

Visual stimuli were generated with the Winvis for Matlab toolbox (Neurometrics Institute, Oakland, CA). We used drifting sinewave gratings with or without perturbation of the spatial structure to test how visual neurons modulate their responses and synchronization in correspondence with these changes. The unperturbed gratings had fixed contrast (50%), spatial frequency (0.5 c/º), and temporal frequency (2Hz), which drove nearly all of the cells in our sample. Several values of orientation and direction of drift were selected, with each providing simultaneous activation of large numbers of cells. We then added spatial noise to the original sinewave gratings to perturb the contour integrity of the stimulus. The spatial noise was created by swapping randomly selected pairs of areas (3x3 pixels, 0.13 × 0.13 $degree^2$) in the original gratings (Figure 6-1). The brightness of each substituted area was uniform and calculated as the average of the initial pixel values. Swapping areas in the original image, as opposed to insertion of random levels, avoids changes in the overall luminance distribution. Each swapped pair was tagged so that no further swapping would happen in these areas. We chose a fixed set of spatial noise levels (all three cats were tested with 10%, 25%, 40% and 55% spatial noise, and two cats were also tested with 100% spatial noise), defined by the total

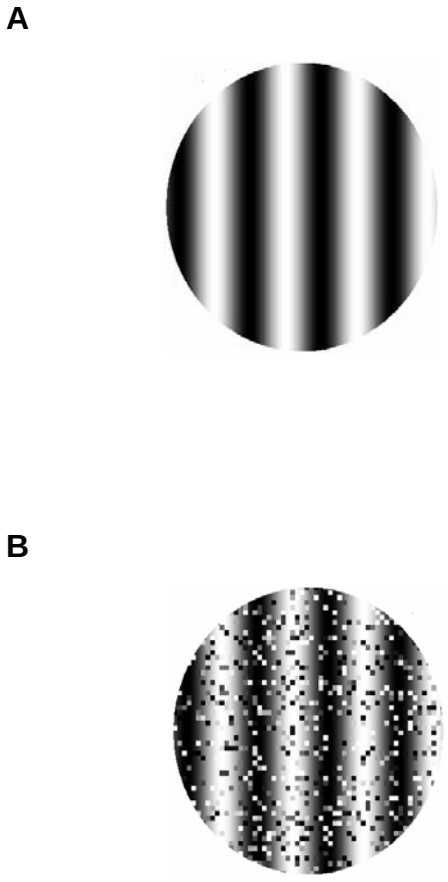

Figure 6-1: Visual Stimuli with and without spatial noise (A) The unperturbed stimulus is a standard sinewave grating with fixed contrast (50%), spatial frequency (0.5 c/º), and temporal frequency (2Hz) drifting at varied orientations. (B) The contour integrity of the stimulus is degraded by adding spatial noise at different levels (25% spatial noise here).

percentage of swapped areas within the original stimulus, to explore how cells modulated their responses to graded deconstruction of spatial integrity.

Since spatial reorganization of the stimulus might influence firing rate as well as synchrony due to changes in the nominal stimulus orientation, we carefully chose the size of the spatial noise elements (dimensions of the swapped areas) so that contour integrity could be perturbed without altering the orientation structure of the stimulus. To test whether our perturbation procedure has any impact on the effective orientation of the stimuli, we tested 34 cells with the original sinewave gratings and the perturbed stimuli with 10 – 55% spatial noise displayed across a full range of orientations (15 – 360 degrees) with a 15 degree increment. The orientation yielding the highest firing rate for the original gratings was defined as a cell's intrinsic orientation preference. When the gratings were perturbed by adding 10% or 55% of spatial noise in the image, 6 cells had peak orientations that deviated from their intrinsic orientation in either condition. When 25% or 40% of noise was added in the image, 8 cells showed peak deviations of their tuning curves. However, all the deviations were within a ±15 degree range. The population averaged orientation tuning curves for each stimulus condition show that adding spatial noise has little impact on the effective orientation of the stimuli (Figure 6-2).

We tested all cells' orientation preference with drifting sinewave gratings displayed for 2 seconds and repeated 25 times. A one-second blank window was interleaved between stimulus presentations to avoid adaptation. After we obtained the orientation preferences for cells that showed vigorous responses (≥ 10 spikes/second), we combined the unperturbed and the perturbed gratings to create the basic stimulus set.

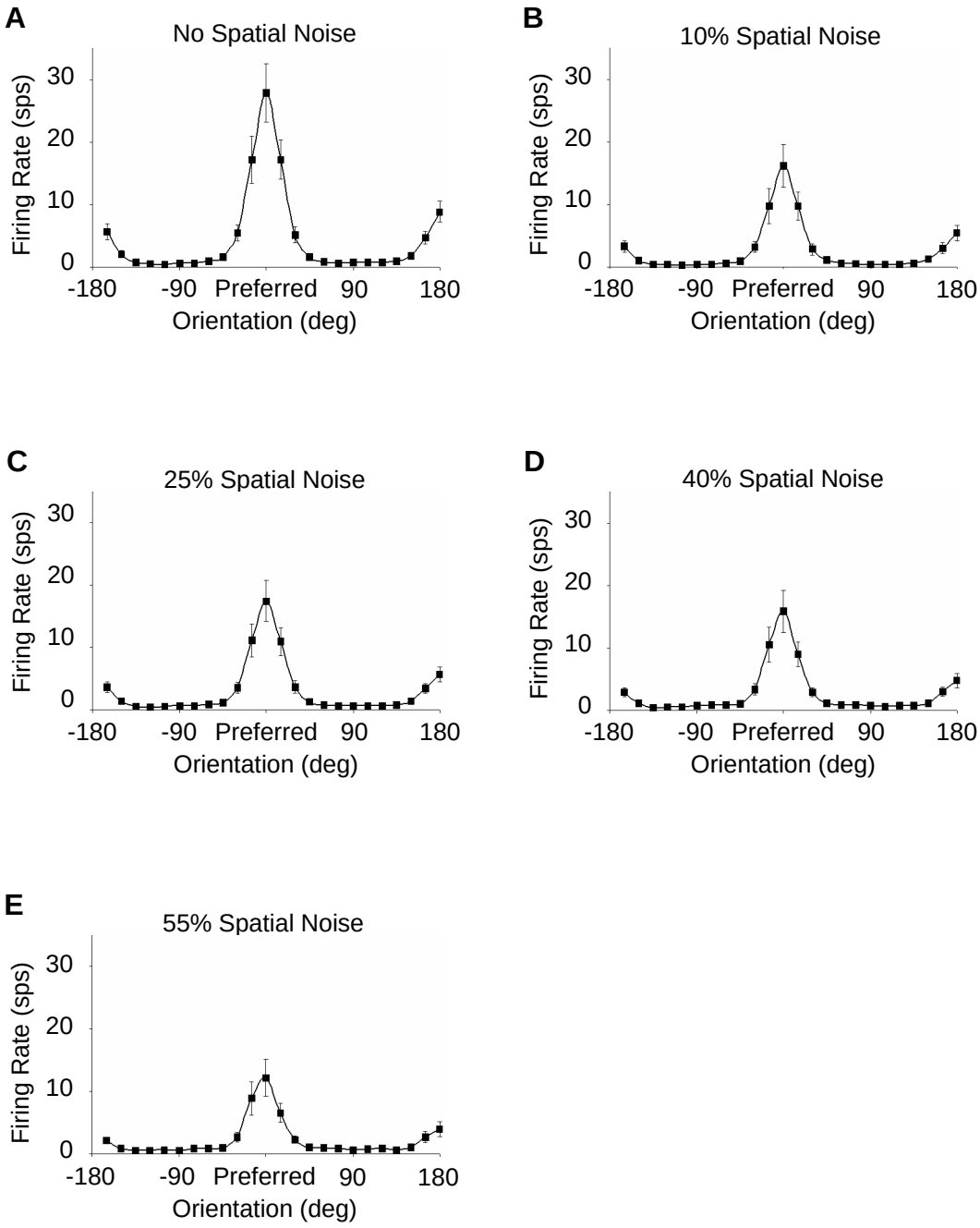

Figure 6-2: The population averaged tuning curves for the original (A) and perturbed gratings (B – E) show that adding spatial noise has little impact on the perceived orientation of the stimuli, though cells' response strength drops with spatial noise. Error bars represent SEM.

Visual stimuli were displayed in random order in a circular aperture (diameter = 10 to 14 degrees) and each presentation lasted 2 seconds. All stimuli were repeated for 100 to 360 trials to ensure reliability of the data. Due to experimental time limits, we only tested the stimuli at certain orientations (normally 8 to 12) that were able to drive a substantial portion of the cell population.

Recording

Recordings were made with a Cyberkinetics 10 × 10 microelectrode array (4 x 4 mm), which was pneumatically inserted to a fixed depth (600 μm) in cat areas 17 and 18 based on Horsley-Clark coordinates. We processed the raw neural signals offline with a spike sorting procedure to remove noise and artifact (Shoham et al., 2003). In this study, we only included channels that recorded single unit activity showing reliable orientation selectivity (i.e., firing rate at the preferred orientation was at least twice that at the worst orientation). Reliable measurement of synchrony and coherence requires a strong response rate, so we selected cells that have their preferred orientation equal or close to the orientation of the visual stimuli (difference between cells' preferred orientation and the orientation of the visual stimulus is equal to or less than 15 degrees). 20, 24, and 23 cells from three cats were included in our final analysis. All cells we studied were classified as complex (Skottun et al., 1991).

Synchrony

Spike timing synchronization between cells was determined from the cross-correlation histogram (CCH), which was derived from the joint peri-stimulus time histogram

(JPSTH) (Aertsen et al., 1989). The two-dimensional JPSTH represents the joint spike count per unit time (here using a 1 msec binwidth) between a pair of cells. To correct for changes in synchrony due to the contribution from the joint elevation of the firing rates, the raw JPSTH is normalized by subtracting the cross-product of the peristimulus time histograms (PSTHs) and then dividing by the standard deviation of the PSTH predictors. This normalization procedure is statistically equivalent to the method of the shift predictor (Perkel et al., 1967; Gerstein and Perkel, 1972; Aertsen et al., 1989), except that the method of JPSTH produces smoother results since the PSTHs are trial averaged results (Aertsen et al., 1989). The normalized CCH is produced by integrating along the principle diagonal of the normalized JPSTH. A pair of cells is considered to be firing synchronously if a discernible peak appears around 0 msec time lag in the CCH, and synchrony is considered significant if the peak value is at least twice the random fluctuations or noise in the CCH. We identified a total of 152 cell pairs with significant synchrony in our sampled population. The width (about 500msec) of the temporal structure in the PSTH reflects the periodic luminance change in the stimuli (Figure 6-3), which is much broader than the width (10msec or less) of the central peak on CCH in our sampled pairs, indicating that synchrony does not result from covariations in response latency and/or excitability (e.g., Brody, 1999ab).

Coherency/Coherence Analysis

Similar to the cross-correlation analysis, coherency analysis also quantifies the synchronization between neural firing but in the frequency domain. Coherency measures the frequency dependence between neural spike trains instead of the timing dependence

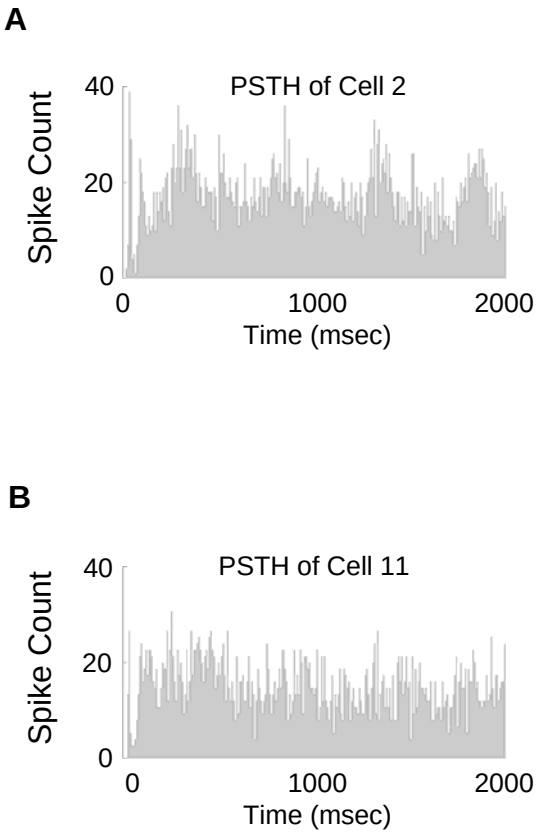

Figure 6-3: Examples of PSTH (A) PSTH of cell 2 responding to unperturbed gratings. (B) PSTH of cell 11 responding to unperturbed gratings.

addressed by the cross-correlation analysis. The direct procedure of calculating coherency is implemented by conducting the Fourier transform of the spike trains to compute the power spectra and the cross spectrum of the two processes. Coherency is then derived by the following equation:

$$\gamma(f) = \frac{S_{12}(f)}{\sqrt{S_{11}(f)S_{22}(f)}} \tag{6-1}$$

in which indices 1 and 2 denote the two different simultaneously recorded neural spike trains (Jarvis and Mitra, 2001). Since coherency is a complex quantity, the modulus of the coherency, known as coherence, is introduced to quantify the association between neural responses in the frequency domain. A windowing procedure is normally applied to reduce the leakage error during the Fourier transform.

We used the multitaper method to compute the coherence in our study. A distinct feature of the multitaper method is that it computes the averaged spectral estimates by applying several orthogonal windowing functions, in which windowing is referred as tapering to differentiate it from segmentation. The coherence estimate from the multitaper method has reduced bias and variance compared to that from the direct estimation procedure (Percival and Walden, 1993; Mitra and Pesaran, 1999; Jarvis and Mitra, 2001). We used the Chronux package 1.0 (Chronux.org) to calculate the coherence spectra of the synchronized cell pairs identified by the JPSTH. Neural spike trains were sampled at a rate of 250 Hz, and the coherence spectra were estimated for the frequency range from 2 to 100 Hz. We applied 5 orthogonal Slepian tapers in calculating the coherence. The 95% confidence intervals of the coherence were calculated with the jackknife method, and a theoretical 95% confidence limit for the coherence was also estimated with multivariate

statistics to determine whether the coherence reaches a significant level (Hannan, 1970; Jarvis and Mitra, 2001).

Temporal Dynamics of Synchrony and Coherence

Two-dimensional plots of CCHs and coherence in a 250 msec moving window were produced with 25 msec step resolution. The beginning of the first time window started 0 msec after stimulus onset. To ensure reliability of the estimation, we only analyzed the temporal dynamics of synchrony and coherence in the 74 pairs of cells that were tested with 360 stimulus trials. Pre-stimulus CCH and coherence were not included in the study since we could not obtain reliable estimates with low spontaneous spike rate (mean = 4.25 spikes/sec). We consider synchrony and coherence to be stabilized when the values of synchrony and coherence first reached 90% of their maximum values along the time axis.

Results

We drifted sinewave gratings with different levels of spatial noise at constant velocities to examine how the perturbation of spatial integrity influences the synchronized responses in visual neurons. The synchronization between neural firing was estimated with the cross-correlation and coherence analyses in the time and frequency domains respectively. We identified a total of 152 pairs of cells exhibiting synchronized firing from recordings in areas 17 and 18 of three paralyzed and anesthetized adult cats. We found that synchrony and coherence systematically dropped when the spatial integrity of the stimuli was deconstructed in stages. When coherence was examined, the gamma

frequency band appears to be more sensitive to the perturbation of the spatial integrity than alpha and beta bands or general spike synchrony. By computing the synchrony and coherence with sliding time windows, we discovered that synchrony develops earlier than coherence, suggesting that spectrally organized cooperation is a network property.

Neural Synchrony Modulation

We first measured the correlation between neural responses in the time domain by inspecting the shape of the normalized CCHs derived through the JPSTH method (Aertsen et al., 1989). A narrow (<10 msec) and discernible peak around 0 msec time lag in the normalized CCH indicates that two neurons are firing synchronously while the magnitude of the peak can be considered the maximum "effective connectivity", measured as a percentage of all spikes, between the cells. Figure 6-4 shows how synchrony is dependent on the integrity of the spatial coherence of the visual stimulus. Cells 2 and 11 have the same orientation preference. When stimulated by intact sinewave gratings, these two cells showed strong synchrony. Synchrony consistently decreased as the spatial integrity of the visual stimulation was systematically perturbed. We examined the population behavior by averaging the CCHs (Figure 6-5) and the synchrony values (Figure 6-8 A) for all cell pairs (N = 152) that we identified as having significant synchrony for unperturbed stimuli. The graded reduction of synchrony across the population suggests that the dependence of synchrony on the integrity of spatial structure is a general phenomenon in the primary visual cortex.

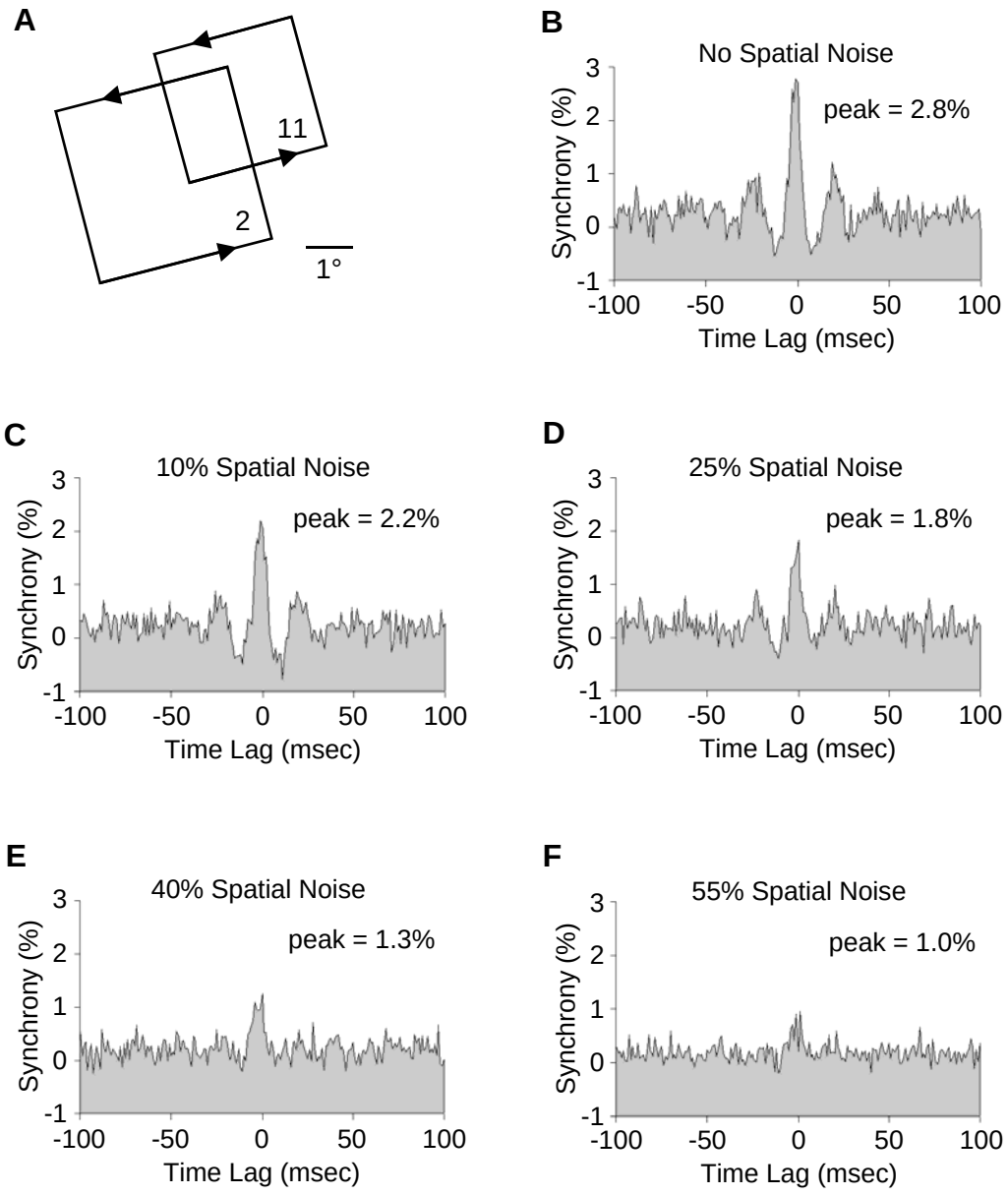

Figure 6-4: Example of synchrony modulation by the perturbation of spatial integrity in the stimuli (A) Cells 2 and 11 have the same orientation preference and partly overlapping receptive fields. (B) The cross-correlation histogram shows strong synchrony from unperturbed sinewave gratings. (C-F) With spatial noise in the stimulus increased from 10% to 55%, the strength of the synchrony between these two cells is systematically reduced.

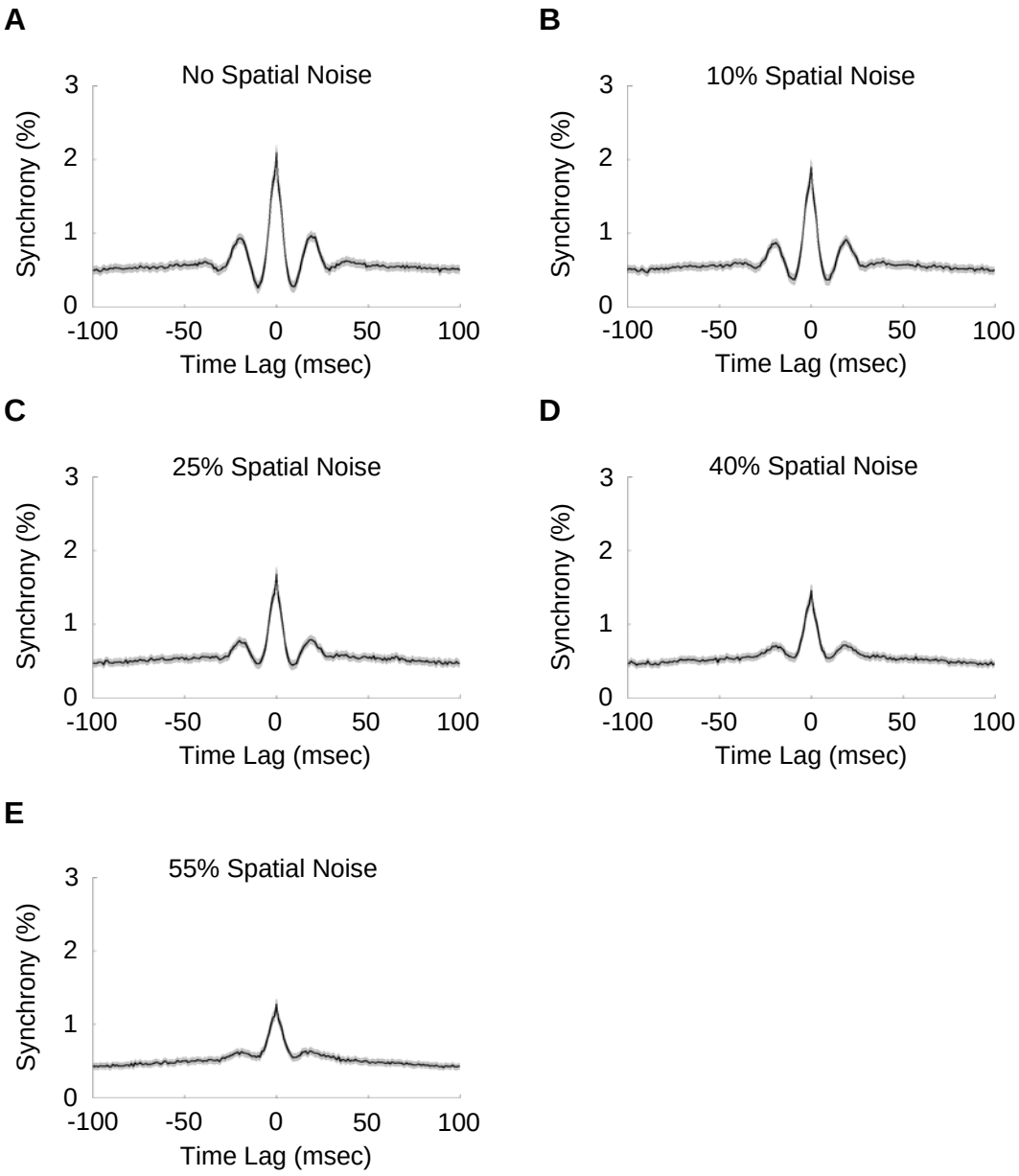

Figure 6-5: CCHs were averaged across all synchronized cell pairs for stimulus conditions with different noise levels (A) Averaged CCH for regular gratings. (B-E) Averaged CCHs for perturbed gratings with noise level increased from 10% to 55%. The gray areas around the averaged CCHs (black curves) indicate SEM.

Coherence Modulation

We also evaluated the cooperation between neural spike trains in the frequency domain by measuring the coherence modulation of synchronized cell pairs as spatial integrity was deconstructed. Coherence spectra were calculated with multitaper spectral estimation, which not only computes the coherence estimation with reduced bias, but also provides variance estimation (Percival and Walden, 1993; Jarvis and Mitra, 2001). Consistent with our findings in the time domain, the synchronized neural spike trains also displayed correlation in the frequency domain. This finding is not surprising since synchrony and coherence analyses are correlated, though they analyze the association between neural responses from different perspectives (Zhou et al., 2007). Figure 6-6 shows an example in which the coherence between two cells dropped with the deconstruction of spatial integrity in the stimulus. We observed that with unperturbed sinewave gratings, the coherence spectrum showed two major peaks, one at around 50 Hz and another at around 10 Hz (Figure 6-6 A). As the spatial noise level in the stimulus increases (Figure 6-6 B-F), the spatial integrity systematically decreases although the overall motion of the stimulus remains constant. We found that the magnitude of the coherence, especially in the gamma frequency band, showed organized reduction. After the spatial integrity of the stimulus was totally destroyed by adding 100% spatial noise in the stimulus, only a small amount of coherence was preserved in the low frequency band (<10Hz) and the coherence in the gamma band totally disappeared. The mean coherence curves for each stimulus condition were generated by averaging the data from all synchronized pairs, in which a trial-shifted predictor was subtracted to remove the background coherence. The same modulation pattern that exhibited in the above example is also seen in the population-averaged

coherence results. Coherence showed graded reduction as the spatial noise level in the stimulus systematically increased (Figure 6-7).

Frien and Eckhorn (2000) reported that, in area V1 of macaque monkeys, the spectral coherence of MUA in the range of 35 – 50 Hz depended more strongly on stimulus orientation than that in the range of 0 – 12 Hz. Also in Macaque V1, Henrie and Shapley (2005) found that, while overall LFP power gradually increases with increased stimulus contrast, the gamma band increases differentially more than in other frequency bands. These results suggest that differential organization of mechanisms signal different spectral components. To explore whether specific frequency bands are differentially sensitive to the deconstruction of spatial integrity, we separated trends in the alpha (5 – 15 Hz), beta (15 – 35 Hz), and gamma bands (35 – 70 Hz) respectively. We quantified the total coherence by integrating the area between the coherence curve and the estimated 95% confidence level at the frequencies where the phase value fell within a range defined by time offset of ± 10 msec. The relationship between phase (ϕ) and time (t) (Jarvis and Mitra, 2001) is defined by:

$$\phi(f) = 2\pi ft \tag{2}$$

The reason that we specifically limit integration within this phase range is because information provided by cooperative neural firing appears to be contained mainly in a time window of less than 10 msec (Softky and Koch, 1993; Samonds et al., 2004). The integrated values for individual bands (alpha, beta, and gamma) are further normalized by dividing the bandwidth of the frequency range so that the relative coherence modulation can be directly compared. Figure 6-8 shows the modulation of synchrony, normalized coherence in different frequency bands, and mean firing rate corresponding to different

Figure 6-6: Example of coherence modulation by the perturbation of spatial structure in the stimuli. The black traces in the plots represent the coherence between cells while the gray dotted curves above and below represent the 95% confidence intervals of the coherence derived from the jack-knifing method. The straight gray dotted line draws the theoretical 95% confidence limit for the coherence estimated via multivariate statistics. (A) With regular drifting sinwave gratings, the coherence spectrum exhibited prominent elevation around 10 and 50 Hz respectively. (B-E) The coherence between cells, especially in the gamma band, decreases with the percentage increase of the spatial noise level in the image. (F) With 100% drifting spatial noise, the spatial structure of stimulus is destroyed while the temporal coherence was maintained. Only a small amount of coherence was preserved in the low frequency band (<10 Hz) while gamma coherence disappeared completely.

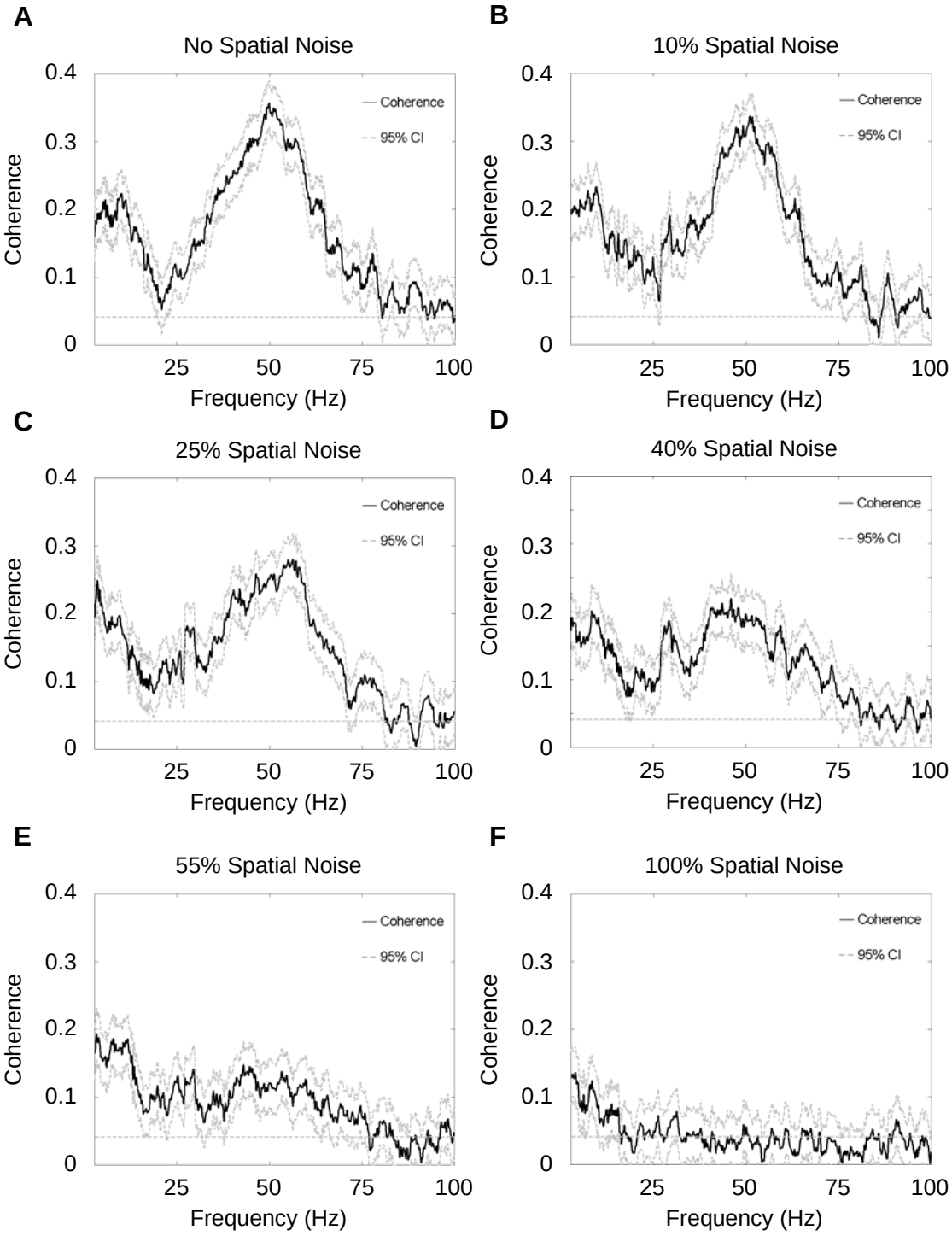
A
No Spatial Noise
B
10% Spatial Noise
C
25% Spatial Noise
D
40% Spatial Noise
E
55% Spatial Noise
F
100% Spatial Noise
Coherence
95% CI
Coherence
0.4
0.3
0.2
0.1
0
25
50
75
100
Frequency (Hz)

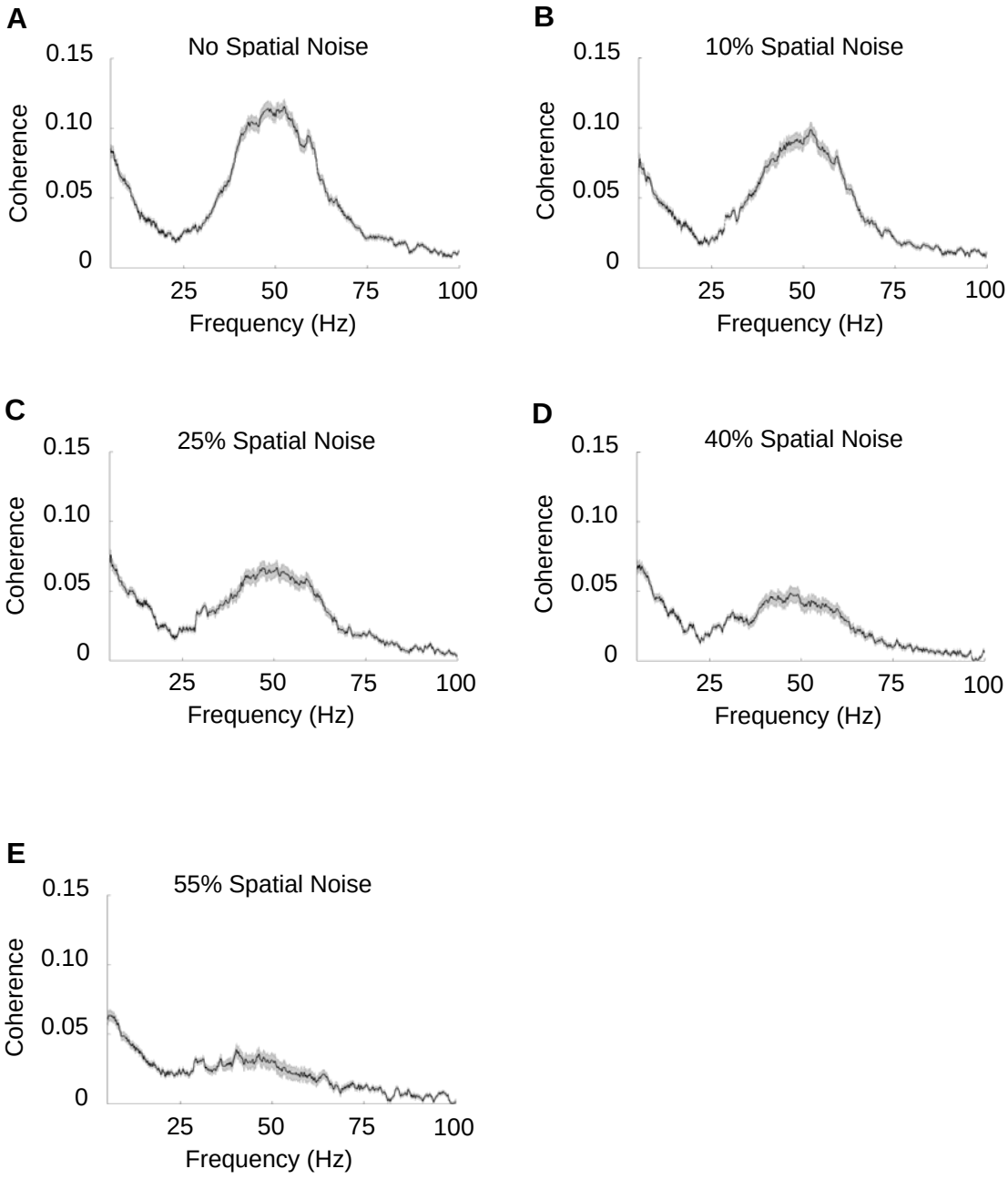

Figure 6-7: Coherence averaged across the population (A) Mean coherence for regular gratings. (B-E) Mean coherence for perturbed drifting gratings with noise levels increased from 10% to 55%. Gray areas around the mean coherence curves (black traces) indicate SEM.

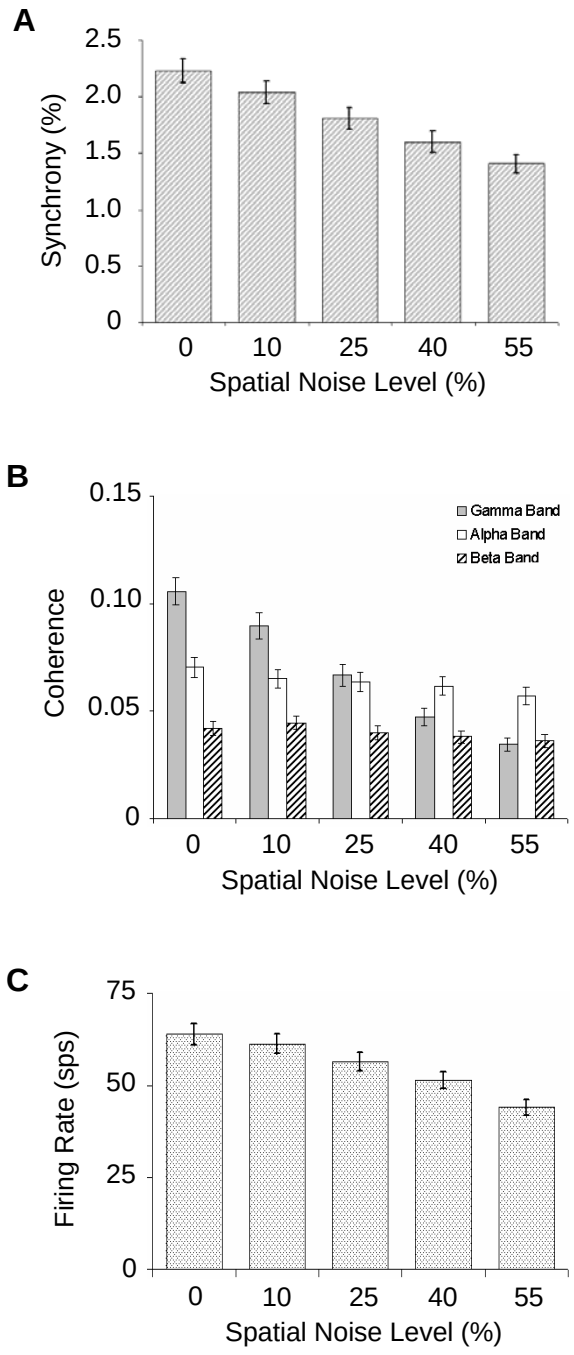

Figure 6-8: Mean response with different levels of spatial noise (A) Mean synchrony values for stimulus conditions with different noise levels. (B) Mean normalized integrated coherence in the alpha, beta, and gamma bands for stimulus conditions with different noise levels. (C) Mean firing rate for stimulus conditions with different noise levels.

spatial noise levels. One-way ANOVA testing shows that synchrony, gamma coherence, and firing rate, but not alpha and beta coherence, can discriminate between different levels of spatial noise (table 6-1). We transformed the means of firing rate, synchrony, and gamma band coherence into percentage values so that the response modulation between different domains can be compared. For example, the mean firing rate under the stimulation of perturbed gratings with 10% spatial noise was transformed by dividing the mean firing rate under stimulation by regular gratings, and then multiplied by 100%. With this transformation, we found that firing rate, synchrony and gamma band coherence reduced to 68.9%, 63.1%, and 32.4% respectively at 55% spatial noise level (Figure 6-9). The transformed mean firing rate, synchrony, and gamma coherence were individually fitted with linear regression lines. Comparing the slopes between different regression lines (Zar, 1999), we found that gamma coherence and synchrony dropped significantly faster than firing rate, and gamma coherence also reduced significantly faster than synchrony, indicating that gamma coherence is the most sensitive in detecting the change of spatial integrity among these three variables (table 6-2). We found that coherence in the alpha and beta bands was well maintained at 81.4% and 86.4% even when the spatial integrity was dramatically degraded with 55% spatial noise. We suspect that the coherence in these low frequency bands is mainly supported by the temporal features, such as common fate, in the stimulus. However, we cannot verify this conjecture since we did not vary the temporal features of the stimuli used here.

Besides modulation of synchrony and coherence by the increase of spatial noise in the stimulus, we also noticed a corresponding reduction of firing rate (Figure 6-8 C). Removing the contribution of firing rate covariation is necessary before evaluating

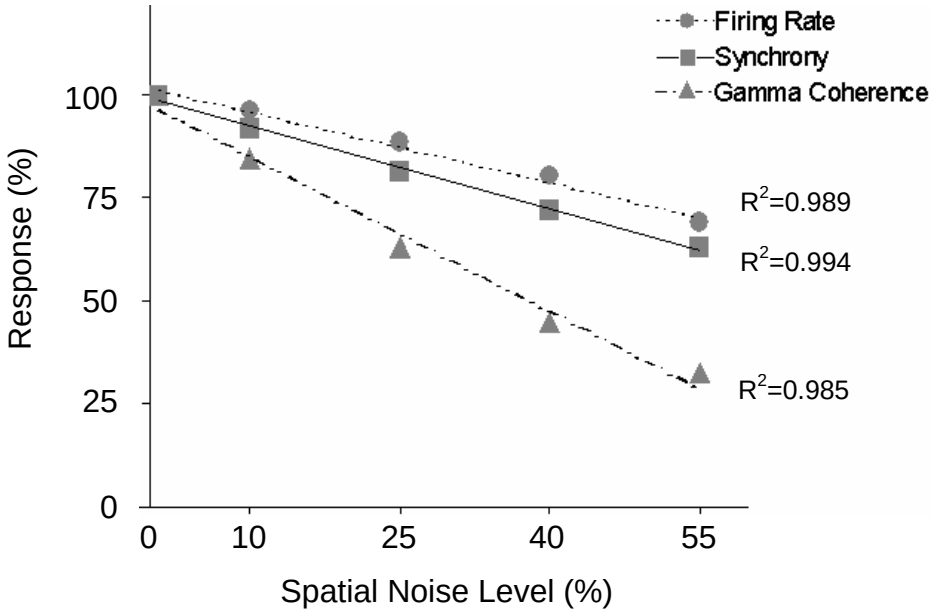

Figure 6-9: The mean firing rate, synchrony, and normalized integrated gamma coherence were transformed to percentage values fitted with linear regression lines for direct comparison.

Table 6-1: One-way ANOVA test ($\alpha = 0.025$) shows that synchrony, gamma coherence, and firing rate can differentiate the different spatial noise levels while coherence in the alpha and beta bands cannot tell the difference.

	p Value
Synchrony	1.53E-009*
Alpha Coherence	0.33
Beta Coherence	0.34
Gamma Coherence	0*
Firing Rate	3.86E-008*

* indicates significant *p* value

Table 6-2: Two-tailed *t*-test ($\alpha = 0.025$), which compares the slopes between different regression lines, shows that synchrony reduces faster than firing rate while gamma coherence reduces faster than both firing rate and synchrony with the increase of spatial noise level.

	p Value
Gamma Coherence – Firing Rate	0.0002*
Synchrony – Firing Rate	0.0179*
Gamma Coherence -- Synchrony	0.0003*

* indicates significant *p* value

cooperation between neurons. The JPSTH method removes the "chance correlation" by subtracting the cross-product of the peristimulus time histograms, which is statistically equivalent to shift predictor (Aertsen et al., 1989). Frequency domain estimators such as coherence analysis provide intrinsic normalized measurement of correlation between neural responses (Jarvis and Mitra, 2001). Therefore, even though the mean firing rate decreased with the progressive reduction of the spatial coherence in the stimuli, the changes in synchronization between spike trains, either in the time or frequency domain, should not be considered as being induced by the firing rate change.

Evolution of Neural Cooperation

Even though there is correlation between JPSTH-derived synchrony and coherence, it is not clear whether these two quantities reflect the same underlying activity. This question can be addressed by observing how synchrony and coherence between neural responses develops over time. We calculated both synchrony and coherence within a 250 msec moving window with 25 msec step resolution throughout the two second duration of stimulation. Figure 6-10 shows an example from a cell pair of the 2-dimensional plots for temporal evolution of coherence. Strong coherence in both the gamma band and lower frequency (<25 Hz) bands results from stimulation with pure sinewave gratings and gratings with low distortion (10% or 25% spatial noise added). However, gamma coherence is either weak or absent with noisier gratings (40%, 55% spatial noise), although the low frequency coherence is less affected. In the population-averaged 2-dimensional coherence plot (Figure 6-11 B) for pure sinewave grating stimuli, strong coherence also appears in the gamma band and the frequency bands lower than 25 Hz.

We observed the evolution of coherence and synchrony by finding the maximum coherence in the high (gamma) and low (5 – 35 Hz) frequency bands and the maximum synchrony along the time axis in the 2-dimensional coherence and synchrony plots (Figure 6-11). The averaged result shows that synchrony develops much earlier than high-frequency coherence. Synchrony reaches its highest magnitude within the second moving time window, which starts 25 msec after stimulus onset, and then gradually declines, stabilizing at about 80% of its maximum level after 700 msec (Figure 6-12 A). Though all tested cell pairs that demonstrated gamma band coherence surpassed the 95% confidence interval for gamma coherence within 300 msec, gamma coherence gradually grows to its highest value at around 900 msec and then slightly decays (Figure 6-12 B). Across all synchronized pairs, the median time when synchrony reaches 90 percent of the highest magnitude is within a 250 msec window starting at 25 msec after stimulus onset while the median for that of high-frequency coherence is within a window starting at 575 msec. Synchrony therefore develops much more quickly than high-frequency coherence, and gamma coherence, though obvious early on, continues to develop over most of a second. The temporal dynamics of synchrony and coherence suggest that even though a rough impression can be obtained from a quick glimpse, a certain amount of time is needed to refine the perceived image. Coherence in the low frequency band (5 – 35 Hz) behaves in a complementary fashion to that in gamma band. The highest level is reached at the onset of stimulation and decays thereafter (Figure 6-12 C). We consider that coherence in the low frequency band (<25 Hz) is mainly induced by the stimulus onset, while gamma coherence develops through internal interaction within the neural network.

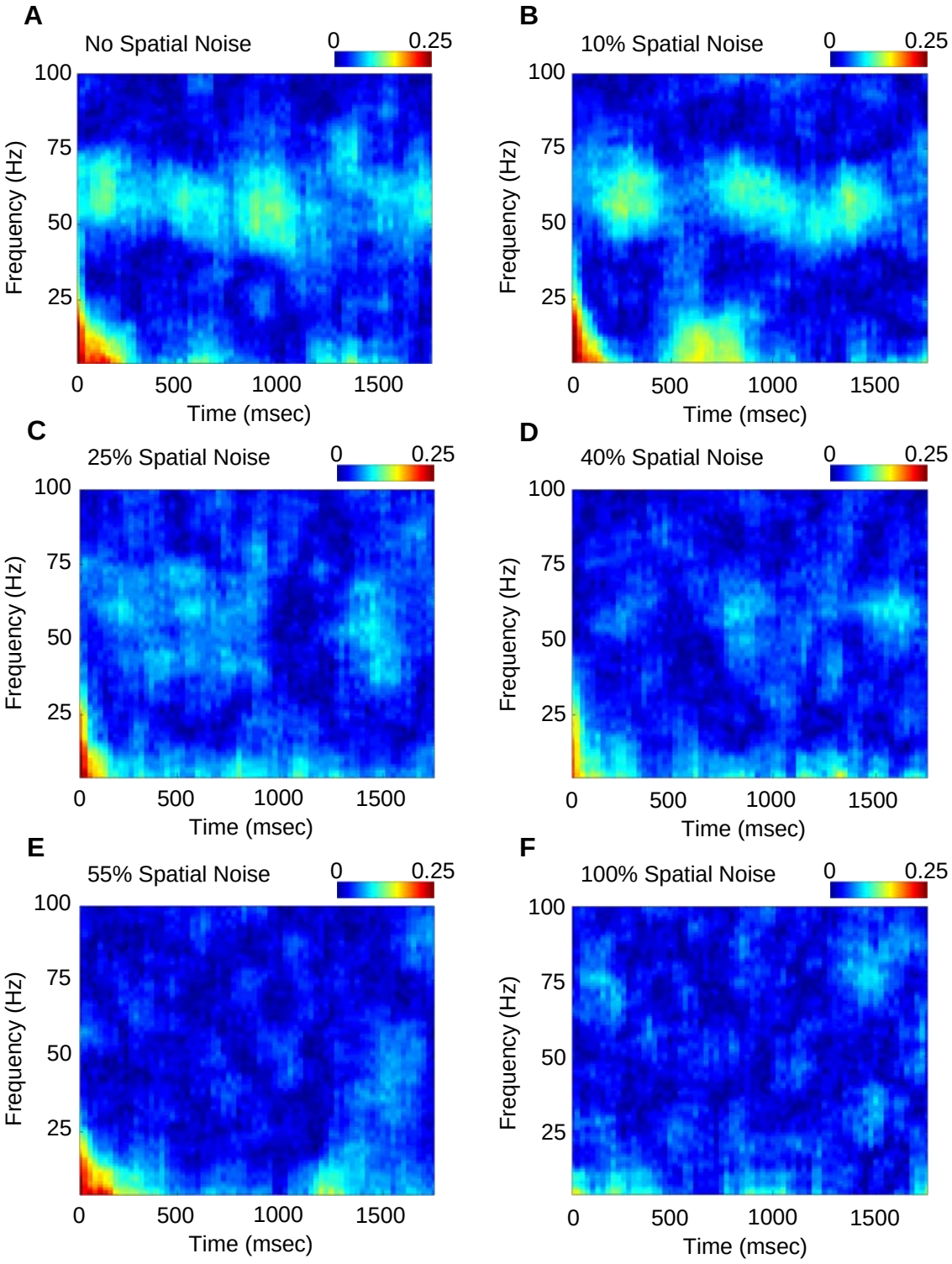

Figure 6-10: Example of coherence evolution over time (A) Coherogram for stimulation with regular sinewave gratings. (B-E) Coherograms for stimulation with noise levels from 10 – 55%. (F) Coherogram for 100% noise level.

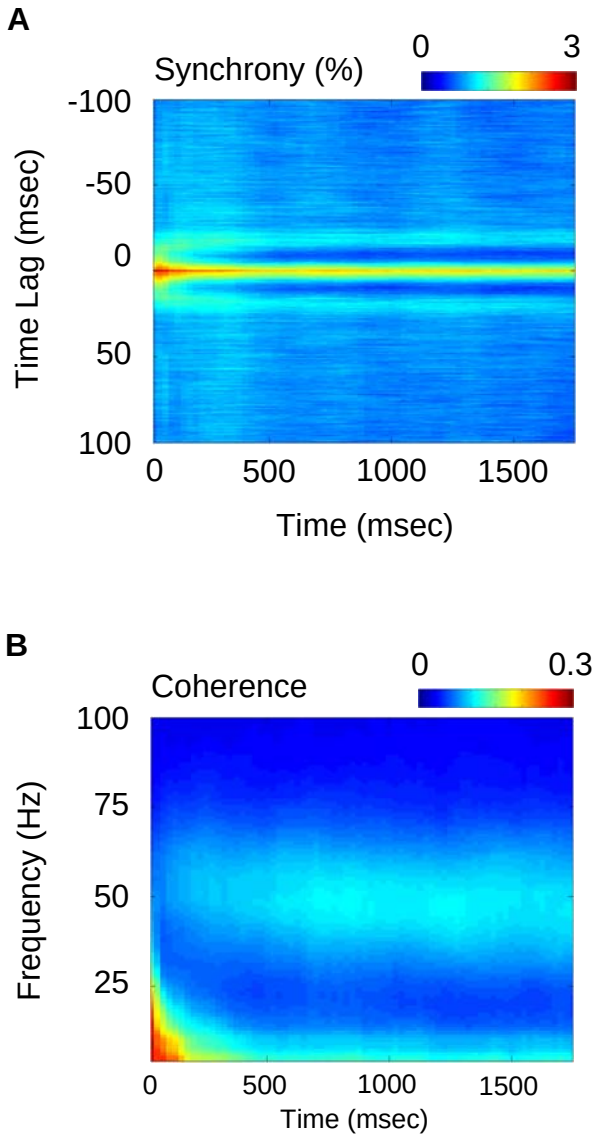

Figure 6-11: (A) Population averaged temporal dynamics of CCH with stimulation of regular gratings. (B) Population averaged temporal dynamics of coherence with stimulation of regular gratings.

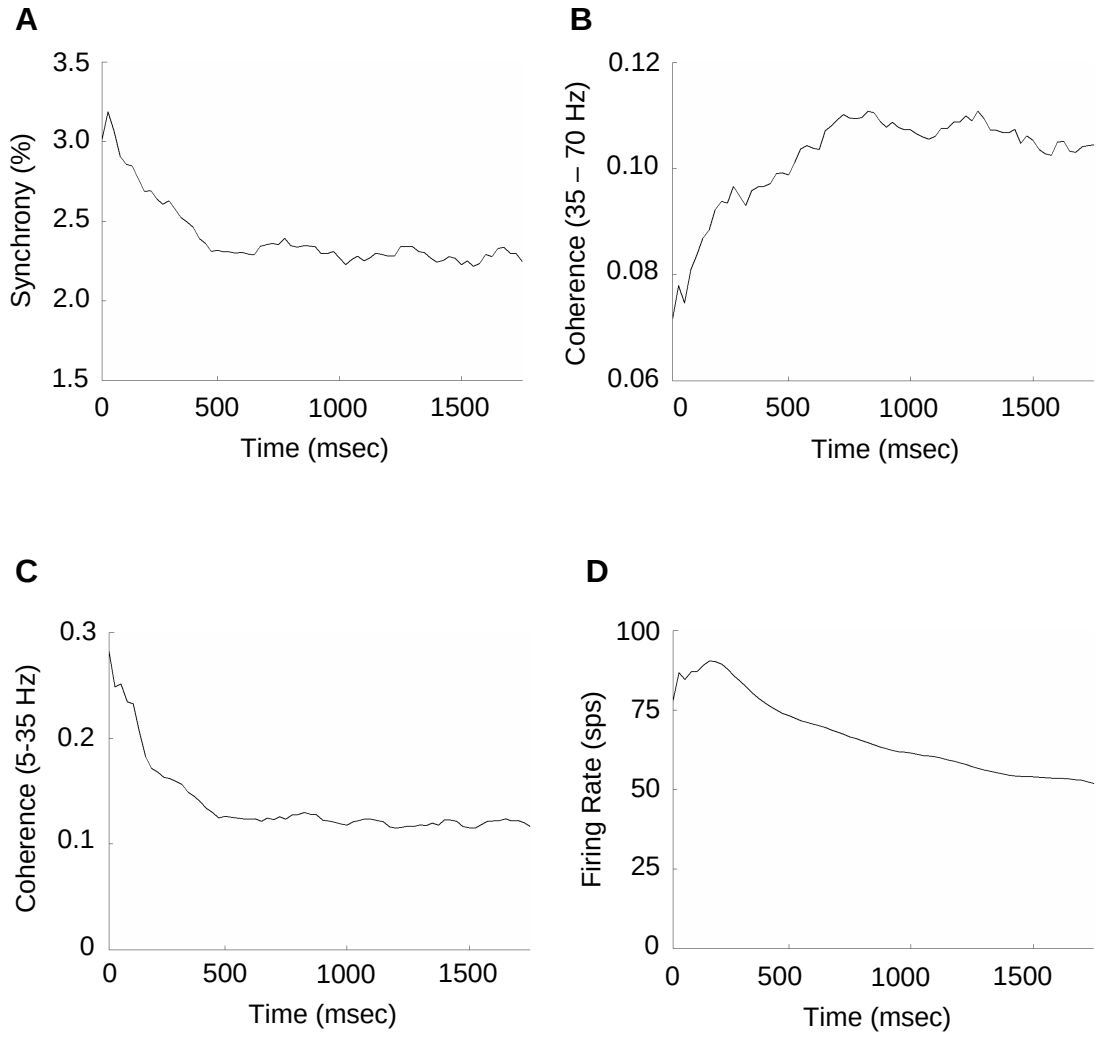

Figure 6-12: (A) Evolution of maximum synchrony vs. time. (B) Evolution of maximum gamma coherence vs. time. (C) Evolution of maximum coherence in the low frequency band (5 – 35 Hz) vs. time. (D) Temporal dynamics of mean firing rate.

Discussion

Here we demonstrate that the correlation between neural responses is influenced by the integrity of the spatial structure of the visual stimulus. Synchrony and coherence derived from JPSTH analysis and spectral estimation significantly and systematically declined when the contour integrity of gratings was deconstructed by increasing spatial noise in the image, indicating that synchronization in neural firing can detect modification of spatial features. We also found that coherence modulation in the gamma band showed a greater loss than in alpha and beta bands as the spatial coherence was reduced, suggesting that gamma oscillation is more sensitive than other frequency bands as an indicator of the change of spatial integrity in visual stimuli. Compared to the coherence change in the gamma band, which decreased by 67.6% with 55% spatial noise in the stimulus, the alpha and beta bands only reduced by 18.6% and 13.6% coherence with the same stimulus. We also found that alpha and beta coherence were well maintained even after the spatial structure in the image was largely destroyed. We thus consider that the lower frequency coherence is mainly induced by the basic temporal structure of the stimulus as opposed to its spatial representation.

Development of neural cooperation

The initiation and development of neural cooperation in the visual system remain largely unstudied. Samonds and Bonds (2005) discovered a strong inverse logarithmic relationship between synchrony and cells' response latency differences, implying that two cells are more likely to synchronize their responses if their response latencies are nearly the same. Fries et al. (2001) found that with similar orientation preferences and

overlapping receptive fields, the spontaneous response of cells in cat primary visual cortex tends to exhibited correlated fluctuations in response latency and that this correlation only occurred when LFPs oscillated in the gamma frequency range. This suggests that, during the perception of contours with spatially contiguous structure or similar orientations, the coherence of spontaneous excitability fluctuation in certain cells, which may originate from either the anatomical connections or short-term synaptic plasticity in the pre-stimulus stage, could result in faster binding after stimulus onset. In our analysis, we found that synchrony reached its maximum value within the first tens of milliseconds, also suggesting that cell pairs that are synchronized are synchronized by the time of their *first* spikes (Samonds and Bonds, 2005). Unlike spike synchronization in the time domain, the frequency dependence between cells develops much more slowly. This does not however mean that its availability is delayed. In 96% of the cell pairs having coherence in the gamma band, detectibility of the coherence reached 95% confidence limits within 250 msec after stimulus onset, but the average gamma coherence does not reach its maximum until around 900 msec (Figure 6-12 B). This suggests that while the overall magnitude of neural cooperation in the time and frequency domains are strongly correlated, they are governed by two different mechanisms. We believe that spike timing synchronization is initially triggered by coherent structure embedded in the visual stimulus, while the frequency dependent component of cooperation is supported by network interactions.

Though only a moderate correlation was found between synchrony and gamma oscillation, oscillatory coupling may provide a framework that supports the organization of synchrony. Synchrony is maintained with little attenuation throughout the stimulation

period if oscillation is apparent, while synchrony decays significantly in the absence of oscillation (Samonds and Bonds, 2005). An *in vitro* study of pyramidal neurons, which have both axons and dendrites extending through multiple layers, shows that back-propagation of the action potential produced in the axon facilitates the generation of calcium action potentials in the dendrite if it coincides with a distal dendritic input within a range of several milliseconds (Larkum et al., 1999). This suggests that pyramidal cells may act to associate the activities of multiple neurons from which the pyramidal cells receive synchronized inputs. The intrinsic oscillatory behavior in pyramidal cells may facilitate maintenance of this association. (Silva et al., 1991). It thus seems reasonable to conjecture that the pyramidal neurons play an important role in the development of neural cooperation. The pyramidal cell detects the coincident firing between neurons, which is initiated by the coherent structures in the visual stimulation, and fires action potentials to coordinate the firing timing of two correlated neurons. The intrinsic rhythmic firing frequency of pyramidal cells, on the other hand, promotes and maintains the synchronized oscillation within the correlated neural population.

Neural Synchronization and Perceptual Grouping

Gestalt theory defines the basic framework for how our brain combines discrete elements to create a "whole" object, which is interpreted from the coherent spatial and temporal cues (Koffka, 1935). However, the biological mechanisms that support the representation and integration of those individually incomplete features through the visual pathway remain unclear. In our current study, we have observed that gamma band coherence has higher sensitivity than independent firing rate and spike synchrony to the degradation of

contour integrity of the stimulus. We also found that coherence modulation in the gamma frequency band, but not in the alpha or beta band, is capable of signaling the difference between stimulus patterns with different noise levels. Our findings suggest that fast frequency association between neurons may play an import role in visual perception, such as pattern recognition and contour integration.

REFERENCES

Aertsen AM, Gerstein GL, Habib MK, Palm G (1989) Dynamics of neuronal firing correlation: modulation of "effective connectivity". J Neurophysiol 61:900-917.

Barlow HB (1972) Single units and sensation: a neuron doctrine for perceptual psychology? Perception 1:371-394.

Castelo-Branco M, Goebel R, Neuenschwander S, Singer W (2000) Neural synchrony correlates with surface segregation rules. Nature 405:685-689.

Dan Y, Alonso J-M, Usrey WM, Reid RC (1998) Coding of visual information by precisely correlated spikes in the lateral geniculate nucleus. Nat Neurosci 1:501-507.

Eckhorn R, Bauer R, Jordan W, Brosch M, Kruse W, Munk M, Reitboeck HJ (1988) Coherent oscillations: a mechanism of feature linking in the visual cortex? Biological Cybernetics V60:121-130.

Engel AK, Kreiter AK, Konig P, Singer W (1991) Synchronization of oscillatory neuronal responses between striate and extrastriate visual cortical areas of the cat. Proc Natl Acad Sci USA 88:6048-6052.

Frien A, Eckhorn R (2000) Functional coupling shows stronger stimulus dependency for fast oscillations than for low-frequency components in striate cortex of awake monkey. Eur J Neurosci 12:1466-1478.

Fries P, Neuenschwander S, Engel AK, Goebel R, Singer W (2001) Rapid feature selective neuronal synchronization through correlated latency shifting. Nat Neurosci 4:194-200.

Gail A, Brinksmeyer HJ, Eckhorn R (2000) Contour decouples gamma activity across texture representation in monkey striate cortex. Cereb Cortex 10:840-850.

Gerstein GL, Perkel DH (1972) Mutual temporal relationships among neuronal spike trains. Biophys J 12:453–473.

Gray CM (1999) The temporal correlation hypothesis of visual feature integration: still alive and well. Neuron 24:31-47.

Gray CM, Singer W (1989) Stimulus-specific neuronal oscillations in orientation columns of cat visual cortex. Proc Natl Acad Sci USA 86:1698-1702.

Gray CM, Konig P, Engel AK, Singer W (1989) Oscillatory responses in cat visual cortex exhibit inter-columnar synchronization which reflects global stimulus properties. Nature 338:334-337.

Hannan EJ (1970) Multiple time series. New York: Wiley.

Henrie JA, Shapley R (2005) LFP power spectra in V1 cortex: the graded effect of stimulus contrast. J Neurophysiol 94:479-490.

Jarvis MR, Mitra PP (2001) Sampling properties of the spectrum and coherency of sequences of action potentials. Neural Comput 13:717-749.

Kohn A, Smith MA (2005) Stimulus dependence of neuronal correlation in primary visual cortex of the macaque. J Neurosci 25:3661-3673.

Konig P, Engel AK, Singer W (1995) Relation between oscillatory activity and long-range synchronization in cat visual cortex. Proc Natl Acad Sci USA 92:290-294.

Lamme VAF, Spekreijse H (1998) Neuronal synchrony does not represent texture segregation. Nature 396:362-366.

Larkum ME, Zhu JJ, Sakmann B (1999) A new cellular mechanism for coupling inputs arriving at different cortical layers. Nature 398:338-341.

Milner PM (1974) A model for visual shape recognition. Psychol Rev 81:521-535.

Mitra PP, Pesaran B (1999) Analysis of dynamic brain imaging data. Biophys J 76:691-708.

Montani F, Kohn A, Smith MA, Schultz SR (2007) The role of correlations in direction and contrast coding in the primary visual cortex. J Neurosci 27:2338-2348.

Palanca BJA, DeAngelis GC (2005) Does neuronal synchrony underlie visual feature grouping? Neuron 46:333-346.

Percival DB, Walden AT (1993) Spectral analysis for physical applications, multitaper and conventional univariate techniques: Cambridge University Press.

Perkel DH, Gerstein GL, Moore GP (1967) Neuronal spike trains and stochastic point processes. II. Simultaneous spike trains. Biophys J 7:419–440.

Samonds JM, Bonds AB (2005) Gamma oscillation maintains stimulus structure-dependent synchronization in cat visual cortex. J Neurophysiol 93:223-236.

Samonds JM, Allison JD, Brown HA, Bonds AB (2003) Cooperation between area 17 neuron pairs enhances fine discrimination of orientation. J Neurosci 23:2416-2425.

Samonds JM, Allison JD, Brown HA, Bonds AB (2004) Cooperative synchronized assemblies enhance orientation discrimination. Proc Natl Acad Sci USA 101:6722-6727.

Samonds JM, Zhou Z, Bernard MR, Bonds AB (2006) Synchronous activity in cat visual cortex encodes collinear and cocircular contours. J Neurophysiol 95:2602-2616.

Shoham S, Fellows MR, Normann RA (2003) Robust, automatic spike sorting using mixtures of multivariate t-distributions. J Neurosci Methods 127:111-122.

Silva LR, Amitai Y, Connors BW (1991) Intrinsic oscillations of neocortex generated by layer 5 pyramidal neurons. Science 251:432-435.

Singer W (1999) Neuronal synchrony: a versatile code for the definition of relations? Neuron 24:49-65.

Singer W, Gray CM (1995) Visual feature integration and the temporal correlation hypothesis. Annu Rev Neurosci 18:555-586.

Skottun BC, De Valois RL, Grosof DH, Movshon JA, Albrecht DG, Bonds AB (1991) Classifying simple and complex cells on the basis of response modulation. Vision Research 31:1079-1086.

Softky WR, Koch C (1993) The highly irregular firing of cortical cells is inconsistent with temporal integration of random EPSPs. J Neurosci 13:334-350.

Thiele A, Stoner G (2003) Neuronal synchrony does not correlate with motion coherence in cortical area MT. Nature 421:366-370.

Usrey WM, Reid RC (1999) Synchronous activity in the visual system. Annu Rev Physiol 61:435-456.

von der Malsburg C (1981) The correlation theory of brain function. In. Goettingen, Germany: Max-Planck-Institute for Biophysical Chemistry.

von der Malsburg C (1999) The what and why of binding: the modeler's perspective. Neuron 24:95-104.

Zar JH (1999) Biostatistical analysis, Fourth Edition Edition. Upper Saddle River, New Jersey: Prentice Hall.

Zhou Z, Bernard MR, Bonds AB (2007) Temporal and frequency analysis of synchronized neural responses in cat visual cortex. In: Vision Science Society Annual Conference. Sarasota, FL.

CHAPTER VII

FUTURE EXPLORATIONS

Examining correlation in neural assemblies larger than two presents two significant challenges: (1) Quantification of multicell correlation and (2) Selection of stimuli that are suitable for generation of synchrony in larger groups.

Quantifying correlation in large neural assemblies

Correlation between cells is normally studied by CCH analysis in the time domain (Perkel et al., 1967; Aertsen et al., 1989) or coherence analysis in the frequency domain (Jarvis and Mitra, 2001), but correlation within pairs of cells does not directly predict correlation across larger groups. The representation of synchrony in multicell assemblies is confounded by both a quantity and a quality of synchronization due to the large number of pairwise interactions. Previous researches have proposed several approaches to describe the cooperation within neural assemblies that contain more than two cell members. For example, gravitational clustering (Gerstein and Aertsen, 1985; Gerstein et al., 1985) maps neural activities into motions of particles in a multidimensional space. The number of neurons in the assembly determines the dimensionality of the space, and the distances between any two particles are uniform in the initial state. Simultaneous neural responses are transformed to particle charges that will proportionally attract other particles to create patterns of clustering. Samonds and Bonds (2004) developed a real-time visualization method that translates the temporal organization of multi-neuron

responses into a spatial display, in which the binary firing pattern of individual neurons within a cell assembly is converted into decimal numbers representing the group firing pattern. However, the results from these two methods are both qualitative instead of quantitative, and the gravitational clustering method still focuses on pairwise distance calculations.

To extend our analysis of the principles governing membership in synchronous assemblies to larger populations, we have developed an intuitive and reliable approach to detect and quantify synchrony within neural assemblies of arbitrary sizes (Bernard et al., 2005). The basic principle of this new method is to reflect the relevance of group synchrony to post-synaptic neurons by modeling the temporal summation of postsynaptic potentials (PSPs). The steps to implement the algorithm of this method are briefly described as follows:

1. Transforming the point process spike train to create PSP trains by convolving each spike with an alpha function (Equation 7-1) which models the general shape of PSP (Figure 7-1 A&B). The length of the alpha function can be defined as 10 msec, since previous researches have shown that the effective temporal summation is around 10 msec or less (Softky and Koch, 1993; Samonds et al., 2003).

$$f(t) = \begin{cases} te^{-t/\tau} & 0 \le t \le 10 \text{ msec} \\ 0 & \text{others} \end{cases} \quad (7\text{-}1)$$

2. Filtering PSP trains created in step 1 to remove partial or entire waveforms that do not overlap with any waveforms from other PSP trains (Figure 7-1 C).
3. Deriving the raw synchrony by calculating the ratio of the total integrated area in the filtered PSP trains to the total integrated area in the original PSP trains.

4. Determining the statistical significance. Chance synchrony is derived by calculating shift predictor (Perkel et al., 1967) under the null hypothesis that all neurons in the assembly are firing independently. More specifically, the score in step 3 is recalculated after shifting PSP trains by one or more stimulus trials. A student t-test can determine if a raw synchrony score is significant or not after the distribution of chance synchrony score being built by deriving multiple shift predictors with different trial shifts.
5. Computing normalized synchrony score by subtracting chance score from raw synchrony score.

The final group synchrony estimate (normalized synchrony) has a value ranging from 0 to 1 while a high normalized score implies strong group correlation with a cell assembly. We have compared results from the PSP method with Aertsen's JPSTH method (1989) in calculating pairwise synchrony, and both methods are consistent in evaluating synchrony within a pair of cells (Figure 7-2).

Testing synchrony with natural image stimuli

So far, studies about information representation and processing in visual cortex mainly rely on observing neural response to the simulation of artificial images. However, the rich structure information contained in natural image stimuli may provide a more convincing explanation about how information is encoded in the visual system. For example, natural images may provide more effective stimulation in further tests of the validity of association field theory. Based on the statistics of natural image scenes and psychophysical studies (Field et al., 1993; Geisler et al., 2001), association field theory

predicts that contour integration may be implemented by the association between orientation-tuned cells dependent on their joint relative orientation and spatial position. In Chapter 4, we have shown that synchrony was not simply an issue of matched tuning preferences between cell pairs, since with suitable stimulation of curvilinear stimuli, some cell pairs with larger orientation preference differences could exhibit more synchrony than those with smaller orientation preference differences, and that synchrony was not well-correlated with distance between recording sites. This implies that the stimulus configuration may be as important as direct anatomical connections in defining correlated activity. This initial examination of association field principles used a limited range of curvatures that only offered a match between stimulus and receptive field cocircularity in a few cell pairs, substantially decreasing the opportunities for synchrony. One of the possible strategies to get a large number of cells with differed orientation preferences to synchronize their responses is to test those cells with natural images (Figure 7-3), which contain many more comprehensive contour configurations than simple artificial images.

Our prediction is, if synchrony is related to behavioral validation of the association field theory (Hess et al., 2003), it will not depend simply on a good spatial match between the stimulus and the cell pairs. Instead, pairs with receptive fields of closer proximity will demonstrate synchrony for more similar orientations and pairs with receptive fields having wider separation will demonstrate synchrony for larger orientation differences. This simply reflects the shift in orientation along fixed curvatures rather than sensitivity to greater or lesser curvature. The extent to which our results are consistent with the association field concept will address whether synchrony in the primary visual

cortex plays a part in defining the association field, thus supporting a linking hypothesis. This will also contribute to our understanding of the relative roles of temporal coherence and architectural constraints in the creation of synchrony.

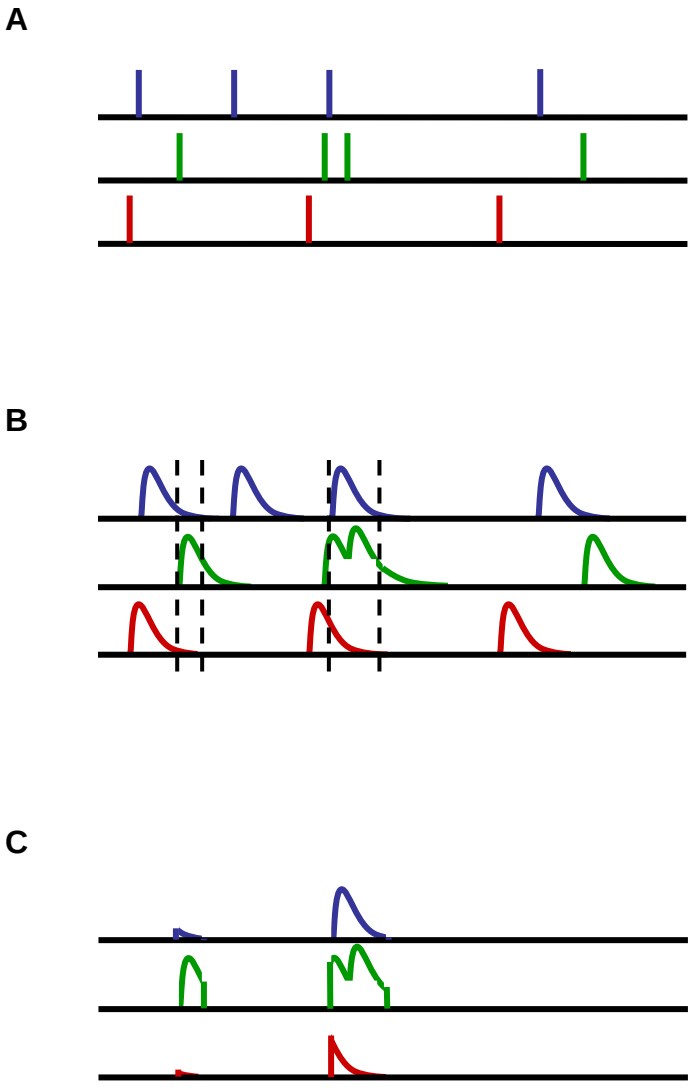

Figure 7-1: Implementing PSP algorithm (A) Spike trains from a cell assembly with three neurons. (B) PSP trains created by convolving each spike train with an alpha function. (C) Filtered trains with non-overlapping waveforms removed from original PSP trains.

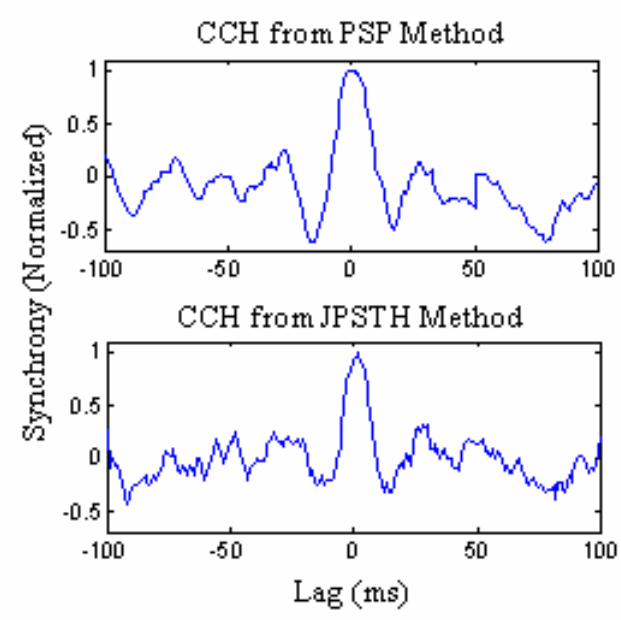

Figure 7-2: Smoothed (5msec moving average window) cross-correlograms for one pair of cells constructed by the PSP (top) and JPSTH (bottom) methods.

Figure 7-3: The comprehensive spatial configurations in natural image stimulation maybe more effective than simple artificial images in driving multiple cells to synchronize their responses if the receptive fields (white rectangles in the picture) of cells are optimally aligned on correlated contours. The image was obtained from http://www.nicisoft.com

REFERENCES

Aertsen AM, Gerstein GL, Habib MK, Palm G (1989) Dynamics of neuronal firing correlation: modulation of "effective connectivity". J Neurophysiol 61:900-917.

Bernard MR, Samonds JM, Zhou Z, Bonds AB (2005) An integration model for detection and quantification of synchronous firing within cell groups. In: Vision Sciences Society 5th Annual Conference, p 676a. Sarasota, FL: J Vision.

Field DJ, Hayes A, Hess RF (1993) Contour integration by the human visual system: Evidence for a local "association field". Vision Research 33:173-193.

Geisler WS, Perry JS, Super BJ, Gallogly DP (2001) Edge co-occurrence in natural images predicts contour grouping performance. Vision Research 41:711-724.

Gerstein GL, Aertsen AM (1985) Representation of cooperative firing activity among simultaneously recorded neurons. J Neurophysiol 54:1513-1528.

Gerstein GL, Perkel DH, Dayhoff JE (1985) Cooperative firing activity in simultaneously recorded populations of neurons: detection and measurement. J Neurosci 5:881-889.

Hess RF, Hayes A, Field DJ (2003) Contour integration and cortical processing. Journal of Physiology-Paris 97:105-119.

Jarvis MR, Mitra PP (2001) Sampling properties of the spectrum and coherency of sequences of action potentials. Neural Comput 13:717-749.

Perkel DH, Gerstein GL, Moore GP (1967) Neuronal spike trains and stochastic point processes. II. Simultaneous spike trains. Biophys J 7:419–440.

Samonds JM, Bonds AB (2004) Real-time visualization of neural synchrony for identifying coordinated cell assemblies. J Neurosci Methods 139:51-60.

Samonds JM, Allison JD, Brown HA, Bonds AB (2003) Cooperation between area 17 neuron pairs enhances fine discrimination of orientation. J Neurosci 23:2416-2425.

Softky WR, Koch C (1993) The highly irregular firing of cortical cells is inconsistent with temporal integration of random EPSPs. J Neurosci 13:334-350.

CHAPTER VIII

CONCLUSIONS

In this work, I investigated how synchronized neural responses within the cat's striate cortex might influence visual perception. The visual stimuli that were applied in my study included not only the classic drifting sinusoid gratings that have been extensively employed in studying neural behavior in the primary visual cortex but also concentric rings and gratings with systematically deconstructed spatial integrity. We found that neural synchronization in lower levels of the cortical visual pathway, i.e. area 17, may provide the basis for contour integration. We summarized our results as follows:

1. Cells in areas 17 and 18 dynamically synchronize their responses based on incoming visual information. The strength of correlation between neurons is dependent not only on the receptive field properties (i.e., orientation preference, location) of the cell pairs, but is more importantly determined by the spatial and temporal features of visual stimulation.
2. Neural synchrony is not a trivial phenomenon caused by response modulation. Instead, spike timing synchrony and frequency coherence between neural spike trains is induced by spatial and temporal structures in a specific stimulus. Cooperation between neural responses is restricted within a specific time range, i.e. less than 10 msec, which matches that for effective temporal summation of synchronized inputs. Perturbing the fine temporal structures in neural responses

not only can interrupt association between neural responses but also may cause information loss.

3. Neural synchronization in both the time and frequency domains has different but related roles in visual perception. Fast development of spike timing synchrony suggests that synchrony is trigged by the coherent temporal features of visual stimulus, while the slow accumulation of frequency coherence, especially in the gamma frequency band, implies that frequency association between neurons plays important role in recognizing detailed spatial structure of stimulus.